TÍTULO

APLICACIÓN DE RESIDUOS DE COMBUSTIÓN DEL CARBÓN PARA EL AUTOSELLADO DE BALSAS MINERAS PRODUCTORAS DE DRENAJE ÁCIDO DE MINA

AUTOR

Dino Lucio Quispe Guzmán

Universidad Internacional de Andalucía y Universidad de Huelva
Facultad de Ciencias Experimentales - Departamento de Geología

"APLICACIÓN DE RESIDUOS DE COMBUSTIÓN DEL CARBÓN PARA EL AUTOSELLADO DE BALSAS MINERAS PRODUCTORAS DE DRENAJE ÁCIDO DE MINA"

Dino Lucio Quispe Guzmán

Tesis presentada para optar al grado de Doctor en Ciencias en la
Universidad Internacional de Andalucía

DIRECTORES:

Dr. Rafael Pérez López
Contratado Ramón y Cajal
del Área de Cristalografía y
Mineralogía del Departamento
de Geología – Facultad de
Ciencias Experimentales de la
Universidad de Huelva

Dr. José Miguel Nieto Liñán
Profesor Titular de Universidad
del Área de Cristalografía y
Mineralogía del Departamento
de Geología – Facultad de
Ciencias Experimentales de la
Universidad de Huelva

AGRADECIMIENTOS

Han pasado cinco largos años y por fin ha concluido esta investigación, esto no hubiera sido posible sin la colaboración directa e indirecta de los compañeros y amigos a los cuales les tengo una eterna gratitud.

No podría empezar sino con el más sincero agradecimiento a mis directores Rafa y José Miguel, que me dieron la oportunidad de lograr un sueño que me había trazado en el mundo de la investigación. Gracias por la paciencia y disponibilidad para corregir mis numerosos errores, y las enseñanzas que me brindaron a lo largo de estos años. También gracias por la amistad que me ofrecieron, el apoyo en todas las circunstancias, incluso fuera del aspecto laboral. No hay palabras para expresar la calidad de personas que son.

De igual forma tengo mucho que agradecer a Carlos Ayora, su apoyo y confianza para permitirme participar de esta investigación. Sus aportaciones, comentarios y consejos me permitieron observar desde muchos puntos de vista la investigación.

Esta tesis no podría haberse visto culminada sin el aporte científico y la amistad de mis amigos y compañeros que durante tanto tiempo compartimos tantas experiencias. De manera muy especial a Fran, Manu, Lola, Marco, Julio, Hans, Joaquín, Pablo, Sergio, Dianita, Awi, Gema, Carlos, Ester… y muchas más personas que podría enumerar. No podría dejar de mencionar a Reinaldo, Carmen y Gabriel, que me brindaron muchos gestos de amistad y aliento para culminar este trabajo. Tengo que agradecer también a muchas más personas de la Universidad de Huelva que de una forma u otra estuvieron colaborando conmigo como: Israel, Dani, Paco, Moisés, Nuno, Rafa, María José, Cinta,

Cristobal… y otras muchas más personas que aunque no los nombre les tengo mucho que agradecer.

Finalmente agradecer en la distancia a mi familia que siempre estuvieron pendientes de mí en el transcurso de estos años. De manera especial a la memoria de mi Padre y Hermana que con júbilo me vieron partir pero me dejaron antes de culminar este trabajo que les hubiera llenado de orgullo. A mí adorada Madre que día a día me acompañaba con sus palabras, a mis Hermanos, Hermana, sobrinas y sobrinos que son mi soporte familiar aunque sea en la distancia.

ÍNDICE:

CAPÍTULO 3. THE ROLE OF MINERALOGY ON ELEMENT MOBILITY IN TWO SULFIDE MINE TAILINGS FROM THE IBERIAN PYRITE BELT (SW SPAIN)

CAPÍTULO 4. FORMATION OF A HARDPAN IN THE CO-DISPOSAL OF FLY ASH AND SULFIDE MINE TAILINGS AND ITS INFLUENCE ON THE GENERATION OF ACID MINE DRAINAGE

CAPÍTULO 5. CONCLUSIONES

BIBLIOGRAFÍA

ANEXO I. Tablas

ANEXO II. Publicaciones

Resumen

La Faja Pirítica Ibérica (FPI) es una de las mayores provincias de sulfuros masivos del mundo. La incesante actividad minera ha supuesto la producción de una enorme cantidad de residuos que han provocado la degradación ambiental de la zona. El problema procede de la oxidación de los sulfuros contenidos en esos residuos. Este proceso resulta en la producción de lixiviados ácidos y con elevada concentración de contaminantes que se conocen como Drenaje Ácido de Mina (AMD). La presente Tesis Doctoral (Capítulo 1) examina el proceso que controla la atenuación de la oxidación y liberación de contaminantes en dos balsas abandonadas de lodos piríticos de flotación en la FPI usando cenizas volantes de combustión del carbón como aditivo alcalino. Con este fin, se ha realizado una caracterización previa del patrón de meteorización de las cenizas volantes y del modelo de oxidación de ambas balsas.

El Capítulo 2 estudia los cambios de movilidad de elementos peligrosos contenidos en el carbón durante la combustión en la central térmica de Santa Catarina (Brasil), así como el potencial de impacto ambiental de sus cenizas residuales. La comparación de los resultados de concentración total y móvil de contaminantes muestra que después de la combustión, los elementos oxidables enlazados a la materia orgánica y sulfuros del carbón son mayoritariamente transferidos a la fracción de elementos solubles y, por tanto, fácilmente bioacumulativos, en las cenizas resultantes, principalmente U, Cr y As. La mayoría de las cenizas volantes que genera la central durante condiciones operacionales normales presentan carácter alcalino (pH > 10). Aunque la presencia de contaminantes móviles podría limitar el reciclado de este residuo como material de construcción, su elevada alcalinidad le confiere potencial para su uso como aditivo neutralizador para el tratamiento de residuos sulfurosos. Además, la posible lixiviación de contaminantes procedentes de las cenizas volantes durante el tratamiento no debe aumentar significativamente las concentraciones en las aguas ya contaminadas por AMD.

El Capítulo 3 se centra en la comprensión de los procesos que controlan la oxidación y generación de AMD bajo un clima semiárido en dos balsas de

1

flotación. En ambas balsas, la oxidación de los sulfuros libera sulfatos y contaminantes al agua de poro que son transportados y concentrados por evaporación en la superficie, causando la precipitación de sales solubles sulfatadas en la estación seca. Estas sales actúan como sumideros temporales de Fe, Cd, Co, Zn, Ni, Cu y Mn ya que se disuelven durante las lluvias en la estación húmeda. Los residuos de flotación contienen 30% de pirita, aunque estos valores ascienden hasta un 80% en los 50 cm superiores de una de las balsas. Esta diferencia es la clave que controla el modelo de oxidación. En la balsa que contiene 30% de pirita, el pH del agua de poro aumenta hasta 3 en la estación húmeda, provocando la sobresaturación y precipitación de fases secundarias en el frente de oxidación. En consecuencia, esta balsa muestra una capa oxidada de color amarillento de 20-25 cm en la parte superior. Por lo contrario, en la balsa que contiene 80% de pirita en la parte superior, el agua de poro es extremadamente ácida (pH < 0.5) durante todo el año, incluso en la estación húmeda, lo cual mantiene en solución la carga contaminante. Por tanto, no hay precipitación de fases secundarias en la zona de oxidación. La ausencia de estos precipitados explica el aparente aspecto no meteorizado de esta balsa, a pesar de su mayor potencial de liberación de contaminantes al medioambiente.

El Capítulo 4 propone una estrategia para el tratamiento del AMD generado en ambas balsas de flotación mediante la adición de una cubierta alcalina de 15 cm de cenizas volantes en parcelas experimentales a escala piloto de campo. Durante el tratamiento, las soluciones alcalinas de las cenizas volantes interactúan con las soluciones ácidas del lodo minero, conduciendo a la precipitación masiva de fases neoformadas en la interfase entre ambos materiales. Con el tiempo se desarrolla una zona cementada o hardpan en el contacto que fue analizada usando radiación sincrotrón. El hardpan está constituido por oxihidroxisulfatos de Fe pobremente cristalinos, jarosita y yeso; además la precipitación de yeso también cementa el nivel de cenizas volantes. La precipitación de estas fases reduce la movilidad de los elementos al modificar su especiación química a formas menos móviles bajo condiciones oxidantes. El hardpan dificulta el acceso de los agentes oxidantes al lodo, disminuyendo la tasa de oxidación de los sulfuros y atenuando la liberación de elementos contaminantes al medioambiente.

2

Abstract

The Iberian Pyritic Belt (IPB) is the one of the largest provinces of massive sulfur worldwide. The incessant mining activity has led to the output of a huge amount of wastes that has caused the environmental degradation in the area. The problem derives from the oxidation of the sulfides contained in these wastes. This process results in the production of acidic leachates with high concentration of pollutants known as Acid Mine Drainage (AMD). The present Ph.D. Thesis (1st Chapter) examines the process that controls the attenuation of both oxidation and release of pollutants in two abandoned impoundments with pyrite-rich flotation tailings at the IPB using fly ash from coal combustion as alkaline additive. With this purpose, both weathering pattern of fly ash and oxidation model of the two sulfide impoundments were previously characterized.

The 2nd Chapter reports about the changes in mobility of hazardous elements contained in coal during combustion at a power plant in Santa Catarina (Brazil) as well as the environmental impact potential of the ash wastes. Comparison of results of total and mobile concentrations of contaminants shows that after combustion, oxidizable elements bound to organic matter and sulfides in coal are mostly transferred to the soluble fraction and, hence, most readily bioaccumulative in ashes, mainly U, Cr and As. Most of fly ash wastes generated by the plant under normal operational conditions are alkaline in nature (pH > 10). Although the mobile contaminants could limit the recycling of this waste as construction material, its high alkalinity gives potential for use as neutralizing additive for the treatment of sulfide-rich wastes. In addition, the possible leaching of pollutants from fly ash during the treatment should not significantly increase concentrations in the waters already contaminated by AMD.

The 3rd Chapter is focused on the understanding of the processes controlling sulfide oxidation and AMD generation under semi-arid climate in the two flotation tailings impoundments. In both impoundments, sulfide oxidation releases sulfate and contaminants to the pore-water that are

transported and concentrated by evaporation in the top surface, causing the precipitation of soluble sulfate salts in the dry season. These salts act as temporary sinks for Fe, Cd, Co, Zn, Ni, Cu and Mn since they are dissolved during rainfall events in the wet season. The flotation tailings have 30% of pyrite, although these values amount up to 80% in the upper 50 cm of one of the impoundments. This difference is key to control the oxidation model. In the impoundment containing 30% of pyrite, pore-water pH increases to 3 in the wet period, causing supersaturation and precipitation of secondary phases in the oxidation front. Consequently, this impoundment shows a 20-25 cm thick yellowish oxidation layer in the top part. In contrast, in the impoundment containing 80% of pyrite in the top part, pore-waters are extremely acidic (pH < 0.5) during the entire year, even in the dry season, which keeps in solution the pollutant load. Therefore, no precipitation of secondary phases occurs in the oxidation zone. The absence of these precipitates explains the apparent unweathered aspect of these tailings, in spite of its much higher potential for release of contaminants to the environment.

The 4th Chapter proposes a strategy for the treatment of AMD generated in both flotation tailings impoundments by addition of an alkaline cover of 15 cm of fly ash on two pilot-scale field experimental plots. During the treatment, alkaline solutions from fly ash interact with acidic solutions from mine tailings, leading to the massive precipitation of newly-formed phases in the interface between both materials. Over time, this interaction promotes the development of a cemented zone or hardpan in the contact, which was analyzed using synchrotron radiation. The hardpan comprises poorly-crystalline Fe oxyhydroxysulfates, jarosite and gypsum; in addition, the precipitation of gypsum also cements the fly ash level. The precipitation of theses phases reduces the mobility of the elements by modification of their chemical speciation into less mobile forms under typical oxidizing conditions. The hardpan also hinders the penetration of oxidizing agents to sulfide mine tailings, which reduces the sulfide oxidation rates and attenuates the release of pollutant elements to the environment.

4

CAPÍTULO 1. INTRODUCCIÓN

1.1. GEOQUÍMICA DEL DRENAJE ÁCIDO DE MINA

1.1.1. Balsas de flotación

La actividad minera está directamente ligada al desarrollo de los pueblos para satisfacer sus necesidades socioeconómicas. Al principio, las extracciones se efectuaban puntualmente de forma artesanal, pero con el tiempo evolucionaron hacia una extracción de forma masiva debido a la creciente necesidad de recursos minerales. Como consecuencia de esta mayor demanda, se han desarrollado nuevos métodos extractivos post-mineros para mejorar la recuperación de metales valiosos. Uno de los cambios más significativos ha sido la implantación de los métodos de procesado de mineral por flotación (King, 1982). La flotación evoluciona constantemente para procesar un mayor volumen de materia mineral y para una mayor variedad de minerales. Esta técnica ha permitido la explotación de yacimientos complejos de baja ley, que antiguamente se consideraban poco rentables (Leja, 1982; Ives, 1984; Johnson y Munro, 2002).

La flotación por espuma es un proceso de separación fisicoquímica que utiliza las diferencias entre las propiedades físicas de los minerales con valor (mena) y los minerales no deseados (ganga) (Crozier, 1992; Laskowski y Poling, 1995; Harris, et al., 2002; Rao, 2004). Teóricamente la flotación implica tres fases: sólido, líquido y espuma; con tres etapas fundamentales en el proceso: a) unión selectiva del mineral a las burbujas de aire de la espuma (floculación), b) el arrastre que ocasiona el agua a través de las burbujas y c) adhesión de partículas valiosas en las burbujas (Trahar y Warren, 1976; Crawford y Ralston, 1988). La unión de los minerales mena a las burbujas es un proceso químicamente selectivo que depende de las propiedades superficiales de los minerales, provocando así la separación de minerales valiosos de la ganga. La aplicación de este método está limitada a partículas relativamente finas (de 10 a 100 μm); si el tamaño fuera mayor se evitaría la adhesión a las burbujas por el elevado peso de las partículas (Finch y Dobby, 1990; Laskowski y Ralston, 1992). En la concentración por flotación generalmente el mineral deseado está en la parte flotante y la parte de la ganga

7

se deja decantar al fondo. Este proceso se denomina flotación directa, siendo el proceso contrario la flotación inversa.

El proceso de flotación se aplica fundamentalmente para concentrar metales base a partir de yacimientos de sulfuros metálicos o para la eliminación de sulfuros en carbones antes de su combustión. Estos residuos se almacenan en pequeños lechos conocidos como balsas de lodos mineros (*tailing impoudments*) para su decantación (Fig. 1.1). Los residuos procedentes de la flotación están formados principalmente por sulfuros (especialmente pirita), silicatos y óxidos con un elevado contenido de agua (Jurjovec et al., 2002; Bernd, 2007). Las balsas a menudo se diseñan sin tener en cuenta los cambios que puedan sufrir durante el tiempo de almacenamiento, donde el material está expuesto a condiciones ambientales cambiantes. Además, los lodos procedentes de las plantas de flotación están compuestos por fracciones de minerales de tamaño de grano fino, a diferencia de los residuos producidos por las operaciones extractivas que son de mayor tamaño (King, 1982; Johnson y Munro, 2002). Estos lodos, al tener partículas muy finas, tienen mayor superficie de contacto susceptible de reacción, lo que supone una mayor disposición para los procesos de oxidación y, por lo tanto de liberación de contaminantes. En especial, la acción del agua, oxígeno, temperatura y la actividad microbiana son los factores que ocasionan y aceleran los procesos de meteorización. Así, el producto de la lixiviación de los sulfuros residuales almacenados en las balsas de flotación genera Drenaje Ácido de Mina (AMD, siglas de *Acid Mine Drainage*), el cual provoca la degradación en la calidad de las aguas, sedimentos y suelos de los sistemas circundantes (Bigham y Nordstrom, 2000; Younger et al., 2002; Akcil y Koldas, 2006).

En los últimos años, con el objetivo de proteger el medioambiente, se han implantado normas de gestión de residuos más estrictas, lo que ha motivado la necesidad de desarrollar sistemas de control para los vertidos residuales. Con esto se ha llegado a optimizar las condiciones de manipulación y mejorar la calidad ambiental de los entornos afectados por las balsas de lodos. El problema radica en entornos mineros abandonados localizados en áreas remotas o donde no exista propietario que pueda considerarse como responsable de los costes de tratamiento de los efluentes resultantes de la meteorización de estos residuos.

8

Fig. 1.1. Fotografía de una antigua balsa de lodos (complejo minero abandonado de Monte Romero, Faja Pirítica Ibérica).

1.1.2. Oxidación de sulfuros y generación de AMD

La pirita es el mineral más abundante en todos los ambientes geológicos asociados a yacimientos de sulfuros, también es un mineral muy abundante en depósitos de carbón. El proceso de oxidación de pirita se inicia cuando el mineral queda expuesto a condiciones ambientales (Buckley y Woods, 1987; Rimstidt y Vaughan 2003), ya sea por exposición natural o por actividad humana. La exposición de pirita (y otros sulfuros) a condiciones atmosféricas oxidantes ocasiona su meteorización mediante un conjunto de reacciones geoquímicas y microbiológicas encadenadas (Ecs. 1.1 a 1.7). El resultado implica la generación de AMD, es decir, drenajes extremadamente ácidos con elevadas concentraciones de sulfatos, metales (Fe, Cu, Pb, Zn, etc.) y metaloides (As, Sb, etc.) (Lowson, 1982; Parker y Robertson, 1999; Younger et al., 2002), así como elevadas concentraciones de elementos procedentes de la hidrólisis ácida de las rocas encajantes del yacimiento (Al, Ca, Mg, etc.). Estos drenajes son una fuente importante de contaminación de aguas superficiales y subterráneas, por lo que se considera una amenaza para el medioambiente. Por tanto, existe una gran variedad de estudios sobre los procesos de oxidación de pirita (por ejemplo, Luther, 1987; Evangelou 1995; Evangelou y Zhang 1995; Nordstrom y Alpers 1999; Keith y Vaughan 2000).

La oxidación de pirita puede producirse en presencia de oxígeno (Ec. 1.1) o bien por la combinación de oxígeno y Fe^{3+} (Ec. 1.1 a 1.3) (Evangelou y

9

Zhang, 1995). El Fe, tanto en su estado divalente como trivalente, desempeña un papel central en la oxidación de la pirita en cuanto a la producción de acidez. La oxidación de pirita en medio acuoso puede expresarse a partir de las siguientes reacciones (Bernd, 2007):

$$FeS_2 + 7/2O_{2(aq)} + H_2O \rightarrow Fe^{2+} + 2SO_4^{2-} + 2H^+ + \varepsilon^o \tag{1.1}$$

$$Fe^{2+} + 1/4\,O_{2(aq)} + H^+ \rightarrow Fe^{3+} + 1/2H_2O + \varepsilon^o \tag{1.2}$$

$$FeS_2 + 14Fe^{3+} + 8H_2O \rightarrow 15Fe^{2+} + 2SO_4^{2-} + 16H^+ + \varepsilon^o \tag{1.3}$$
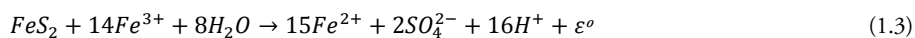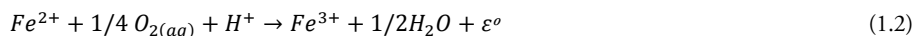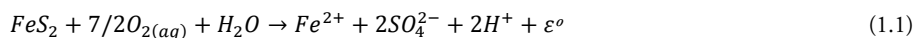
En todas las reacciones se libera energía debido a que la oxidación de la pirita es exotérmica. La oxidación de la pirita por acción del oxígeno disuelto produce SO_4^{2-}, Fe^{2+} y H^+ (Ec. 1.1). El Fe^{2+} generado se oxida por acción del oxígeno disuelto provocando la formación de Fe^{3+} (Ec. 1.2). La liberación de H^+ produce la disminución del pH del agua. El Fe^{3+} generado en la Ec. 1.2 actúa como un agente oxidante de la pirita (Ec. 1.3). La oxidación de la pirita causada por el Fe^{3+} a su vez genera también Fe^{2+}. Este Fe^{2+} se vuelve a oxidar por acción del oxígeno disuelto a Fe^{3+} que de nuevo oxida a la pirita y genera Fe^{2+}, así sucesivamente formando un ciclo continuo de oxidación de Fe^{2+} a Fe^{3+} (Fig. 1.2) (Bernd, 2007).
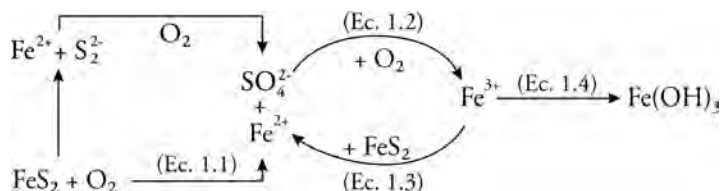
Fig. 1.2. Diagrama simplificado del ciclo de reacciones de oxidación de la pirita (Banks et al., 1997; Bernd, 2007).

La abundancia del Fe^{3+} como agente oxidante está limitada por el pH de la solución, presentándose una relación inversa entre el pH y la solubilidad del Fe^{3+}. A pH superiores a 3, el Fe^{3+} precipita formando oxi-hidróxidos de hierro (Ec. 1.4).

$$Fe^{2+} + 3H_2O \leftrightarrow Fe(OH)_3 + 3H^+ \tag{1.4}$$

La precipitación de Fe^{3+} libera protones a la solución, acidificando aún más el medio. Esta reacción de hidrólisis reduce el pH lo cual permite que el Fe^{3+} permanezca disuelto.

La oxidación de otros sulfuros como la galena, la esfalerita o la calcopirita no se han estudiado con tanto detalle como la de la pirita, ya que no genera acidez, aunque se liberan otros metales potencialmente tóxicos en solución (Ejemplos, Ecs. 1.5 a 1.7).

Galena $\qquad PbS + 2O_{(aq)} \leftrightarrow Pb^{2+} + SO_4^{2-}$ (1.5)

Esfalerita $\qquad ZnS + 2O_{(aq)} \leftrightarrow Zn^{2+} + SO_4^{2-}$ (1.6)

Calcopirita $\qquad CuFeS_2 + 4O_{2(aq)} \leftrightarrow Cu^{2+} + Fe^{2+} + 2SO_4^{2-}$ (1.7)
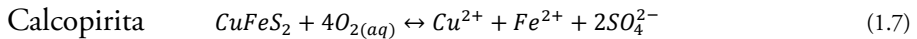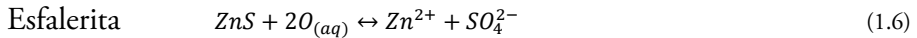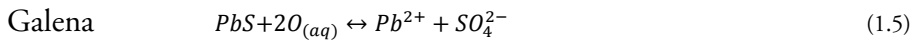
En ambientes naturales, los procesos de oxidación de la pirita están catalizados por la actuación de microorganismos, los cuales aceleran las reacciones descritas anteriormente (Langmuir, 1997). Algunos estudios sobre microorganismos que actúan en los procesos de oxidación se han centrado en las siguientes bacterias extremófilas: Acidithiobacillus ferrooxidans, Leptospirillum ferrooxidans, Acidithiobacillus thiooxidans, Metallogenium, y algunas otras. De todas ellas, cabe destacar la actuación fundamental de Acidithiobacillus ferrooxidans (Schippers y Sand, 1999).

La oxidación por acción bacteriana de sulfuros se atribuye a dos tipos de reacciones metabólicas (directas e indirectas) que no son excluyentes entre sí. En el mecanismo directo, la bacteria entra en contacto físico con el sulfuro, el cual se oxida mediante reacciones enzimáticas. En el mecanismo indirecto, las bacterias no actúan directamente sobre la superficie de los sulfuros, sino que catalizan las reacciones que ocurren próximas a dicha superficie. Este proceso indirecto no se restringe solo a los sulfuros metálicos, sino también puede afectar a arseniuros, carbonatos y óxidos.

1.1.3. Mecanismos de neutralización de acidez

Las aguas ácidas, al tener los valores de pH tan bajos, contienen la mayoría de los elementos potencialmente contaminantes en solución. La meteorización de los aluminosilicatos a menudo existentes en los entornos mineros no es suficientemente rápida y, aunque contribuyen a la neutralización de la acidez generada, estos minerales por sí solos no son capaces de tamponar las soluciones a un pH elevado. La disolución de estos aluminosilicatos aporta a la solución ácida grandes cantidades de elementos entre los que cabe destacar Al, Si, Ca, Mg, K, Na, etc. El proceso químico de neutralización tiene como finalidad agregar sustancias alcalinas tales como carbonatos capaces de elevar los valores de pH a niveles aceptables. Este aumento de pH disminuye la solubilidad de los elementos considerados contaminantes, favoreciendo su precipitación. En la reacción, se consumen iones H^+ y se generan iones bicarbonatos. La mejora de la calidad de las soluciones se produce por precipitación de sulfatos y oxihidróxidos.

La neutralización podría ser un mecanismo eficaz en la eliminación de metales tales como Cd, Cu, Fe, Ni y Zn (Bernd, 2007). Sin embargo, la solubilidad de los metales varía con el pH y no todo los metales pueden ser precipitados a un mismo valor de pH (Kuyucak, 2001; Brown et al., 2002). Por ejemplo, los metales trivalentes alcanzan su mínimo de solubilidad a un pH cercano a la neutralidad y, sin embargo, los metales divalentes precipitan a valores más altos de pH. Por otro lado, la adsorción superficial y coprecipitación de contaminantes en los precipitados férricos son mecanismos que también juegan un papel muy importante en la inmovilización y atenuación de la contaminación (Stumm y Sulzberger, 1992; Webster et al., 1994; McGregor et al., 1998; entre otros).

1.1.4. Técnicas de tratamiento

Existen numerosas investigaciones enfocadas a reducir el impacto que generan los drenajes ácidos producidos en entornos mineros. En la actualidad estos estudios se pueden clasificar en dos categorías: 1) los que se refieren específicamente al tratamiento de las aguas ácidas; y 2) los destinados al

tratamiento de los residuos sólidos para evitar que sigan lixiviando dichas aguas ácidas.

1.1.4.1. Tratamiento del AMD

Los métodos de tratamiento del AMD se refieren básicamente a dos formas, los sistemas activos o convencionales y los sistemas pasivos (Younger et al., 2002). El tratamiento activo se basa en la mejora de la calidad del agua por métodos que requieren del suministro continuo de energía artificial y reactivos químicos. El tratamiento pasivo es una alternativa al tratamiento activo y se basa en la mejora de la calidad del agua usando únicamente fuentes de energía biodisponibles de forma natural. El tratamiento pasivo no implica la utilización continua de reactivos químicos y tampoco requiere de mantenimiento frecuente (Younger et al., 2002; Walton-Day, 2003). Estos procesos de tratamiento son lentos porque necesitan más tiempo de residencia del agua en los lechos de tratamiento. De forma contraria, en los tratamientos activos el tiempo de residencia es mucho más corto, pero requiere de un mantenimiento continuo (Kleinmann, 1990; Phipps et al., 1991; Skousen et al., 1998).

Los tratamientos activos ocasionan elevados costes económicos mientras que los pasivos son de bajo coste (Phipps et al., 1991; Skousen et al., 1998). Este hecho ha permitido que en las últimas décadas se hayan realizado numerosos estudios sobre tratamientos pasivos. La técnica de tratamiento pasivo más común es la oxidación de aguas ácidas para transformar los metales en solución a sus formas oxidadas menos solubles. Para lograrlo se añaden reactivos alcalinos tales como calcita para incrementar los valores de pH para luego provocar la precipitación metálica (Turner y McCoy, 1990; Blowes et al., 2000).

Se pueden considerar diferentes tipos de métodos pasivos: humedales aerobios (Hedin et al., 1994; Skousen et al., 1998), sistemas de aireación, drenes de caliza anóxicos (Turner y McCoy, 1990), barreras reactivas permeables (Blowes et al., 2000) y sistemas de reducción y producción de alcalinidad (Kepler y McCleary, 1994; Watzlaf, 1997). Todos estos métodos han sido creados para el tratamiento de aguas con concentraciones bajas a medias de metales y acidez, característica típica de zonas mineras de carbón. En

los últimos años, para la descontaminación eficaz de AMD con una carga extremadamente alta de metales y acidez, típico de distritos mineros de sulfuros metálicos, se ha desarrollado un novedoso sistema pasivo denominado DAS (Dispersed Alkaline Substrate, Caraballo et al., 2011; Macías et al., 2012).

1.1.4.2. *Tratamiento de escombreras mineras*

El principio fundamental del tratamiento de las escombreras es diseñar y aplicar métodos para inhibir o retardar los procesos químicos, físicos y microbiológicos que dan lugar a la generación de los drenajes ácidos. Esto implica que el método debe minimizar los índices de reacción de los residuos sulfurosos que contiene; atenuando su lixiviación y por lo tanto la liberación de metales contaminantes (Johnson et al., 2000; Younger et al., 2002). Para cumplir estos objetivos es necesario tener en cuenta 5 pasos: a) reducir el contacto con el oxígeno, b) reducir la infiltración de agua c) aislar los minerales sulfurosos, d) controlar el pH del agua de poro y e) controlar los procesos bio-geoquímicos (Bernd, 2007).

La problemática básica de las escombreras mineras es el enorme volumen que acumulan de residuos ricos en sulfuros, cuya meteorización conduce a la generación de AMD. En algunos casos, la neutralización de acidez y la retención de metales se producen de forma natural cuando la escombrera contiene minerales alcalinos tales como la calcita. De forma contraria, cuando los derivados de la acciones extractivas acumulados exceden la capacidad neutralizadora del entorno (Jurjovec et al., 2002) o bien el entorno no tiene capacidad neutralizadora (por ausencia de materiales alcalinos), el resultado es la formación inevitable de AMD.

Cuando un producto de carácter alcalino entra en contacto con el residuo minero, se produce un aumento de los valores de pH de los lixiviados. Esto se traduce en una neutralización de la acidez, una reducción de la solubilidad del Fe liberado y, con el tiempo resulta en una atenuación del proceso de oxidación de los sulfuros, especialmente pirita (Blowes et al., 2004). El Fe^{2+} se oxida a Fe^{3+}, proceso rápido a pH alcalino, y precipita como un oxi-hidróxido férrico, eliminando a éste y a otros metales (por coprecipitación y/o adsorción) de la solución. Por otro lado, la precipitación inmediata de las fases

14

férricas puede tener lugar sobre la superficie de la pirita, originando un revestimiento que puede afectar a la velocidad de disolución del mineral, hasta el punto de inhibirla. Este proceso fue definido como microencapsulación (Evangelou, 1995). La técnica más común empleada en el tratamiento de un residuo minero donde se desarrolla el proceso de microencapsulación es la adición de calcita (Nicholson et al., 1988, 1990; Mylona et al., 2000; entre otros).

Existen otros ensayos encaminados a prevenir o retardar la producción de AMD. Así, Farah et al. (1997) propusieron la aplicación de aislantes fabricados con cemento o resinas naturales sobre residuos mineros dispuestos en enormes pilas expuestas a condiciones de meteorización naturales. Ambos tipos de aislantes forman una capa cuya principal función es la de proteger a los residuos de su oxidación, y por tanto, retardar la generación de AMD. Los aislantes con cemento son menos efectivos que las resinas naturales, ya que éstos forman una película que es susceptible de astillarse y escamarse siendo incapaz de resistir los efectos de la meteorización.

1.2. RESIDUOS DE LA COMBUSTIÓN DEL CARBÓN

1.2.1. Combustión del carbón

Los carbones son combustibles fósiles sólidos utilizados principalmente en las centrales térmicas, donde se genera energía eléctrica a partir de la energía térmica producida durante su quema. La creciente demanda de energía eléctrica ha creado la necesidad de incrementar la construcción de grandes centrales térmicas. Esto implica un incremento en el consumo de carbón y, para cumplir esta demanda, ha sido necesario incrementar la explotación mundial de carbón en los últimos años.

El carbón utilizado en las centrales térmicas es triturado, pulverizado y posteriormente introducido por inyección mediante aire caliente dentro de las cámaras de combustión. Este método es el más utilizado en las centrales térmicas del mundo (Fig. 1.3). Estas cámaras son de tipo supercrítico con circulación asistida donde se generan vapores a altas presiones y temperaturas. Estos vapores activan las turbinas encargadas de producir la energía eléctrica.

15

Durante la combustión, la parte orgánica es oxidada y volatilizada, mientras que la fracción mineral es transformada en sólidos residuales como cenizas volantes y cenizas de fondo. En general, las cenizas volantes son partículas de tamaño de grano muy fino las cuales son arrastradas por el flujo de gases generados durante la combustión. Con el fin de evitar la emisión de estas partículas a la atmosfera, son recuperadas mediante sistemas de retención, siendo el más importante los precipitadores electrostáticos (Smith, 1987; Megía, 1998). Las fracciones residuales más pesadas, conocidas como cenizas de fondo, al no ser arrastradas por los gases caen depositadas en las cámaras de combustión. El porcentaje generado de cada residuo depende de la disposición de la planta y el tipo de calderas empleadas en la combustión, así como de la naturaleza de la materia prima.
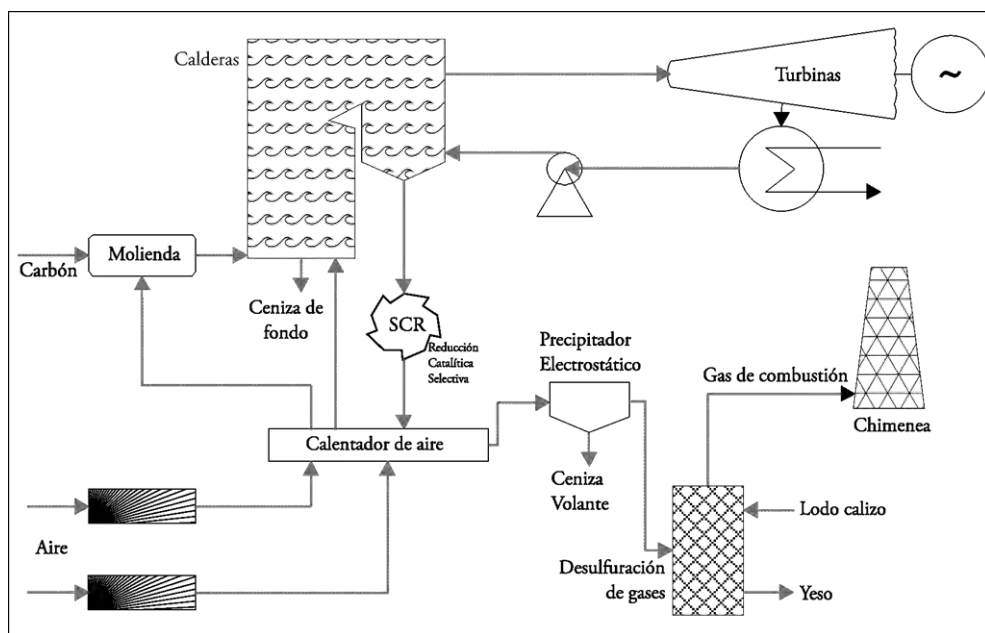
Fig. 1.3. Esquema típico de una planta termica de combustion de carbón (IEA, 2007).

El modo de almacenamiento de los residuos adquiere cierta importancia para una posible utilización en el futuro. Idealmente, el almacenamiento debe producirse en seco ya que tiene la ventaja de que las propiedades fisicoquímicas

16

permanezcan inalteradas. Sin embargo, el almacenamiento en zonas cercanas a las plantas térmicas ocupa cada vez superficies mayores, lo que conlleva al aumento considerable de los costes de transporte y restauración medioambiental. La acumulación de cenizas de combustión a menudo se produce en espacios abiertos, lo cual puede suponer un riesgo ambiental importante ya que su meteorización en periodos húmedos puede provocar la lixiviación y liberación de algunos elementos contaminantes (Potgieter-Vermaak et al., 2006).

En los últimos tiempos, las legislaciones han variado considerablemente en lo referente a la calidad de los lixiviados procedentes de los residuos de la combustión del carbón, lo que condiciona la acumulación de estos, y por lo tanto supone un fuerte incremento en los costes de gestión de residuos.

1.2.2. Cenizas volantes

El carbón utilizado en la industria para la generación de energía eléctrica produce aproximadamente un 40% de residuos sólidos, de este el 80% corresponde a cenizas volantes (Silva et al., 2009a). Además de representar la mayor parte de los residuos generados, son los de menor tamaño de grano y los más reactivos químicamente. Las cenizas volantes están compuestas por aglomerados de micro-esferas de tamaño de grano muy fino (entre 0.2 y 200 μm) constituidas principalmente por Si y Al y en menor proporción Fe, Na, K, Ca, P, Ti y S; también pueden contener elevados contenidos de elementos traza como As, Ba, Cd, Cr, Hg, Pb y Se. El contenido elevado de estos elementos podría limitar la aplicación de las cenizas volantes debido a las restricciones ambientales.

En cuanto a la mineralogía, las cenizas volantes están constituidas mayoritariamente por un vidrio amorfo aluminosilicatado, mullita y cuarzo, con menores contenidos de cal, óxidos de hierro, anhidrita y feldespato potásico (Querol et al., 1999). La composición química y las propiedades fisicoquímicas de las cenizas volantes están bien documentadas y sus diferencias están relacionas principalmente con el tipo de carbón utilizado y el método de combustión de las plantas térmicas (Querol et al., 1995; Rice et al., 1997; Vassilev y Vassileva, 2005). Las cenizas volantes tienen un elevado potencial

para neutralizar acidez debido a la presencia de la fase vítrea y de la cal. La cal en contacto con el agua se disuelve relativamente rápido produciendo soluciones con un pH de alrededor de 12. Sin embargo, la alcalinidad no expira cuando la cal se consume ya que la disolución del vidrio también produce alcalinidad (pH alrededor de 10) y es un proceso relativamente más lento, manteniendo el potencial neutralizador de acidez a largo plazo (Pérez-López et al., 2009).

1.2.3. Producción y aplicaciones

La producción mundial de residuos de combustión está liderada por China, Rusia y Estados Unidos, en este orden. En la Unión Europea se generan 100 millones de toneladas de residuos anuales. En la actualidad, los residuos de combustión son utilizados principalmente en la industria de la construcción (IEA, 2007; ECOBA, 2011). Las cenizas volantes tienen propiedades reactivas al entrar en contacto con el agua y un elevado poder aglomerante. La utilización de las cenizas volantes como aditivo en el hormigón puede ser de dos maneras: como elemento activo debido a su carácter puzolánico o como elemento inerte (árido). La utilización de las cenizas en la fabricación de hormigón reduce en gran medida el uso del cemento, lo cual tiene un valor añadido porque reduce el consumo energético y la materia prima que se consumiría en la fabricación del cemento sustituido (Goñi et al., 1997; Manz, 1997). En la Unión Europea aproximado un 50% de las cenizas volantes y cenizas de fondo son reutilizadas como material de construcción (Fig. 1.4). La reutilización de las cenizas en España es aproximadamente 65% (ECOBA, 2011).

Como consecuencia del no reciclado total de las cenizas volantes, del carácter acumulativo de este residuo y del incremento de las restricciones medioambientales, en los últimos años se ha hecho imprescindible la búsqueda de nuevas aplicaciones que sean respetuosas con el medioambiente. Numerosas investigaciones se centran en convertir los residuos en productos de interés para mercados específicos y, de esta forma, reducir el impacto ambiental que deriva de su almacenamiento indiscriminado. Por ejemplo, algunas de sus aplicaciones potenciales serían: su utilización como polvos reactivos de fundición (Andres et

18

al., 1995), para la recuperación de metales a partir de las cenizas (Pickles et al., 1990), para la producción de fertilizantes (Ghosh, 1997; Saylak et al., 1997;), para la producción de cerámicas (Queralt et al., 1997; Anderson et al., 2001), para la síntesis de zeolitas (Höller y Wrishing 1985), en la fabricación de materiales ignífugos (Vilches et al., 2001), para la estabilización de residuos mineros y la neutralización de AMD (Jarvis y Brooks, 1996; Potgieter-Vermaak et al., 2006; Pérez-López et al., 2007a).
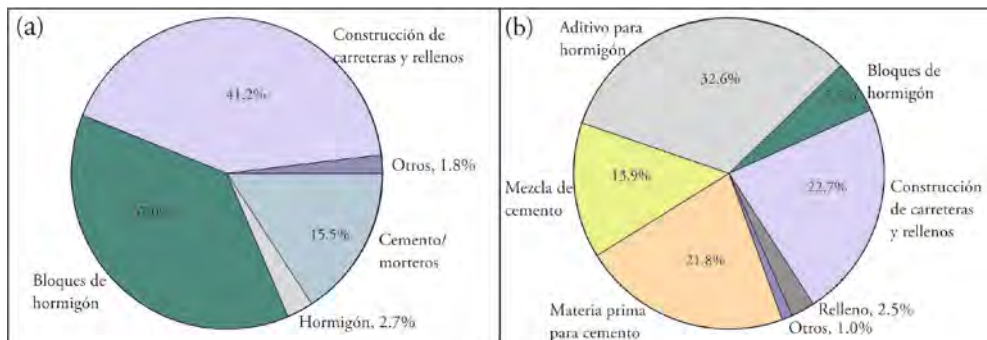
Fig. 1.4. Usos de los residuos de combustión de carbón en Europa (cenizas de fondo (a) y cenizas volantes (b)) (ECOBA, 2011).

1.3. ESTRUCTURA, JUSTIFICACIÓN Y OBJETIVOS

A continuación se describe la estructura de la presente Tesis Doctoral que se ha divido en 5 capítulos. El primer capítulo muestra una introducción general y los objetivos, y el último capítulo unas conclusiones generales. Los capítulos 2, 3 y 4 son los capítulos principales basados en artículos científicos publicados, los cuales tienen una estructura basada en una introducción, metodología, resultados y discusión, y conclusiones. Esta estructura, aunque parezca repetitiva y redundante, pretende aportar independencia a cada capítulo individual para así facilitar su comprensión.

1.3.1. Capítulo 2: "Changes in mobility of hazardous elements during coal combustion in Santa Catarina power plant (Brazil)"

La demanda energética mundial sufre un constante crecimiento y para satisfacer estas necesidades se están proponiendo ampliar los complejos

energéticos de generación eléctrica, principalmente alimentados con carbón. Esto hace suponer que la demanda de carbón se incrementará y, por lo tanto, la generación de residuos de combustión también (IEA, 2007; ECOBA, 2011). Este es el caso de Brasil, debido al auge económico que están desarrollando tienen la necesidad de incrementar la producción de energía, lo que conlleva a una mayor demanda de carbón y mayor generación de residuos. Brasil se localiza en una zona tropical con lluvias constantes y ambiente extremadamente húmedo. En estos ambientes, los residuos de la combustión del carbón no permanecen estables en las zonas de acopio ya que se encuentran expuestas a continua meteorización (Silva et al., 2009a). Además, las zonas de almacenamiento están situadas cercanas a zonas agrícolas que pueden estar influenciadas por la actividad que conlleva la combustión del carbón.

La aplicación de los residuos de combustión en Brasil aun no está bien extendida debido a la falta de estudios sobre su comportamiento bajo diferentes condiciones de meteorización en las zonas de almacenamiento. De igual forma, no existen estudios sobre la transferencia de metales desde el procesado de la materia prima hasta los residuos derivados de la combustión. Esta falta de conocimiento podría limitar el desarrollo de tecnologías de aprovechamiento de estos materiales para sus posibles aplicaciones futuras. Este capítulo está enfocado en la caracterización del carbón y sus cenizas de combustión obtenidas en la principal central térmica de Latinoamérica (Santa Catarina, Brasil). En este capítulo se persiguen los siguientes sub-objetivos específicos:

- Estudiar la mineralogía y el contenido total de elementos potencialmente tóxicos en el carbón y en los residuos de combustión.

- Evaluar el porcentaje de transferencia de estos elementos desde el carbón a las diferentes cenizas de combustión.

- Evaluar el grado de movilidad de estos elementos bajo diferentes condiciones ambientales de meteorización mediante técnicas de laboratorio de extracción secuencial.

- Combinar los datos de la extracción secuencial con el volumen anual producido de cada tipo de cenizas para establecer el riesgo potencial de contaminación ambiental de la central térmica.

20

1.3.2. Capítulo 3: "The role of mineralogy on element mobility in two sulfide mine tailings from the Iberian Pyrite Belt (SW Spain)"

La Faja Pirítica Ibérica (FPI) es la mayor provincia de sulfuros masivos del mundo (Sáez et al., 1999). Se localiza en el suroeste de la Península Ibérica y ha sufrido una incesante actividad minera que se remonta a 5000 años de historia (Leblanc et al., 2000; Nocete et al., 2005). A excepción de algunos permisos de exploración y varios proyectos en fase de explotación, la mayor parte de la actividad minera ha cesado casi por completo en la actualidad, dejando una gran cantidad de residuos mineros ricos en sulfuros en un centenar de distritos mineros abandonados (Pinedo Vara, 1963). Estos residuos se encuentran dispuestos en escombreras y balsas mineras expuestas abiertamente a una continua meteorización. Estas acumulaciones impactan de forma severa en la calidad ambiental de la región debido a la elevada producción de AMD derivado de la oxidación de los sulfuros residuales. Estos lixiviados son a su vez drenados por la red hídrica de la zona que, en consecuencia, se caracteriza por presentar en su mayor parte una extrema acidez y una elevada carga de metales disueltos potencialmente contaminantes. Esta polución, a través de los ríos Tinto, Odiel y Guadiana, es transportada hasta alcanzar el Golfo de Cádiz y el Océano Atlántico (Sáinz et al., 2002; Fernández-Remolar et al., 2004; Cánovas et al., 2007; Delgado et al., 2009; Sarmiento et al., 2009).

Las balsas de lodos de flotación pueden considerarse uno de los focos principales de generación de AMD en la FPI por su elevada concentración de sulfuros. Estas balsas están abandonadas sin ningún tipo de control, y el libre acceso de oxígeno y la elevada área superficial de las partículas micrométricas son factores que aceleran el proceso de oxidación y la liberación de contaminantes al medioambiente. Además, la FPI está sometida a un clima semiárido de tipo Mediterráneo, con una estación húmeda-lluviosa en invierno y una estación seca-cálida en verano. Esta humedad alternante, las moderadas y altas temperaturas y la completa ausencia de carbonatos en la región provocan la meteorización activa de la pirita y una importante producción de AMD. Este capítulo trata de llenar el vacío de información existente sobre los procesos de oxidación de lodos de flotación bajo condiciones áridas o semiáridas mediante el estudio de dos balsas abandonadas en el distrito minero de Monte Romero (FPI). Este objetivo a su vez persigue los siguientes sub-objetivos específicos:

- Caracterizar la composición mineralógica y química del lodo minero a diferentes profundidades.

- Evaluar el grado de movilidad de los contaminantes bajo diferentes condiciones de meteorización mediante extracción secuencial.

- Estudiar la composición química del agua de poro y del gas de poro, y realizar una modelización geoquímica que correlacione estos datos con las observaciones mineralógicas.

- Establecer un modelo de oxidación que explique la producción de aguas ácidas de mina por meteorización de balsas de flotación en clima semiárido.

1.3.3. Capítulo 4: "Formation of a hardpan in the co-disposal of fly ash and sulfide mine tailings and its influence on the generation of acid mine drainage"

Una vez conocido el patrón de meteorización de las cenizas volantes (Capítulo 2) y de las balsas de flotación (Capítulo 3), la idea sería diseñar e implementar acciones preventivas orientadas a minimizar la generación de lixiviados por el acopio a la intemperie de ambos residuos. Hasta ahora, el tratamiento de AMD en la FPI se centraba en sistemas pasivos enfocados en tratar directamente lixiviados con extrema acidez y elevada concentración de metales (Caraballo et al., 2011; Macías et al., 2012). Aunque estos sistemas funcionan satisfactoriamente, este estudio intenta ir más allá con el tratamiento de los residuos sulfurosos que son la fuente de producción de estos lixiviados. Como se comentó anteriormente, la calcita es el aditivo alcalino comúnmente usado para el tratamiento de residuos mineros. Sin embargo, las cenizas volantes de la combustión de carbón también tiene aplicaciones potenciales como agente neutralizador de acidez.

La hipótesis de partida sería aportar una única solución sostenible y atractiva para el tratamiento simultáneo de cenizas volantes y lodos de flotación. Las ventajas de usar cenizas volantes como aditivo alcalino para tratar residuos mineros incluyen que son un sub-producto ampliamente disponible y generalmente barato en comparación con la calcita. De hecho, las cenizas volantes están recibiendo actualmente una considerable atención en el

22

tratamiento químico mediante su adición a suelos contaminados por metales o residuos mineros (Dermatas y Meng, 2003; Wang et al., 2006; Polat et al., 2007). Además, algunos estudios previos de laboratorio han demostrado que la adición de una cobertera de cenizas volantes sobre lodos de flotación también puede inducir una neutralización de la acidez, la retención de metales y la mejora de la calidad de los lixiviados que se produzcan (Pérez-López et al., 2007a,b). Los resultados obtenidos en estos experimentos de laboratorio han sido tan alentadores que plenamente justifican la necesidad de su implementación en ensayos de campo a escala piloto, antes de un futuro tratamiento a gran escala. Dicho tratamiento a escala piloto es el principal objetivo de este capítulo. Este objetivo también persigue los siguientes sub-objetivos específicos:

- Construir parcelas experimentales con una cubierta superior de cenizas volantes sobre las dos balsas de lodos abandonadas en el distrito minero de Monte Romero (FPI).

- Comparar el grado de movilidad de contaminantes observado en el lodo minero sin tratamiento con el observado en las parcelas experimentales enmendadas con cenizas volantes.

- Caracterizar los precipitados neoformados en las parcelas experimentales usando microanálisis con rayos X basados en radiación sincrotrón.

- Monitorizar el acceso de oxígeno atmosférico a ambas balsas, y evaluar como la adición de cenizas volantes puede afectar al progreso de la oxidación y generación de aguas ácidas de mina.

CAPÍTULO 2. CHANGES IN MOBILITY OF HAZARDOUS ELEMENTS DURING COAL COMBUSTION IN SANTA CATARINA POWER PLANT (BRAZIL)

Abstract

This paper reports about changes in mobility of hazardous elements contained in coal during combustion at a power plant in Santa Catarina (Brazil) and the environmental impact potential of ashes. Total and mobile element concentrations were determined by digestion and sequential extraction. Comparison of results within the mobile fraction showed that after combustion, oxidizable elements bound to organic matter and sulfides in coal were mostly transformed into elements easily soluble in water or slightly acidic conditions and, hence, most readily bioaccumulative in the environment in ashes, mainly U, Cr, and As. Capacity of ashes as a source of mobile pollutants was quantified by combining sequential extraction and annual production. Just considering the easily soluble fraction, coal ashes could leach up to 839 tons of Al, 144 tons of Fe, 100 tons of Mn, 4.6 tons of Zn, 3.1 tons of Cr, 1.7 tons of As, 1.5 tons of Cu, 490 kg of U, and 20 kg of Pb every year. Bottom ashes are disposed of in landfill sites close to the plant. Fly ashes are recycled as construction material. Diagnostic processes do not consider checking for these highly mobile hazardous elements. Hence, uncontrolled dumping and use of these by-products may pose significant risks to environment and human health.

2.1. INTRODUCTION

In Brazil, coal has been used for decades as fossil fuel in thermoelectric plants for the generation of electric power (Levandowski and Kalkreuth, 2008). Coal represents the Brazil's largest source of non-renewable energy, accounting for 50% of the total, followed by nuclear fuel (27%), oil (8%) and natural gas (2.5%). The coal demand reaches 18.4 Mt per year (Gurmendi, 2007). During the 1970´s, there was a sharp increment in mining activities in order to increase the national production of coal. Consequently, the region was declared under environmental danger in 1980. Currently, the power production from the coal combustion is estimated to generate around 1500 MW distributed in seven power plants, which represents 11% of the total energy generated in Brazil. This is the reason why attention was prioritized in order to reduce environmental degradation, without altering the demand for coal in power plants (Silva et al., 2009a,b, 2010a).

Due to high concentrations of mineral matter such as sulfides, clays, and quartz, Brazilian coal must be pulverized and beneficiated, specifically with flotation, before its combustion. Then, the coal is burned inside a boiler, producing a solid combustion-by-product known as coal ash (fly ash and bottom ash). Fly ash comprises the fine particles that rise with the flue gases and are recovered by electrostatic precipitators, while bottom ash is the heavy residual fraction that remains at the bottom of the boiler. Brazilian power plants produce more than 3 Mt of combustion ash every year, from which 65-85% is fly ash and 15-35% is bottom ash. Fly ashes are used in concrete products (Yılmaz and Olgun, 2008). However, in many countries such as United States of America, the total production exceeds its potential applications (Manz, 1997). Many investigations are focused on the search for possible applications of fly ash such as agricultural amendments (Hammermeister et al., 1998), zeolite synthesis (Penilla et al., 2006), and treatment of sulfide-mining wastes (Pérez-López et al., 2007a). Bottom ashes are often of little use and are disposed in storage areas.

In the burning process, many hazardous elements present in the coal in a volatile form may vaporize. A portion of elements in the boiler enter into

29

bottom ash, and the rest of the inorganic materials are entrained in the flux of combustion gases, in fly ash or vapor. Coal ash is composed of amorphous inorganic components, minerals such as silicates, oxides and hydroxides mainly of iron, sulfates, carbonates, phosphates and sulfides, and organic constituent or unburnt coal (char) (Vassilev and Vassileva, 1996a,b). It is crucial to perform a complete chemical and mineralogical characterization of ashes in order to establish the contamination risk potential of power plants over their surrounding environment and human health, as well as their possible industrial usage. In residues with hazardous elements associated with different solid fractions such as combustion ashes, the total amount of pollutants is not a good measure of their risk potential for the environment and human health. Mobility and toxicity of the impurities depend on the chemical form in which they are linked in the solid phase, i.e. on the chemical speciation in solids.

The methods commonly used for characterization of coal and ashes are in detail described elsewhere (Vassilev and Tascón, 2003; Vassilev and Vassileva, 2005). Composition of bulk samples and individual fractions separated by ashing, physical, or chemical treatments, always controlled by mineralogical observations, has a great importance to determine the speciation of hazardous elements in solid phases. However, this methodology may turn out analytically very complex since it requires the intervention of a large number of techniques. Recently, the three-step sequential extraction method, proposed by the European Community Bureau of Reference (BCR) (Ure et al., 1993) and improved in subsequent studies (Rauret et al., 1999; Sahuquillo et al., 1999), has become very popular because it has good interlaboratory reproducibility and it is suitable for analysis of a large variety of matrices, including coal ashes (e.g. Petit and Rucandio, 1999; Smeda and Zyrnicki, 2002). The standardized-BCR sequential extraction meets the minimum number of steps to determine the mobility of metals in the main environmental conditions (weak acid leaching, reducing conditions and oxidation), which greatly simplifies the studies of speciation.

There are some evaluation studies about environmental impact performed on coals and their combustion products in power plants around the world (e.g. Hower et al., 2005; Goodarzi, 2006; Valentim et al., 2009), Brazil included (e.g. Levandowski and Kalkreuth, 2008; Silva et al., 2009a,b, 2010a).

30

In Brazil, these investigations are focused on the mineralogy, total metal content and, at best, in the mobility of the metal water-soluble fraction. However, there are no studies about speciation of metals in other fractions that may be potentially mobile depending on the weathering conditions and may be determined only by sequential extraction. This report is focused on the characterization of coal and its combustion ashes obtained at the main power plant of Latin America: Santa Catarina (Brazil). The objectives are to: (1) study the mineralogy and total content of potentially toxic elements, (2) evaluate the mobility degree of these elements in different weathering conditions by the BCR sequential extraction, and (3) combine the data from sequential extraction with the annual volume produced of each ash type in order to establish the risk potential of environmental contamination from the residues obtained at the power plant, according to the methodology proposed by Pérez-López et al. (2008).

2.2. MATERIALS AND METHODS

2.2.1. Study area

The economy in the state of Santa Catarina (southern Brazil) within the last century is associated with coal mining. Its 'Jorge Lacerda' (TRACTEBEL company) power plant has the largest capacity in South America (Fig. 2.1). It generates 857 MW/h of electricity with a consumption of 200,000 t of coal/month. The plant produces 80,000 t/month of ashes, of which 80% is fly ash and 20% is bottom ash. This plant is one of the largest worldwide producers of ash (Silva et al., 2009b). Fly ashes when leaving the precipitators are taken by trucks to be recycled for cement manufacture; while bottom ashes are disposed of in open landfill sites close to the plant.

2.2.2. Sample collection

Three types of materials were studied: (1) feed coal after flotation, (2) fly ash, and (3) bottom ash. Fly ashes were collected from the electrostatic precipitators, while bottom ashes were collected when exiting the boiler. The sampling of coal, fly ash and bottom ash was carried out at two different burning periods: (a) combustion under normal operational conditions; and (b)

31

combustion aided by oil as part of the boiler start-up procedure. In order to maintain the representativeness of sampling, the materials were collected simultaneously in each combustion period within five days following ASTM D 2234-89 (1991).

Fig. 2.1. Location of Santa Catarina power plant.

2.2.3. Analytical procedures

2.2.3.1. pH determination

The pH of the samples was determined using a Crison© combined glass electrode after the addition of 10 ml of deionized water to 1 g of sample in a centrifuge tube and the agitation of the suspension for 1h.

2.2.3.2. Mineralogical characterization

The mineralogical characterization was performed using X-ray diffraction (XRD) with a BRUKER diffractometer D8-Advance. This device uses KαCu radiation at 40 kV and 30 mA, with a scanning range of 3º to 65º and a rate of 0.3°-2θ/min. Morphology and composition of particles and minerals were investigated using a Field Emission Scanning Electron Microscope (FE-SEM;

32

Zeiss Model ULTRA plus) equipped with an energy dispersive X-ray spectrometer (EDS).

2.2.3.3. Bulk analysis

The bulk analysis of the samples was performed at Acme Analytical Laboratories LTD (Vancouver, Canada) by digestion with four acids ($HCl:HNO_3:HF:HClO_4$) in a microwave for 1h. The analysis was carried out by inductively coupled plasma-atomic emission spectroscopy (ICP-AES; Jarrel Ash Atomcomp 975) for major elements, and inductively coupled plasma-mass spectroscopy (ICP-MS; Perkin Elmer Elman 6000) for trace elements. The reproducibility of the results was demonstrated through the analysis of in-house reference materials.

2.2.3.4. Sequential extraction

The BCR sequential extraction divides the metal content of a solid into four solution fractions (Table 2.1). This method is not able to determine the chemical composition of each solid component separately; rather it just extracts sets of solid compounds to release mobile metals under specific environmental conditions. Fraction 1 (F1: easily soluble fraction) is composed of interchangeable metals, associated with carbonates and those soluble in water or under slight acidic conditions. This fraction contains the most mobile elements, thus being the most bioavailable and, consequently, the most potentially dangerous for the environment. Fractions 2 and 3 may also be a threat to the environment, depending on the redox conditions. Fraction 2 (F2: reducible fraction) is composed of metals bound to Fe and Mn oxyhydroxides that may be released if the environmental conditions change from oxic to anoxic. Fraction 3 (F3: oxidizable fraction) extracts the metals bound to organic matter and sulfides under oxidizing conditions. The sum of the first three fractions of the sequential extraction represents the total metal content associated with the mobile phase. Finally, the non-mobile fraction, or Fraction 4 (F4: residual fraction), consists of metals strongly bound to the structures of amorphous and crystalline phases that are only extracted by aqua regia digestion. Therefore, it is unlikely that the metals within Fraction 4 are

33

released, unless they are exposed to extreme weathering conditions (McGrath and Cunliffe, 1985).

Table 2.1. The BCR-sequential extraction procedure used for metal speciation.

Step	Fractions	Extractant (1 g of dry solid)	Shaking time and temperature
F1	Water/acid soluble and exchangeable	40 mL of 0.11 M CH_3COOH	16 h at room temperature (RT)
F2	Reducible	40 mL of 0.5 M $HONH_2HCl$ (pH 2)	16 h at RT
F3	Oxidizable	10 mL of 8.8 M H_2O_2 (pH 2) + 10 mL of 8.8 M H_2O_2 (pH 2), add 50 mL of 1 M $NH_4C_2H_3O_2$ (pH	1 h at RT and 1 h a 85º C, 1 h at 85º C and 16 h at RT
F4	Residual *	10 mL of aqua regia 3:1 (12 M HCl : 15.8 M HNO_3)	Heating on hot plate to dryness

*Digestion of the residual material is not step of the BCR protocol.

The solutions from the sequential extraction were analyzed, at the Research Services of the University of Huelva and the Institute 'Jaume Almera' in Barcelona, using ICP-AES (Jobin Yvon Ultima 2) for major elements and ICP-MS (Perkin Elmer Elan 6000) for trace elements. Emphasis was placed on the metals that are present in highest concentrations: Al, As, Cd, Cr, Cu, Fe, Mn, Pb, S, Th, U, and Zn, some of which have high environmental concern. Henceforth, the term metal includes metals, metalloids (i.e. As) and non-metals (i.e. S). In order to validate the results, a pseudo-total digestion with aqua regia of the original samples was performed following a procedure similar to the step 4 of the sequential extraction. The control of the results is performed by comparing the sum of the four steps of the sequential extraction with the results obtained from the pseudo-total digestion with aqua regia by calculating the recovery percentage (Ec. 2.1):

$$\text{Recovery} = \frac{\text{Step 1+step 2+step 3+step 4}}{\text{Pseudo}-\text{total digestion}} \text{x100} \qquad (2.1)$$

The mean recovery percentages of the coal samples and the combustion ashes were 129 ± 26%, 135 ± 20%, 82 ± 28%, 137 ± 36%, 112 ± 7%, 114 ± 14%, 102 ± 4%, 118 ± 16%, 102 ± 13%, 104 ± 13%, 102 ± 11%, and 85 ± 18% for Al, As, Cd, Cr, Cu, Fe, Mn, Pb, S, Th, U, and Zn. These good

34

recovery values show the high reproducibility of the data obtained in this study. The high standard deviation and recovery values for some of the elements (e.g. As and Cr) are a consequence of the very low concentrations analyzed for some samples, and therefore, the high variability must not affect the results considerably.

2.3. RESULTS

2.3.1. Mineralogical characterization

The high mineral matter of coal samples and the relatively low-sulfur content confirm previously published data (Silva et al., 2009a, 2010a). As determined by XRD and FE-SEM/EDS, the mineral matter in the coals is dominated by kaolinite, quartz, and illite, with minor proportions of feldspars, calcite, anatase, rutile, and sulfides. In contrast, ashes have high amorphous minerals and mullite contents. In the case of fly ash and bottom ash collected during oil co-firing, they also contain significant proportions of char. All ash samples also contain quartz and trace amounts of sulfides, mainly pyrite but also other such as pyrrhotite and marcasite, as revealed by FE-SEM/EDS (Fig. 2.2).

2.3.2. Geochemical characterization

Table 2.2 summarizes the pH values and the total composition of the coal, fly ash, and bottom ash samples. There are no significant differences in the chemical composition of major and trace elements between the coal sampled during combustion under normal operational conditions and that sampled during combustion with oil at the boiler start-up. The major element concentrations in the combustion ashes are, in general, similar, and all of them are classified as sialic ashes according to the recent classification proposed by Vassilev and Vassileva (2007). The pH of the coal samples is 6.2, which indicates that the capacity of acidity production of pyrite is neutralized by calcite. The pH of fly and bottom ashes produced during normal operations is 11.7 and 10.0, respectively; while the pH of fly and bottom ashes from the boilers co-fired with oil is 4.0 and 9.8, respectively.
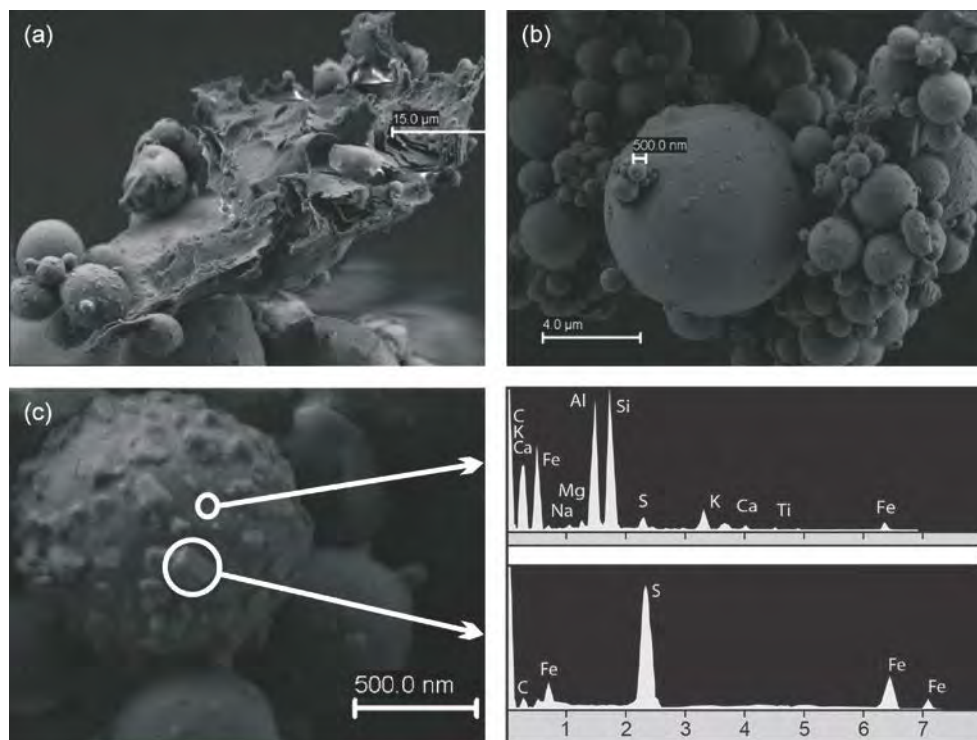
Fig. 2.2. FE-SEM illustrations of (a and b) fly ash and (c) pyrite grains on ultra-fine sphere in bottom ash. EDS analysis for pyrite were endorsed by micro-XRD (selected area electron diffraction and/or microbeam diffraction) detectors coupled to a high-resolution transmission electron microscope. Similar results were reported in recent studies (Silva et al., 2011).

In short-term dissolution processes, the acid-base properties of coal ashes are usually determined by the ratio between the acidic and alkaline components in the soluble fraction. Fly and bottom ashes usually show an alkaline character due mainly to high contents of CaO and MgO. However, sometimes fly ash leachates can be acidic. This is due to the sorption of SO_2 from the gas stream onto particle surfaces in the cleansing system (e.g. Spears and Lee, 2004; Ward et al., 2009). The sulfate condensed on the particles forms sulfuric acid in contact with water and lowers the pH of the fly ash-water interaction. Acid-generating phosphates adsorbed over fly ash particles and pyrite could also contribute as source of acidity (Yan et al., 2007). Fly and bottom ashes coming from normal operational conditions of combustion in Santa Catarina power plant show an alkaline character. In contrast, the coal burned together with oil produces fly ashes of acidic character. This is because the start-up of the boilers

generates a greater amount of gaseous sulfur which is entrained by the flux of gases and subsequently absorbed over the fly ash particles (Navarrette et al., 2004). In fact, both fly ashes have similar contents of Ca and Mg; however, the concentration of S in the acidic fly ashes that were co-fired is 0.5 wt% while it is below the detection limit for alkaline fly ashes (Table 2.2). Albeit, the bottom ashes co-fired with oil, by contrast, do not show an acidic character as a consequence of a higher alkaline earth to sulfate ratio relative to their corresponding fly ashes.

Table 2.2. Compilation of pH and bulk analysis in feed coal, fly ash and bottom ash.

Sample	Without oil[a]			With oil [b]		
	Coal	Fly ash	Bottom ash	Coal	Fly ash	Bottom ash
pH	6.2	11.7	10.0	6.2	4.0	9.8
Major elements (%)						
SiO_2	n.m.	58 [c]	57 [c]	n.m.	51 [c]	49 [c]
Al_2O_3	10	24	22	10	34	19
Fe_2O_3	1.8	5.4	5.7	2.1	4.5	4.6
MgO	0.30	0.70	0.68	0.27	0.91	0.56
CaO	0.52	1.7	1.3	0.48	2.0	0.98
Na_2O	0.28	0.56	0.64	0.22	0.59	0.53
K_2O	1.2	2.5	2.3	1.2	3.1	2.0
TiO_2	0.42	1.1	0.94	0.44	1.3	0.8
P_2O_5	0.03	0.07	0.05	0.03	0.22	0.05
MnO	0.02	0.04	0.04	0.01	0.05	0.03
LOI	n.m.	5.5	6.6	n.m.	10	20
SO_3	4.5	l.d.	l.d.	5.6	1.7	0.7
Trace element concentrations (mg kg^{-1})						
As	4.0	21	1.0	7.0	134	3.0
Cd	0.30	0.80	0.40	0.40	3.8	0.20
Cr	60	112	110	62	179	100
Cu	18	40	35	19	57	32
Pb	20	49	7.8	25	177	11
Th	13	38	34	14	60	27
U	6.4	16	15	5.7	27	12
Zn	77	180	39	109	796	58

l.d.: Below detection limit; n.m.: not measured.
[a] Sampled during combustion under normal operational conditions.
[b] Sampled during combustion aided by oil for the start-up of the boilers.
[c] Data taken from Silva et al. (2010a).

Coal is the main source of trace elements that enter the combustion boilers. The oil used for the start-up of the boilers does not represent a

significant additional source of trace elements (Silva et al., 2010a). During combustion, these elements are partitioned among the fly and bottom ashes and emission gases. The metals studied have a moderate volatility during combustion and tend to escape with the flux of gases in a gaseous phase or bound to aerosol particles (Clarke, 1993). The pollution-control system before the release to the atmosphere enables the condensation of these relatively volatile metals over the surface of the fly ash particles. This explains why the fly ashes show much higher concentrations of these metals than their corresponding bottom ashes (Table 2.2).

The type of combustion also produces differences in the loss-on-ignition (LOI) and in the metal content of the coal ashes (Table 2.2). Fly and bottom ashes from oil co-firing show a LOI higher than those obtained from normal combustion due to a higher proportion of char, as stated in the mineralogical characterization. In fact, incomplete combustion often occurs during the start-up of the boilers (Navarrete et al., 2004). Moreover, the greatest amount of sulfur generated in the flux of gases during the start-up favors a greater entrainment of metals in the form of aerosols than under normal operational conditions. The condensation of those initial gases in the cleansing systems produces fly ashes with greater amount of sulfur and metals absorbed on the particles, as shown in Table 2.2. However, the differences in the composition of both bottom ashes are not so significant.

2.3.3. Sequential extraction data

Extracted contents of sulfur and hazardous elements in coal and the combustion ashes in each step of the sequential extraction are shown in Table 2.3. The percentage values extracted from each element with respect to the sum of the 4 fractions are shown in Figure 2.3 for coal, fly ashes and bottom ashes.

The distribution of metals was similar in both coal samples (Fig. 2.3a,b). Coal has a high percentage of metals associated with the mobile fraction (F1+F2+F3). The concentrations of metals in terms of their relative abundance in the mobile fraction occurred in the following order: Cd (100%) > Mn (95%) > S (93%) > Fe (92%) > As (81%) > Zn (80%) > Cu (76%) > Pb (69%). As expected, most of the S and metals are associated with the oxidizable fraction (bound to organic matter and sulfides, F3): Cd > S > Fe > Cu > Zn >

As > Pb. Coal also shows high contents of Mn associated with the most bioavailable fraction (easily soluble, F1). Arsenic, Pb, and Cr are associated with the reducible fraction (bound to oxides, F2). Finally, the fraction that is least potentially toxic for the environment, i.e. the non-mobile fraction strongly bound to structures of amorphous and crystalline phases (residual, F4), is mainly composed of Th (98%), Al (80%), U (71%), and Cr (61%).

The relative content of mobile metals within the fly ash from normal combustion shows the following order of abundance (Fig. 2.3c): S (100%) > As (93%) > Mn (76%) > U (53%) > Cr (45%) > Cu (38%) > Zn (29%) > Al (27%) > Pb (23%). In this fraction the most significant characteristics are the high percentages of S, Mn, Cr, Zn, Al, and U within the easily soluble fraction; As, Fe, Pb, and U within the reducible fraction; and Pb, Cu, Al, Zn, and Cr within the oxidizable fraction. Almost all the Cd (100%), Th (100%), and Fe (96%), and high percentages of Pb (77%), Al (73%), Zn (71%), Cu (62%), Cr (55%), and U (47%) are within the residual fraction and, thus, not a threat to the environment. The fly ashes from the start-up of the boilers are similar with the exception that they show higher relative and absolute concentrations of sulfur and most metals within the easily soluble fraction (Table 2.3; Fig. 2.3d).

In the bottom ash from coal combustion without oil, the order of relative abundance within the mobile fraction is (Fig. 2.3e): As (84%) > S (81%) > Cu (62%) > Mn (60%) > Cr (42%) > Zn (40%) > U (37%) > Al (32%) > Pb (25%) > Fe (20%). The mobile fraction shows high percentages of Mn and Zn within the easily soluble fraction; As, Fe, and Pb within the reducible fraction; and Th, S, U, Cu, Cr, Al, Zn, Pb, and Fe associated with the oxidizable fraction. Among these fractions, the oxidizable fraction shows the greatest relative abundance. Finally, the non-mobile fraction consists mostly of: Th (98%), Fe (80%), Pb (75%), Al (68%), U (63%), Zn (60%), Cr (58%), Mn (40%), and Cu (38%). Cadmium was not detected in any fraction of the sequential extraction. The bottom ash produced during the start-up of the boilers show a distribution of metal mobility similar to that shown by the ash produced during normal combustion (Fig. 2.3f).

Table 2.3. Results obtained for BCR sequential extraction of feed coal, fly ash and bottom ash.

Sample	Step	Al	As	Cd	Cr	Cu	Fe	Mn	Pb	S	Th	U	Zn
		Toxic elemnts (mg kg^{-1})											
Coal	F1	35	0.29	l.d.	0.08	0.31	151	93	0.16	518	l.d.	l.d.	5.0
(without oil) [a]	F2	136	3.9	l.d.	1.3	0.53	439	13	3.6	104	l.d.	0.10	3.6
	F3	648	6.0	0.17	2.8	30	9717	13	9.4	11262	0.12	0.45	49
	F4	3309	2.1	l.d.	6.0	12	957	7.0	5.7	917	7.5	1.1	11
Fly ash	F1	913	2.2	l.d.	3.9	1.6	99	117	l.d.	794	l.d.	0.63	5.6
(without oil) [a]	F2	715	19	l.d.	2.3	1.6	675	39	0.74	71	l.d.	0.67	3.0
	F3	943	2.7	l.d.	3.2	2.2	263	19	1.0	48	l.d.	0.55	4.9
	F4	6910	1.9	0.09	12	9.0	22357	55	5.8	n.d.	5.7	1.7	34
Bottom ash	F1	719	0.10	l.d.	0.76	1.3	351	53	0.09	120	l.d.	l.d.	1.8
(without oil) [a]	F2	838	3.8	l.d.	1.4	1.9	2036	19	0.31	56	l.d.	0.17	1.4
	F3	1447	0.32	l.d.	2.8	6.1	1248	15	0.25	798	0.10	0.58	2.3
	F4	6387	0.81	l.d.	6.9	5.8	14291	57	2.0	224	4.2	1.3	8.0
Coal	F1	20	0.22	l.d.	l.d.	0.76	236	79	0.17	639	l.d.	l.d.	5.8
(with oil) [b]	F2	128	3.8	l.d.	0.84	0.72	439	11	4.4	92	l.d.	l.d.	3.1
	F3	599	7.3	0.21	2.1	14	12375	14	11	14521	0.19	0.30	67
	F4	2994	3.0	l.d.	4.9	4.1	1198	4.2	7.4	958	7.3	1.0	23
Fly ash	F1	2436	15	0.45	15	7.1	26	63	0.28	6229	l.d.	2.5	57
(with oil) [b]	F2	719	98	l.d.	3.9	2.7	1118	15	6.3	124	l.d.	2.8	6.6
	F3	1597	19	0.13	5.4	3.5	369	12	7.4	210	l.d.	3.0	22
	F4	9503	7.6	0.45	21	8.2	14294	67	27	n.d.	9.5	3.8	136
Bottom ash	F1	1000	0.13	l.d.	1.1	1.4	192	81	0.09	640	l.d.	l.d.	10
(with oil) [b]	F2	960	4.1	l.d.	1.6	1.7	2759	20	0.75	276	l.d.	0.17	2.5
	F3	2499	0.60	l.d.	3.4	11	2199	11	0.82	2049	l.d.	0.86	7.9
	F4	5318	1.9	l.d.	7.5	8.6	16913	31	0.91	264	5.8	1.2	10

l.d.: Below detection limit; n.d.: not detected.

[a] Sampled during combustion under normal operational conditions.

[b] Sampled during combustion aided by oil for the start-up of the boilers.

Note that the bulk chemical attack extracts an additional amount of metals that is not released by the four steps of the sequential extraction. The sequential extraction extracted with respect to the bulk analysis of coal approx. 7% of Al; 15% of Cr; 24% of U; 55% of Cd and Th; 72% of S; and almost all of Zn, Fe, Pb, Mn, Cu, and As. The average values extracted over the bulk for coal ashes are approx. 8% of Al; 15-25% of Th, Cr, Cd, Pb, and U; 35% of Zn; 45-55% of Cu, Fe, and Mn; and almost all of S and As. The remaining metals not extracted in the 4-step sequential procedure are immobile even in extreme environmental regimes (McGrath and Cunliffe, 1985).
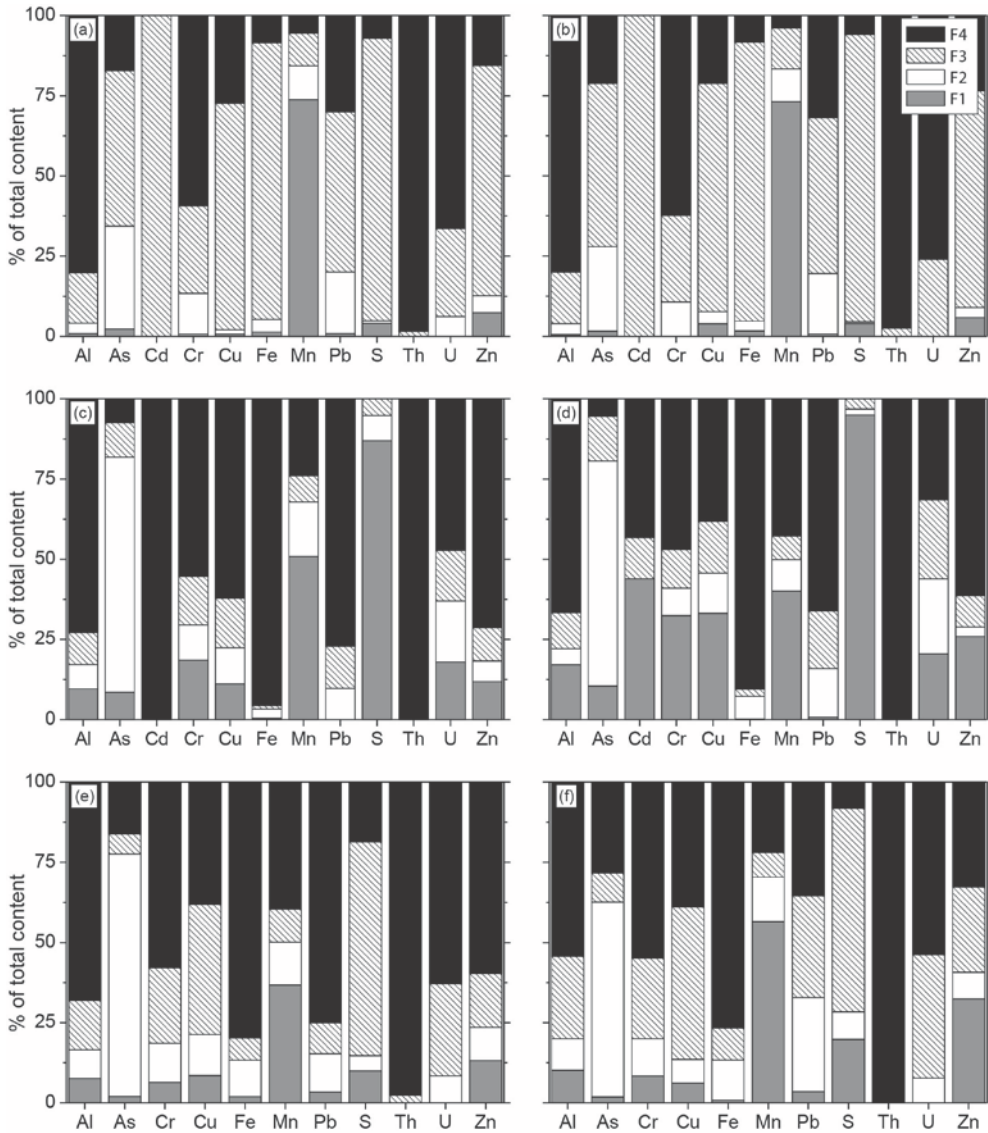
Fig. 2.3. Percentage of hazardous elements extracted in the sequential extraction for (a and b) feed coal, (c and d) fly ashes, and (e and f) bottom ashes. Sampling was performed during combustion (a, c and e) under normal operational conditions and (b, d and f) with oil at the boiler start-up.

Comparing the results, the combustion of coal causes the following changes in the mobility state of metals entering the boilers (Fig. 2.3): (1) most metals go from being within the mobile fraction in coal, mainly within the

41

oxidizable fraction, to being strongly associated with the structure of amorphous glass and minerals that make up the combustion ashes (non-mobile fraction); (2) within the mobile fraction, metals associated with the oxidizable fraction in the combustion ashes are present in lower relative proportion and correspond to sulfide traces and char; and (3) the coal ashes show higher relative concentration of sulfur and metals associated with the easily soluble fraction than raw coal. The easily soluble fraction in the combustion ashes is higher in fly ashes than in bottom ashes and represents the SO_2 and relatively volatile metals that are dragged along with the gases and condensed on the surface of the fine particles in the pollution-control systems. This process is especially significant during the start-up of the boilers producing fly ashes with more metals and sulfur absorbed which in contact with water gives the residue an acidic character. Char is more abundant in the bottom ashes. Bottom ashes have lower concentrations of sulfur than fly ashes and, in addition, much of it is associated with the fraction that is not soluble in water, which determines the non-acidic character of this residue even during the start-up of the boilers. All these observations corroborate the hypotheses discussed in the previous section.

2.4. DISCUSSION

2.4.1. Dynamics of contaminants from coal to combustion ashes

A calculation of mass balance or relative enrichment (RE) index was performed in order to determine the partition or transference of trace elements between coal and ashes during combustion following the equation (2.2). Such procedure allows also calculating the degree of volatilization of elements in the boiler (Meij, 1995).

$$RE\,(\%) = \frac{[M]_{FLY\ ASH} \times C_{FLY\ ASH} + [M]_{BOTTOM\ ASH} \times C_{BOTTOM\ ASH}}{[M]_{FEED\ COAL}} \times 100 \qquad (2.2)$$

where [M] is the total elemental concentration, and C is the amount of fly or bottom ashes generated by combustion of 1 g coal. Considering that 40% of burned coal becomes ash, and of this, around 80% is fly ash and the remaining 20% is bottom ash, $C_{FLY\ ASH}$ is 0.32 and $C_{BOTTOM\ ASH}$ is 0.08. The relative enrichments during normal combustion are close to 100% (Table 2.4),

i.e. the volatile emission of the metals studied is very low, but all of them are partitioned within the ashes instead. Between 80-85% of Al, Cr, Cu, Fe, Mn, Th and U; 90% of Cd; and 95-100% of As, Pb, and Zn are transferred to fly ashes, and the rest to bottom ashes. These data indicate that volatilization of elements occurs but most of them are captured by condensation on fly ash particles. During the start-up of the boilers, the combustion temperature is lower and, therefore, significantly high recovery percentages are also expected. However, the mass balance only approaches 100% considering an incomplete combustion that produces a smaller amount of ash and leaves a greater proportion of char, which is consistent with the mineralogy and LOI of the ashes generated under these conditions.

Table 2.4. Relative enrichment (RE) index of total, mobile and easily soluble elements from feed coal to combustion ashes.

	Toxic elements										
	Al	As	Cd	Cr	Cu	Fe	Mn	Pb	Th	U	Zn
Total-RE [a] (%)	93	70	96	74	87	120	110	80	111	99	79
Mobile-RE [b] (%)	130	78	0	82	8	6	53	5	7	119	8
Easily soluble-RE [c] (%)	997	248	-	1662	200	40	45	5	-	∞ [d]	39

$RE = \frac{[M]_{FLY\,ASH} \times C_{FLY\,ASH} + [M]_{BOTTOM\,ASH} \times C_{BOTTOM\,ASH}}{[M]_{FEED\,COAL}}$ x 100. [M]= metal content in (a) total, (b) mobile (F1 + F2 + F3) and (c) easily-soluble (F1) fractions. (d) Infinite (∞) refers to mobile content in coal = 0 (or not detected) and in combustion ashes ≠ 0.

The actual contaminating capacity of a substance does not depend on the total metal content, but on the fraction that may potentially affect the environment, i.e. mobile metals. As stated above, although coal burning reduces the relative mobility of most toxic metals (F1+F2+F3) that enter the boiler, it increases the relative proportion attributed exclusively to the easily soluble fraction and, therefore, most dangerous for the environment (F1). Hence, it is important to check what may happen with the absolute concentrations by repeating the calculation of the mass balance, using both metallic fractions separately. Considering the mobile fraction under all weathering conditions, i.e. leaching in water or slightly acidic conditions (F1), reducing conditions (F2) and exposure to oxidation (F3), metals during coal

43

combustion remain mobile within the ashes with relative enrichment indices of 5-10% for Pb, Fe, Th, Cu, and Zn, and 50-85% for Mn, As, and Cr. All the Cd is now associated with the non-mobile fraction of the residue; although, approximately 100% of the Al and U keep the same mobility within both materials (Table 2.4). The combined concentration of all mobile metals within coal is approximately six times greater than in the combustion ashes. Therefore, from an environmental point of view, these findings indicate that coal could become a more hazardous material when exposed than the combustion ashes due to higher concentrations of impurities located within the mobile fraction.

Considering the most mobile fraction leachable in water or slightly acidic conditions (F1), Pb, Zn, Fe, and Mn are also present in higher concentrations in coal than in ashes (relative enrichment index < 100%); while there is no Cd nor Th within the easily soluble fraction neither in coal nor in ashes. However, Cu, As, Al, Cr, and U are present in much higher absolute concentrations in the combustion ashes than in coal (relative enrichment index > 100%; Table 2.4). In fact, the easily soluble content of U is below the detection limit within coal, while high concentrations of this element are associated with the easily soluble fraction in fly ashes. Concretely, hydrated uranium phosphates soluble in slightly acidic conditions such as ningyoite may often occur in the fly ashes (Vassilev and Vassileva, 1996a,b). The total concentration of the sum of all easily soluble metals within the combustion ashes is approximately as twice as that in coal. Therefore, the sub-products of the power plant represent a greater threat for the environment under rain water leaching conditions than the coal from which they were produced.

2.4.2. Dynamics of contaminants from combustion ashes to the environment

The mass balance described in the previous section allows evaluation of the potential risk of the combustion ashes according to relative comparisons with respect to coal. Moreover, this risk derives from the use of a laboratory extraction that uses a small aliquot of sample. However, residues normally appear in large volumes exposed to weathering conditions, perhaps generating a significant impact on the environment. Pérez-López et al. (2008) described a method applicable to the techniques of sequential extraction to extrapolate the

44

theoretical risk potential obtained at the laboratory for a residue at a regional scale. This simple procedure gives an idea of the polluting capacity of a residue over its surrounding environment by the combination of two factors: (1) the absolute amount of mobile pollutants obtained at the laboratory (i.e. Table 2.3) and (2) the annual total mass produced of each residue (i.e. Table 2.5). The weighting of both factors would allow estimation of the total amount of mobile pollutants that would be released every year under different environmental conditions - exposure of residues to water, reducing conditions and oxidizing conditions. In this way, we can evaluate the risk potential caused by the production of ashes from coal combustion at the Santa Catarina power plant.

Table 2.5. Total amount of trace elements contained in the easily-soluble, reducible (bound to oxides) and oxidizable (bound to organic mater and sulfide) fractions of the fly and bottom ashes produced annually in Santa Catarina power plant.

FRACTION		TOXIC ELEMENTS (tons)										
		Al	As	Cd	Cr	Cu	Fe	Mn	Pb	Th	U	Zn
Water-soluble fraction of burning 2.4 million tons of coal a year:												
Fly ash	768000 tons	701	1.7	0	3.0	1.2	76	90	0.0	0	0.49	4.3
Bottom ash	192000 tons	138	0.02	0	0.15	0.25	67	10	0.02	0	0	0.34
Reducible fraction of burning 2.4 million tons of coal a year:												
Fly ash	768000 tons	549	14	0	1.7	1.3	518	30	0.56	0	0.52	2.3
Bottom ash	192000 tons	161	0.73	0	0.28	0.37	391	3.7	0.06	0	0.03	0.26
Oxidizable fraction of burning 2.4 million tons of coal a year:												
Fly ash	768000 tons	724	2.1	0	2.4	1.7	202	15	0.77	0	0.43	3.8
Bottom ash	192000 tons	278	0.06	0	0.53	1.2	240	2.9	0.05	0.02	0.11	0.43
Mobile total impact	960000 tons	2551	19	0	8.1	6.0	1495	152	1.5	0.02	1.6	11

The amount of coal burned at the power plant is approximately 2.4 Mt/year. Approximately 768,000 t of fly ash and 192,000 t of bottom ash are generated every year. The total mobile pollutants (F1+F2+F3) that exit the boilers every year associated with the sum of both combustion ashes were

45

calculated to be as follows: 2551 tons of Al, 1495 tons of Fe, 152 tons of Mn, 19 tons of As, 11 tons of Zn, 8.1 tons of Cr, 6.0 tons of Cu, 1.6 tons of U, 1.5 tons of Pb, and 20 kg of Th (Table 2.5). Between 55% and 95% of each of these amounts of metals are associated with fly ashes, except for Th (100%) which is found in a greater proportion within the bottom ashes. Only from pollutants that are leachable in water or slightly acidic conditions there is an annual production of 839 tons of Al, 144 tons of Fe, 100 tons of Mn, 4.6 tons of Zn, 3.1 tons of Cr, 1.7 tons of As, 1.5 tons of Cu, 490 kg of U, and 20 kg of Pb (Table 2.5). These calculations were performed assuming that all the ashes come from a conventional combustion. By sequestering easily soluble contaminants, precipitation of secondary solid phases can slightly reduce the environmental risk. However, the secondary minerals act only as a temporary sink since metals are commonly retained in some of the mobile fractions of the residue and they can be again released when changing the environmental conditions. These results provide an idea of the extreme potential of contamination by metals that the power plant has.

This type of information must be considered as part of the management assessment of the environmental risk potential carried out by the company of the Santa Catarina thermoelectric plant. Checking the toxic impurities and their effects on the environment at the ponds where the combustion ashes are stored is crucial since these residues are freely exposed to weathering conditions. The runoff from the ash ponds may represent a high potential risk for the ecological receptors, especially in the case of bottom ashes as they are not recycled and are permanently stored near the plant. The fly ashes are directly sold for cement production. However, about 2% of fly ashes are not captured by electrostatic precipitators. The fine fly particles, mainly in the range of nano-particles (Silva et al., 2010b), which are released during atmospheric emissions, and transport and usage of this by-product, may represent a high risk to environment and public health. Some studies demonstrated that the damage in lungs and heart due to inhalation of particles is directly related to their metal content (Gurgueira et al., 2002). Therefore, special attention must be paid when using fly ashes as a construction material in Brazil due to the high concentrations of potentially toxic metals such as Cr, As, and U. Since the world production of fly ashes (currently 600 Mt/year) is

increasing exponentially in time, we recommend evaluating the environmental and human health risk potential associated with any thermoelectric plant of the world and especially where these residues are recycled and/or stored on site.

2.5. CONCLUSIONS

The present study has illustrated the impact potential for the environment and for the human health by hazardous elements, derived from the storage, transport, and usage of the combustion by-products as construction materials, at the Santa Catarina power plant (Brazil). Based only on total analysis, approx. 100% of the trace elements studied in coal are transferred to ashes during combustion, and hence, the volatile emission is very low in the power plant. Although volatilization of elements occurs, most of them condense on fly ash particles. However, since combustion of coal alters the mobility of trace elements, potential risks to the environment must be considered based on the extractable metal content. In fact, coal ashes show higher concentrations of most elements than raw coal in the metal fraction that is easily soluble in water or slightly acidic conditions, i.e. the potentially most toxic pollutants for the environment.

The methodology proposed for assessing the environmental risk is based on the weighting of the data from the sequential extractions with annual amount produced. Considering the mobile metal fraction within the combustion ashes, the total pollutant amounts that exit the boilers of the plant every year and that may potentially affect the surrounding environment are approximately 2551 tons of Al, 1495 tons of Fe, 152 tons of Mn, 19 tons of As, 11 tons of Zn, 8.1 tons of Cr, 6.0 tons of Cu, 1.6 tons of U, 1.5 tons of Pb and 20 kg of Th. The easily soluble fraction contains around 65% of Mn; 30-40% of Zn, Cr, Al and U; 25% of Cu; 10% of Fe and As; and 1% of Pb. From these results, implementing controls over the different toxic impurities present within these residues before they are sold as construction material is recommended. This is applicable to Brazil where all combustion ashes produced (mainly fly ashes) are recycled, although it is extensible to any power plant around the world.

47

CAPÍTULO 3. THE ROLE OF MINERALOGY ON ELEMENT MOBILITY IN TWO SULFIDE MINE TAILINGS FROM THE IBERIAN PYRITE BELT (SW SPAIN)

Abstract

A detailed study of two adjacent mine tailings impoundments comparing mineralogical and geochemical analyses of the solids with geochemical analysis of the pore-water and -gas was carried out in the Monte Romero sulfide mining district (Iberian Pyrite Belt, SW Spain). Since 1978, both facilities have been exposed to weathering in a semi-arid climate with dry-warm and wet-rainy seasons. In these impoundments, sulfide oxidation releases sulfate and contaminants to the pore-water that are transported and concentrated by evaporation in the top surface of the tailings, causing precipitation of soluble iron sulfate salts in dry seasons. These salts act as temporary sinks for minor elements such as Cd, Co, Zn, Ni, Cu and Mn, which are again released during rainfall events in wet seasons. Stored flotation tailings have an average pyrite content of 30 wt% although average amounts up to 80% are present in the upper 50 cm of one of the impoundments. According to the results of the current study, this difference is key to control the oxidation model in both tailings. In the impoundment containing 30 wt% of pyrite, pore-water pH increases in wet periods to 3.1 average by rainwater dilution, causing supersaturation and precipitation of secondary Fe^{3+} phases such as jarosite, goethite and schwertmannite. Consequently, this impoundment shows a 20-25 cm thick yellowish oxidation layer in the top part. In contrast, in the impoundment containing 80 wt% of pyrite in the top part extremely acidic pore-waters (pH < 0.5) are present in both dry and wet seasons, and no precipitation of secondary Fe^{3+} phases occurs in the oxidation zone. The absence of secondary precipitates explains the apparent unweathered aspect of these tailings, in spite of its much higher remobilization of contaminants to the surface runoff or groundwaters.

3.1. INTRODUCTION

Mine tailings are typically composed of fine-sand to silt-size particles of quartz, aluminosilicates, carbonates, oxides and sulfides that are separated from the ore and deposited in impoundments. When the fine-grained sulfides, mainly pyrite or pyrrhotite, present in these tailings are exposed to atmospheric oxygen, their oxidation produces acidic water with large contents of sulfate, iron and other metal(loid)s. In absence of preventive or remediation strategies, the result may be the discharge of highly acidic and concentrated waters, known as acid mine drainage (AMD), from the impoundment into adjacent bodies of surface water and/or to nearby aquifers.

To minimize waste weathering, mine tailings are usually kept saturated with or covered by water during mining operations (Holmström and Ohlander, 1999). However, this water layer may disappear in the long run, allowing the access of dissolved oxygen to the sulfide minerals. Then, an oxidation zone of variable thickness may form immediately below the tailings surface. The development of this oxidation zone is limited by the diffusion of oxygen from the tailings surface, which may be enhanced by the presence of coarse pores and subsequent low water saturation (Reardon and Moddle, 1985). The oxidation zone is usually easily distinguishable by yellow-reddish Fe^{3+} oxyhydroxysulfates either dispersed or forming more or less continuous hardpans. Some examples of such oxidation zones are described in detail in Waite Amulet (Quebec, Canada; Blowes and Jambor, 1990; Blowes et al., 1991), Laver (Sweden; Ljungberg and Öhlander, 2001), Lynn Lake (Manitoba, Canada; Gunsinger et al., 2006) and Haveri (Finland; Parviainen, 2009), among many others.

In some cases with high proportion of sulfides, such as Heath Steele (New Brunswick, Canada) or Sherridon (Manitoba, Canada), the downward flow from the vadose zone is Fe^{2+}-rich and leads to the deeper precipitation of another cementation zone mainly made up of Fe^{2+}-sulfates (Blowes and Jambor, 1990; Moncur et al., 2005). Both types of cementation layers (formed by Fe^{3+} or Fe^{2+} minerals) are thought to lessen the transport of oxygen and act

as a zone of element accumulation and, therefore, may moderate the environmental impact of tailings weathering. The addition of carbonates in the tailing material is thought to buffer the acidity and promote the development of hardpans (Blowes et al., 1991).

In addition to Fe-sulfides and oxygen, another key parameter for the generation of AMD and for the precipitation of secondary minerals is the climate. Under humid climate conditions, such as in the examples previously referred to, sulfide oxidation and neutralization reactions may release elements that can be transported downwards to deeper aquifers or surface waters. In contrast, in arid climates, an upward migration to more oxidizing conditions via capillary forces may develop. As pointed out by earlier studies (Dold and Fontboté, 2001; Acero et al., 2009), the upward element transport in strongly acidic oxidation zones under arid conditions may lead to the formation of water-soluble sulfate minerals at the surface of tailings. In the case of carbonate-rich tailings, the acidity produced by sulfide oxidation may be neutralized, which enhances sorption processes able to strongly limit the mobility of the divalent cations (Dold and Fontboté, 2002).

In contrast to the large amount of earlier works on the processes associated with sulfide oxidation and with the subsequent precipitation of secondary phases under humid climatic conditions, the studies focused on the singularities of these processes under arid or semiarid conditions are much scarcer. Therefore, there is a lack of key information for the selection, design and implementation of remedial or preventive actions oriented to restore the mined surroundings and minimize the AMD generation in this type of systems.

To bridge this gap, the present study will focus on the identification of the parameters controlling the weathering of tailings and the development of oxidation fronts under field conditions in the Iberian Pyrite Belt (IPB, SW Spain). The IPB has a semi-arid climate, with a humid-rainy season in winter and a dry-warm season in summer. This alternating humidity, the high to moderate temperatures and the complete absence of carbonates in the region trigger an active weathering of pyrite and important AMD production. With the purpose of obtaining invaluable information about the sulfide weathering

processes under these conditions, two adjacent tailings impoundments 35 to 40 years old at Monte Romero mining district have been selected for a detailed characterization of their mineralogy, pore-water hydrochemistry and pore-gas composition at different depths. The two tailings show that different starting pyrite concentration may result in significant differences in weathering patterns, being the 'apparently' less weathered the more active in mobilization of contaminants. Hence, both impoundments can be considered representative from two different evolutions in one of the largest mining provinces with semiarid climate in the world.

3.2. MATERIALS AND METHODS

3.2.1. Study area

The Monte Romero mining district (IPB) exploited and processed by flotation, mainly between 1970 and 1978, different complex massive sulfide ores to obtain copper, zinc and lead concentrates. In the earlier operation stages, the processing plant treated ore from the Monte Romero Mine by a differential flotation process. Later on, the plant changed to a global flotation process, besides processing ore from other mine at the IPB (San Telmo Mine). The pyrite-rich waste from the flotation process was stored in the two aforementioned tailings impoundments (Fig. 3.1). Despite their similar origin and proximity, the appearance of both impoundments is fairly different: one of them (yellowish impoundment, YI, from now on) shows a 20 cm thick yellowish top layer, whereas the other (grayish impoundment, GI, from now on) is uniformly grayish at different depths and does not present any apparent oxidation layer. At present, both ponds are abandoned and constitute a potential source of AMD production.

3.2.2. Sampling and analysis

3.2.2.1. Tailings

Solid samples from the tailings were collected in two field campaigns; one during the dry season (September 2009) and the other during the rainy season (March 2010). Core samples from the shallowest tailings portions were taken by means of 60 cm-long polyethylene tubes. Deeper tailings samples

were collected at different depths from bore-holes carried out using a soil auger. Air-dried tailings samples were prepared for mineralogical and geochemical studies. Mineralogical characterization was performed using X-Ray Diffraction (XRD) with a BRUKER diffractometer D8-Advance with Cu Kα radiation. Diffractometer settings were 40 kV, 30 mA, a scan range of 3-65º 2θ and a rate of 0.3 º 2θ/min. Analysis of diffraction patterns was performed with the XPowder software (Martín-Ramos, 2004). Furthermore, semi-quantitative chemical analyses and imaging of certain areas were obtained by the use of a JEOL JSM 5410 Scanning Electron Microscope with an Energy Dispersive System (SEM-EDS; JEOL JSM-5410).
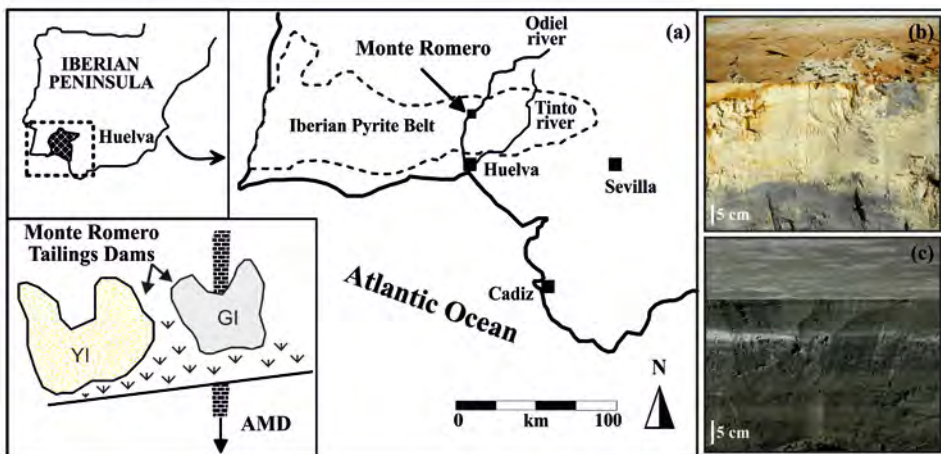
Fig. 3.1. (a) Map of the Monte Romero mine area (IPB, SW Iberian Peninsula) and plan view of the two mine tailings impoundments. Field pictures of the (b) YI and (c) GI.

For geochemical characterization, acid digestions with aqua regia and sequential extractions were applied to the tailings samples. Aqua regia digestion was performed to assess the pseudo-total element contents, which is considered as a measure of the maximum potential hazard that could occur in long term or in extreme environmental regimes (McGrath and Cunliffe, 1985), whereas sequential extractions provide information about the mobility of different elements and their relative mineralogical or organic components in the tailings. Sequential extraction was performed using the three-step Community Bureau of Reference (BCR) procedure outlined by Rauret et al. (1999), and adding the

56

aqua regia extraction as a fourth step. Following the BCR-procedure (Table 3.1), elements are speciated into four fractions; easily-soluble fraction (F1; exchangeable and associated with phases soluble in water or under slight acidic conditions), reducible fraction (F2; bound to Fe-Mn oxyhydroxides), oxidizable fraction (F3; bound to sulfides and organic matter), and residual fraction (F4; non-mobile elements strongly bound to crystalline structures). Quality control of the extraction procedures was performed by calculating the recovery as the sum of the four BCR fractions divided by the amount of pseudo-total elements released by aqua regia digestion, expressed as percentage.

Table 3.1. BCR-sequential extraction procedure used for speciation.

Step	Fractions	Extractant (1 g of dry solid)	Shaking time and temperature
F1	Water/acid soluble and exchangeable	40 mL of 0.11 M CH_3COOH	16 h at room temperature (RT)
F2	Reducible	40 mL of 0.5 M $HONH_2HCl$ (pH 2)	16 h at RT
F3	Oxidizable	10 mL of 8.8 M H_2O_2 (pH 2) + 10 mL of 8.8 M H_2O_2 (pH 2), add 50 mL of 1 M $NH_4C_2H_3O_2$ (pH	1 h at RT and 1 h a 85º C, 1 h at 85º C and 16 h at RT
F4	Residual *	10 mL of aqua regia 3:1 (12 M HCl : 15.8 M HNO_3)	Heating on hot plate to dryness

*Digestion of the residual material is not step of the BCR protocol.

3.2.2.2. Pore-gas

Oxygen concentrations in pore-gas were in-situ analyzed during rainy and dry seasons (March and July 2010, respectively) in vertical profiles of increasing depth up to water saturation at 10 cm intervals using a portable gas-meter ANAGAS CD98 (Environmental Instruments, Leamington Spa, England) coupled to a steel-rod through a vacuum system. The sensitivity ranges from 0% to 30% ± 0.1% for O_2 concentration. The measurement device includes an integral pump for facilitating the gas circulation. The complete stoppage of the gas pump during the measurement is indicative of water-saturation and, hence, of the presence of the water table.

57

3.2.2.3. Pore-water

Pore-water solutions were also sampled during rainy and dry seasons (February 2006 and May 2010, respectively) along the depth profiles in the two tailings ponds. In-situ pore-water extraction and filtration were simultaneously conducted using suction cup lysimeters and hollow-fibre tube sampler devices (Rhizon samplers; Eijkelkamp Agrisearch Equipment, Netherlands). For superficial sampling, lysimeters were directly inserted into the tailings while, for deeper sampling, pore-water was extracted from the corresponding wet tailings samples collected with the soil auger. Both pH and potential redox were measured in the field using Crison instruments. Redox potential was corrected in order to obtain the Eh, with respect to the standard hydrogen electrode (Nordstrom and Wilde, 1998). Filtered pore-solutions were immediately divided into two aliquots in the field; one of them was acidified with HNO_3 for major and trace element analysis, and the other one was buffered to pH 4.5 with an ammonium acetate/acetic acid buffer and Fe^{2+} complexed with a phenantroline solution for Fe^{2+}/Fe^{3+} determination according to the method outlined by Rodier et al. (1996). Moreover, two additional pore-water sampling campaigns were also performed with more detail in the upper part of the YI during the dry season (May and June 2005). Due to the low-moisture content of the tailings during both samplings, ex-situ pore-water extraction was carried out by the high-pressure squeezing technique (Patterson et al., 1978) as adapted by Fernández et al. (2004). Aliquots of pore-water were taken for analysis of pH, redox potential, Fe^{2+}/Fe^{3+} species and general hydrochemical analyses.

3.2.2.4. Aqueous chemistry

Extractants of the geochemical studies and pore-water solutions were analyzed using Inductively Coupled Plasma-Atomic Emission Spectroscopy (ICP-AES; Thermo Jarrell Ash) for determination of major elements (Al, Ba, Ca, Fe, K, Mg, Na, P, S and Si) and Inductively Coupled Plasma-Mass Spectroscopy (ICP-MS; Thermo X-Series II) for trace elements (As, Cd, Co, Cr, Cu, Mn, Ni, Pb, Sb, Sr, Ti, V, Zn). Detection limits were: 0.2 mg/L for S; 0.1 mg/L for Na; 0.05 mg/L for Fe, K, Mg and Si; 0.02 mg/L for Al, Ca and P; 0.005 mg/L for Ba; and 1 µg/L for the trace elements. In the analyses of ICP-

AES and ICP-MS, calibration with sets of standards was performed when the regression coefficient exceeded 0.999. Three laboratory standards, prepared with metal concentrations within the range of the samples, were analyzed with every 10 samples to check for accuracy. Furthermore, dilutions from 1:2 to 1:100 were performed to ensure that the concentration of the samples was within the concentration range of the standards. Blank solutions with the same acid matrix of the samples were also analyzed. The average measurement error was less than 5%.

Determinations of Fe^{2+} and total Fe (following reduction with hydroxylamine hydrochloride) in the pore-water solutions were immediately undertaken in the laboratory by colorimetry at 510 nm using a Hach DR/890 colorimeter on the same day of the sampling. The detection limit was 0.3 mg/L and precision was better than 5%; Fe^{3+} was calculated as the difference between total Fe and Fe^{2+}.

3.3.3. Geochemical modeling

The geochemical code PHREEQC-2 (Parkhurst and Appelo, 2005) was used for the interpretation of the solubility constrains on pore-water hydrochemistry. Since most of the solutions showed high ionic strength, ranging from 0.1 to 15 M, Pitzer ion interaction parameters (Pitzer, 1973) with the database compiled by Tosca et al. (2005) were used in the calculations. This database was expanded to include, among others, interaction coefficients for copper and zinc (Reardon and Beckie, 1987; Reardon, 1988). Solubility products and reactions were taken from the WATEQ4F database (Ball and Nordstrom, 1991), except some solid phases detailed in the annex that were taken from other studies (Reardon, 1988; Delany and Lundeen, 1990; Yu et al., 1999; Tosca et al., 2005). Moreover, thermodynamic consistency of the modified database was ensured by comparison of calculated and experimental solubility values for several single and binary salt systems, as explained in Acero et al. (2007a). The model was used to determine saturation indices with respect to relevant mineral phases that may play a key role in the mobilization/immobilization of dissolved species. Negative saturation indices indicate that the pore-waters are undersaturated with respect to the target minerals and, therefore, their dissolution is thermodynamically favored over

59

precipitation. On the contrary, positive saturation indices indicate that mineral precipitation is favored. Finally, saturation indices close to zero indicate that pore-waters are close to equilibrium with respect to a given mineral phase and neither dissolution nor precipitation is thermodynamically supported.

3.3. RESULTS AND DISCUSSION

3.3.1. Stratigraphy and mineralogy

Monte Romero mine tailings in the YI display a well-defined oxidized upper layer and a less altered lower transition layer in the vadose zone (Fig. 3.1). Water saturation varies annually along this zone according to the seasonal periods, i.e. from strongly unsaturated in the dry-warm season to high water-saturation in the wet-rainy season. This upper level corresponds to the sulfide oxidation front and is the zone where most mineralogical and hydrochemical changes seem to occur. The oxidized zone appears from the surface to a depth of approx. 20-25 cm over the entire impoundment area and is characterized by reddish-yellowish ochre colors. The transition zone has 10-15 cm in thickness and is grayish-black. The remaining deeper mine tailings, which down to 350 cm depth, show dark gray color and water saturation throughout the year (Fig. 3.1).

The oxidized zone in the YI is mineralogically characterized mainly by clay minerals (approx. 60 wt%), quartz (25%), H_3O-jarosite (10%), gypsum (5%) and barite (<5%), and sulfides are almost absent (Table 3.2). The clay mineralogy is dominated by muscovite/illite and clinochlore. Poorly-crystalline goethite and/or schwertmannite are also abundant and occur as microbotryoidal masses and globular-like aggregates composed mainly of Fe and S (Fig. 3.2a,b). Jarosite and these micrometric Fe-rich agglomerates account for the yellowish color of the zone. Both the lack of sulfide minerals and the abundance of secondary Fe^{3+} phases indicate that YI tailings have been exposed to atmospheric conditions for extended periods. In the transition zone, the amounts of secondary Fe^{3+} phases decrease with the increasing amounts of pyrite towards the water-saturated zone. In this zone, the surfaces of pyrite grains are only slightly altered and frequently coated with iron precipitates (Fig. 3.2c). In the saturated zone, grayish tailings are dominantly composed of clay

60

minerals (approx. 40 wt%), pyrite (30%), quartz (20%), gypsum (5%), sphalerite (<5%) and barite (<5%) (Table 3.2). In this zone, secondary Fe^{3+} precipitates were not detected and sulfides do not show any sign of alteration. Carbonate minerals have not been detected at any depth in the mine tailings.
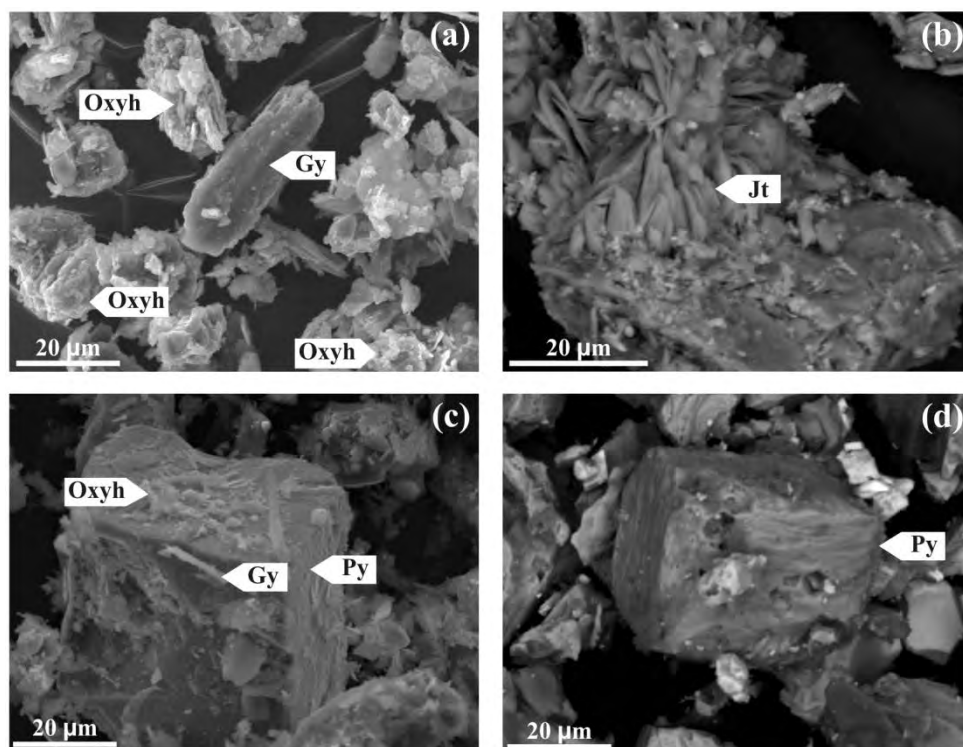
Fig. 3.2. SEM images of: (a,b) oxidized upper layer of the YI, (c) altered pyrite from the transition zone of the YI; and (d) altered pyrite from the upper oxidized part (with no secondary Fe^{3+} phases) of the GI. Gy: gypsum, Jt: jarosite, Oxyh: poorly-crystalline Fe oxyhydroxysulfates, Py: pyrite.

In contrast to the above-described features, the GI does not present any yellowish oxidation top layer; although the shallowest 20 cm part is also subject to the same seasonal variations described for the YI and the deeper tailings are totally water-saturated (Fig. 3.1). Secondary Fe^{3+} phases such as jarosite, goethite and schwertmannite were neither identified by XRD nor by SEM-EDS even in the top part of the tailings.

61

Table 3.2. Mineralogical composition (wt%) for the two mine tailings impoundments

Results for the yellowish impoundment:

Samples	Mineral phase (%)							
Depth (cm)	Barite	Clinochlore	Gypsum	Jarosite	Muscovite	Pyrite	Quartz	Sphalerite
0	0.50	2.40	5.60	6.90	57.0	-	27.6	-
5	0.90	3.80	3.70	9.70	54.5	-	22.8	-
10	0.30	5.10	3.10	7.50	53.8	-	29.9	-
15	0.30	3.80	3.80	6.90	56.1	-	28.8	-
20	0.60	3.00	7.70	-	43.7	18.2	21.5	2.70
25	2.00	2.40	7.60	2.70	52.4	7.70	23.1	2.30
30	0.90	2.20	4.20	-	54.9	10.8	25.4	1.60
35	1.60	1.20	2.50	-	57.0	8.60	27.5	1.50
55	5.20	9.10	8.00	-	44.3	10.3	21.3	1.80
70	4.10	8.80	6.10	-	36.7	14.5	27.0	2.80
85	3.70	2.50	2.40	-	32.1	30.0	25.0	4.10
125	2.70	6.00	4.50	-	29.3	31.7	20.5	5.30
135	3.00	5.00	3.70	-	38.8	11.8	32.4	5.40
150	4.40	10.5	6.00	-	30.5	30.2	14.2	4.20
175	7.20	6.90	2.40	-	24.5	42.2	11.0	5.60
200	4.70	5.00	7.10	-	34.6	32.9	12.9	2.80
250	5.10	8.80	5.10	-	27.1	33.6	16.5	3.85
300	4.40	6.40	4.50	-	31.0	30.3	18.9	4.50
350	4.20	4.90	8.20	-	29.6	36.9	12.3	3.90

Results for the grayish impoundment:

Samples	Mineral phase (%)							
Depth (cm)	Barite	Clinochlore	Gypsum	Jarosite	Muscovite	Pyrite	Quartz	Sphalerite
0	15.2	-	-	-	-	75.2	4.70	4.80
5	14.7	-	-	-	-	80.3	3.10	1.90
10	6.90	-	-	-	-	86.4	2.80	3.90
15	15.6	-	-	-	-	57.9	21.0	5.40
20	9.50	-	-	-	-	78.0	6.30	6.20
30	7.20	-	-	-	-	86.4	2.20	4.20
50	9.90	-	-	-	-	75.6	11.0	3.50
70	5.60	2.90	3.10	-	29.1	33.1	22.3	3.90
100	6.40	6.40	6.90	-	22.3	41.9	11.7	4.50
130	4.30	6.00	4.40	-	31.6	29.8	19.3	4.60
175	7.50	4.00	6.10	-	17.4	47.7	11.5	5.80
200	3.20	10.5	5.90	-	30.4	30.2	16.6	3.20
225	5.00	8.30	3.90	-	40.6	15.8	23.0	3.10
275	2.90	8.70	5.70	-	41.1	19.3	19.0	3.10
300	3.30	10.8	7.20	-	38.0	20.3	18.0	2.40
350	4.60	6.70	5.90	-	29.2	33.6	15.9	4.10

Hence, the complete profile from the surface to 400 cm depth is dark gray in color, identical to the water-saturated zone of the YI and, therefore, no 'apparent' weathering is occurring. The apparent lack of weathering in the GI is surprising because both impoundments store apparently the same mine

tailings under identical climatic conditions. In fact, most of the mine tailings (from 50 to 400 cm) in the GI are mainly composed by clay minerals (approx. 40 wt%), pyrite (30%), quartz (15%), gypsum (5%), sphalerite (<5%) and barite (<5%) (Table 3.2). These mineralogical features are almost identical to those found in the water-saturated zone of the YI. However, the mineralogical composition of the shallowest part of the tailings (from 0 to 50 cm) is clearly different and characterized by high contents of pyrite (approx. 80 wt%), with minor amounts of barite (10%), quartz (5%) and sphalerite (<5%) and lack of clay minerals (Table 3.2). Other minor sulfides present in both tailings include chalcopyrite (<2%) and galena (<0.5%). Texturally, pyrite grains in the upper superficial part are slightly altered, in contrast with those found in the water-saturated zone of this impoundment (Fig. 3.2d).

During the dry season, the development of abundant efflorescent sulfate salts is observed to occur on the surface of both studied tailings due to evaporative concentration under extreme dryness conditions. As determined by XRD, the mineralogy of these salts seems to correspond to Fe^{2+} sulfates (rozenite, szomolnokite and melanterite) and Mg sulfates (hexahydrite), with minor amounts of mixed salts of Fe^{2+}-Al-Mg (halotrichite and pickeringite) and gypsum.

3.3.2. Sequential extractions

The study of pseudo-total and mobile element was mainly focused on the shallowest zone from both impoundments to elucidate the weathering model in each of them. However, some samples from the less altered zone were also considered for comparison purposes. Extracted contents of elements in the aqua regia digestion and in each step of the sequential extraction are shown and compared in detail in Table A1 of the annex. The percentage values extracted from each element with respect to the sum of the four fractions are shown in Figures 3.3, 3.4 and 3.5. The sums of the four sequential extraction fractions are in good agreement with the pseudo-total digestion within a ±15% error, which shows the high reproducibility of the data obtained in this study. Pseudo-total and mobile contents of S and Fe are mainly governed by the huge occurrence of pyrite in the tailings, and hence, their distribution along tailings profiles will be useful for studying the sulfide oxidation and AMD generation.
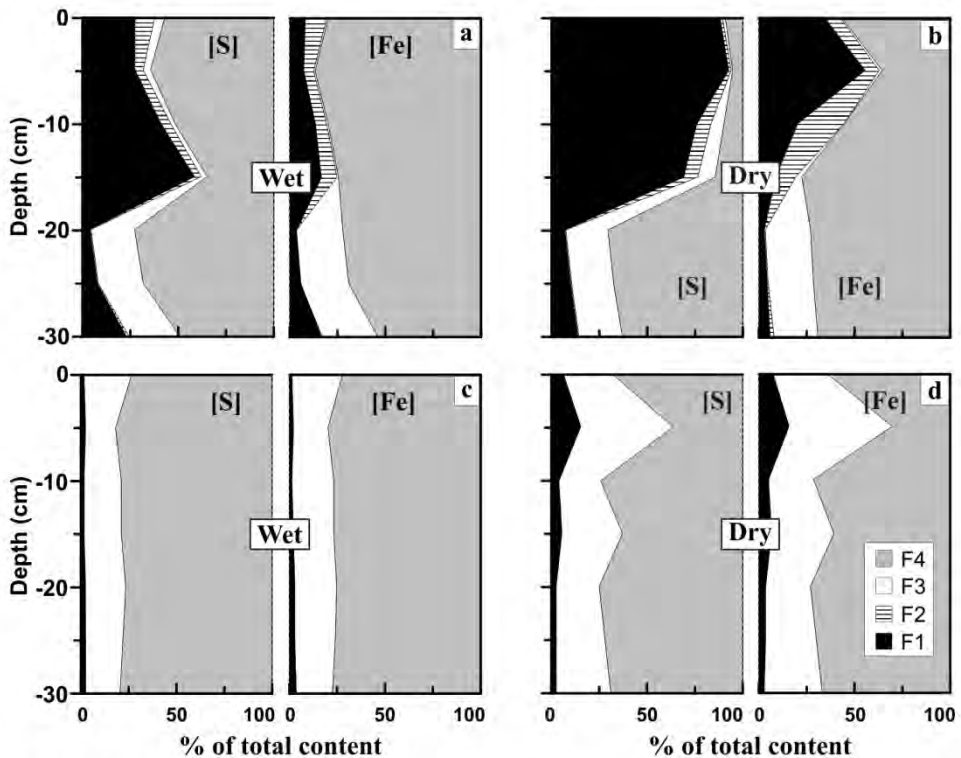
Fig. 3.3. Vertical profiles for the S and Fe percentages extracted in the sequential extraction in the (a,b) YI and (c,d) GI during wet and dry seasons, respectively.

Aqua regia digestion results show that pseudo-total element concentrations in the oxidized surface zone of the YI for both seasonal periods vary as follows: 1256-8039 mg/kg Al, 253-854 mg/kg As, 129-1311 mg/kg Cu, 13.1-51.3 g/kg Fe, 21.5-216 mg/kg Mn, 4.93-52.3 g/kg S, 323-6581 mg/kg Zn, and up to 15.2 mg/kg Cd, 2.90 mg/kg Co and 8.62 mg/kg Ni. In contrast, the less-oxidized zone of the same impoundment shows much higher pseudo-total concentrations: 603-2393 mg/kg As, 3.30-32.5 mg/kg Cd, 2.94-40.3 mg/kg Co, 926-4112 mg/kg Cu, 59.6-240 g/kg Fe, 27.1-95.8 mg/kg Mn, 4.09-10.6 mg/kg Ni, 73.2-273 g/kg S and 1150-14522 mg/kg Zn, except for Al (873-1674 mg/kg). Obviously, the oxidation process leads to a substantial depletion with time of the element contents associated with sulfide minerals in the shallowest part of this impoundment and to a relative enrichment in more weathering-resistant aluminosilicate minerals (Table A1 in the annex).

In the GI, pseudo-total concentrations for the complete profile in both seasons range as follow: 83-802 mg/kg Al, 418-1678 mg/kg As, 0.90-8.72 mg/kg Cd, 11.9-66.7 mg/kg Co, 139-687 mg/kg Cu, 101-368 g/kg Fe, 10.5-39.1 mg/kg Mn, 4.50-13.6 mg/kg Ni, 119-386 g/kg S and 320-3244 mg/kg Zn. Although no apparent oxidized top layer occurs in this impoundment, the samples from the shallowest part also show pseudo-total concentrations slightly lower than the less-oxidized samples. However, these differences are less significant than in the YI (Table A1 in the annex).

In the oxidized layer of the YI, the average percentages leached in the F1 from sequential extractions are 81% and 38% for S, and 29% and 11% for Fe in the dry and wet periods, respectively (Fig. 3.3a,b). This fraction corresponds to soluble salts precipitated in this shallowest part after water rise by capillarity and concentration by evaporation during the dry-warm period, which are later easily dissolved by rainfall events during the wet-rainy period. Accordingly, the results for this oxidized part of the profile have a strong seasonal dependence, with higher values in dry periods than in wet periods. On the contrary, the percentages released in F1 in the less-oxidized zone are clearly lower and less variable seasonally, with annual averages of 12% and 7% for S and Fe, respectively (Fig. 3.3a,b). These values are in good agreement with the weaker influence of evaporation and seasonal changes on this part of the tailings profile. Additionally, the oxidized yellowish layer of the YI tailings shows higher S and, mainly, Fe concentrations in the F2 than in the less-oxidized grayish zone. In contrast, S and Fe concentrations in the F3 are much higher in the less-oxidized zone than in the oxidized top layer. Consistent with the mineralogy, approximately 5-10% of S and Fe is bound to Fe oxyhydroxysulfates in the oxidation front versus <1% in the less-oxidized zone (Fig. 3.3a,b). On the contrary, approx. 25% of S and Fe in the less-oxidized zone is bound to sulfide minerals versus <5% in the oxidation front (Fig. 3.3a,b).
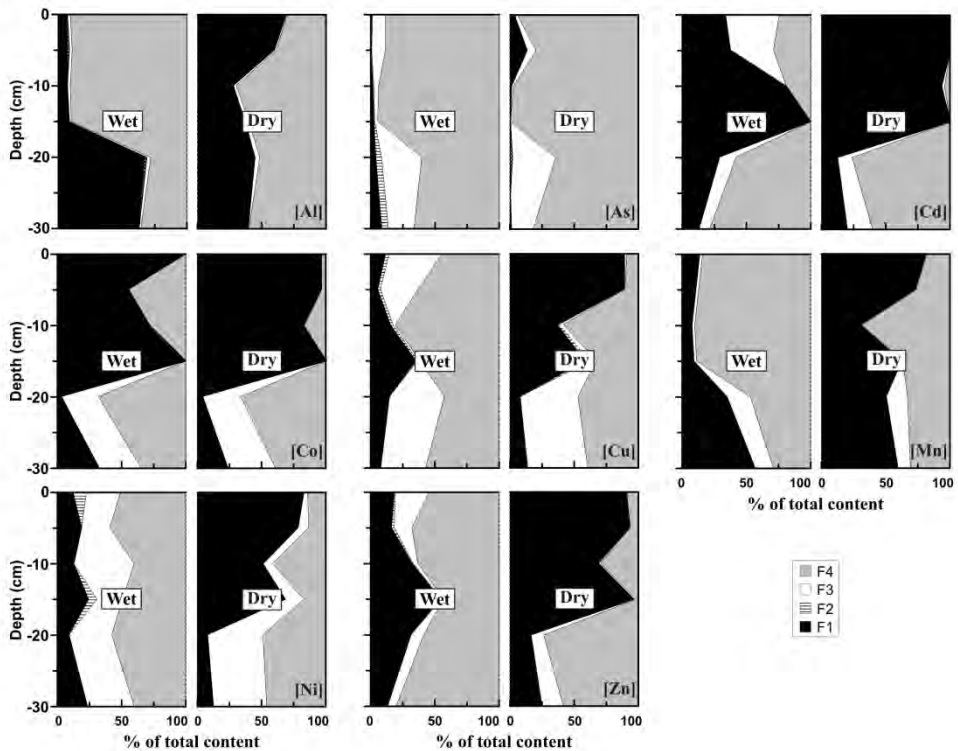
Fig. 3.4. Vertical profiles for Al, As, Cd, Co, Cu, Mn, Ni and Zn percentages extracted in the sequential extraction in the YI during wet and dry seasons.

In the shallowest zone of the GI (up to 20 cm depth), average S and Fe percentages in the F1 are again higher in the dry periods (8%) due to precipitation of soluble evaporitic salts than in wet periods (1%) due to their dissolution in rainwater (Fig. 3.3c,d). As in the other impoundment, the amount of evaporitic salts in dry period decreases with the depth, reaching similar S and Fe concentrations in both seasons with average values in the less-oxidized zone of 2% and 3%, respectively (Fig. 3.3c,d). Unlike the YI, however, no differentiation was found in the depth distribution of S and Fe associated with F2 and F3 between the shallowest and deepest zones. Due to the lack of an oxidized upper layer rich in secondary Fe^{3+} phases in the GI, the concentrations of S and Fe released in the F2 are relatively low throughout the profile, i.e. much less than 1% (Fig. 3.3c,d). In contrast, the abundant presence of sulfides, mainly pyrite, throughout the profile governs the relatively high

66

values of S and Fe associated with the F3, i.e. approx. 25% (Fig. 3.3c,d). Higher absolute concentrations of S and Fe associated with the F3 are found in the GI than in the less-oxidized zone of the YI logically due to higher pyrite content (Table A1 in the annex).
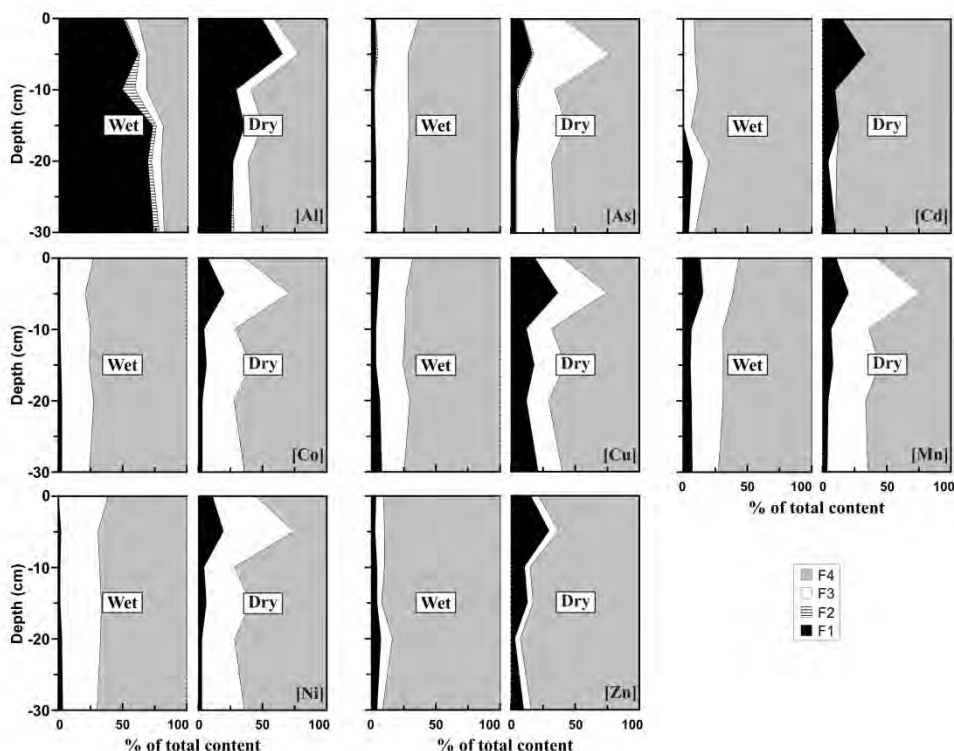
Fig. 3.5. Vertical profiles for Al, As, Cd, Co, Cu, Mn, Ni and Zn percentages extracted in the sequential extraction in the GI during wet and dry seasons.

Parallel to S and Fe, it is worth noting that both impoundments show high concentrations of contaminants in the F1 of the shallowest zone samples associated with evaporitic soluble salts that precipitate in dry period, thus being the most dangerous and bio-available fraction for the environment. These concentrations decrease substantially in depth and in wet period by dissolution (Table A1 in the annex). In relative terms, the percentages extracted from these evaporitic salts in the oxidized layer of the YI during the dry season are also high, ranging from 60% to 100%, for Cd, Co, Zn, Ni, Cu and Mn; although very low percentages of As were observed (<5%) (Fig. 3.4). In comparison with

67

the YI, the relative percentages associated with evaporitic salts in the upper level of the GI are lower, ranging from 10% to 20% (Fig. 3.5), because higher percentages of these elements are also bound to sulfides. Although the element content in evaporitic salts exceeds in dry conditions, one point to note is that these seasonal differences are far more significant in the YI than those observed in the GI. Thus, the element contents in the F1 in the wet period are from 15 to 85 times lower than in dry period for the YI, and only between 1 and 8 times lower for the GI (Table A1 in the annex). This observation means that the highest content of evaporitic soluble salts must occur in the GI during the wet seasons.

3.3.3. Pore-gas and -water

The water tables during the pore-gas sampling were at depths of 40-50 and 60-70 cm in the YI and GI, respectively. As expected, the highest levels were measured during the wet period. In the unsaturated zone of both impoundments, the pore-gas oxygen concentrations decrease from around 20% at the surface (atmospheric conditions) to values below the detection limit (0.5%) at the depth of the water table (Fig. 3.6). In the wet season, higher partial water-saturation occurs and, hence, the sulfide oxidation slows down. Consequently, the decline in oxygen concentration with depth is slower and more gradual in both tailings. In the dry season, however, the sulfide surfaces are almost completely water-free and hence available for their oxidation. Thus, oxygen is rapidly depleted in the first few centimeters. This faster depletion is especially evident in the GI with higher pyrite percentages in the shallowest 50 cm (Fig. 3.6).

Pore-water in the oxidation zone of the mine tailings is subject to cyclical changes in pH, Eh and chemical composition according to seasonal variations. During dry seasons, the pH is extremely acidic in the vadose zone of both impoundments, with values as low as 1.66 and 0.20 for the YI and GI, respectively (Fig. 3.7a); while the Eh shows oxidizing values of up to 562 mV and 470 mV for the YI and GI, respectively (Fig. 3.7b). Pore-water SO_4 and Fe concentrations are of up to 235 g/L and 67.3 g/L for the YI, and 42.1 g/L and 9.93 g/L for the GI, respectively (Fig. 3.7c,d). Fe^{2+} percentages with respect to

total Fe for both seasonal periods in the oxidation zone are about 40% and 70% for the YI and GI, respectively. According to the geochemical modeling (see Table A2 in the annex), the pore-water of both impoundments exhibits undersaturation with respect to any possible secondary products of pyrite oxidation (Fe^{3+}) oxyhydroxysulfates such as K-jarosite, H_3O-jarosite, Na-jarosite, goethite and schwertmannite). In contrast, geochemical calculations suggest that pore-waters are often supersaturated with respect to some water-soluble iron sulfate salts, such as bilinite and copiapite (Table A2 in the annex), which occur due to strong concentration by evaporation in dry-warm periods.
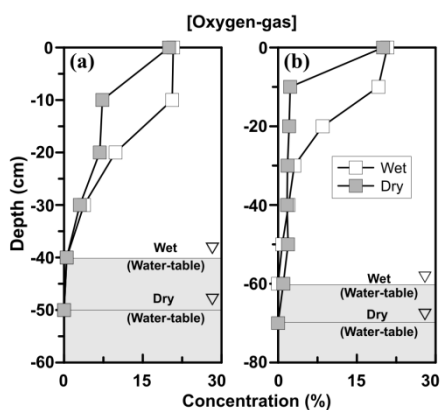
Fig. 3.6. Vertical profiles for pore-gas oxygen concentration in the (a) YI and (b) GI.

During wet seasons, however, an opposite behavior is observed in the oxidation zone of both impoundments. In the YI, the pH increases, reaching values of up to 3.11 due to dilution by rainwater input (Fig. 3.7a); while the Eh is maintained with values of up to 514 mV (Fig. 3.7b). Pore-water SO_4 and Fe concentrations are much lower than during the dry season, reaching maximum values of 2.93 g/L and 275 mg/L, respectively (Fig. 3.7c,d). This decrease is due not only to the direct dilution effect by rainwater input but also to the increase of pH, which leads to pore-water supersaturation with respect to jarosite-group minerals, goethite and schwertmannite (Table A2 in the annex). The potential precipitation of these secondary ferric phases is perfectly consistent with the mineralogical characterization. Regarding the trace elements, their concentrations in the oxidation layer also significantly decrease in the wet period, which could be likely due to their incorporation to

secondary phases (Fig. 3.8). These findings are also supported by a sulfur-iron pɛ-pH stability diagram calculated for the pore-water composition range observed in the tailings impoundments (Fig. 3.9). However, pore-solutions are undersaturated with respect to soluble sulfate salts. The decrease of concentrations by precipitation of secondary oxidation products would counteract the increase by dissolution during the first rainfalls of the evaporitic salts formed in the dry-warm season.
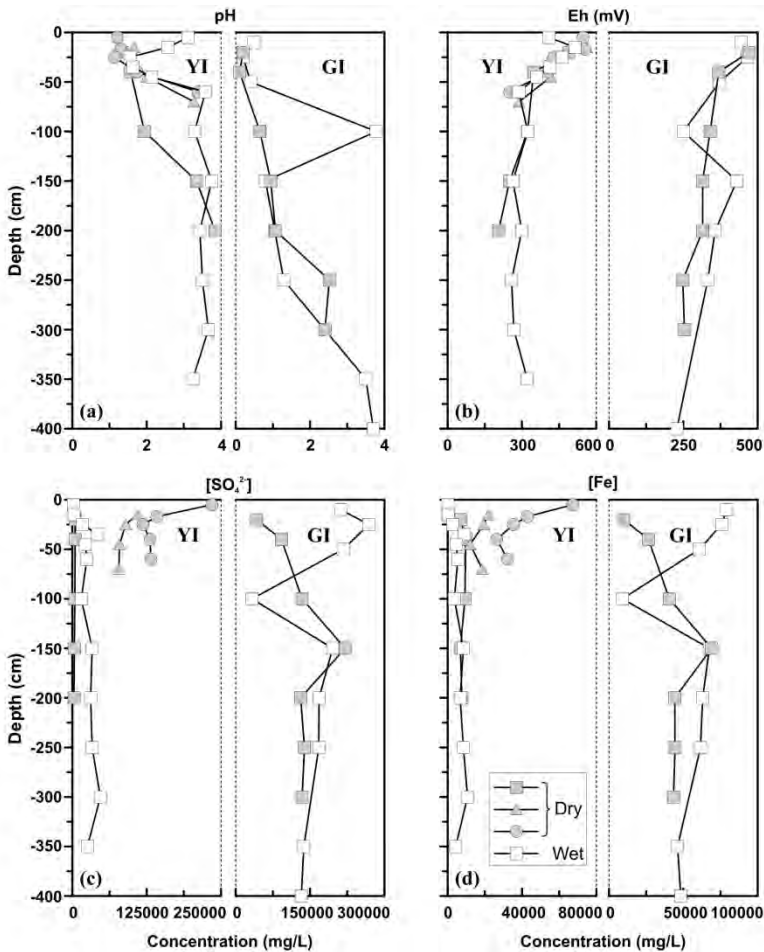
Fig. 3.7. Vertical profiles for pore-water (a) pH, (b) Eh, (c) SO_4 and (d) Fe concentrations in the YI and GI.
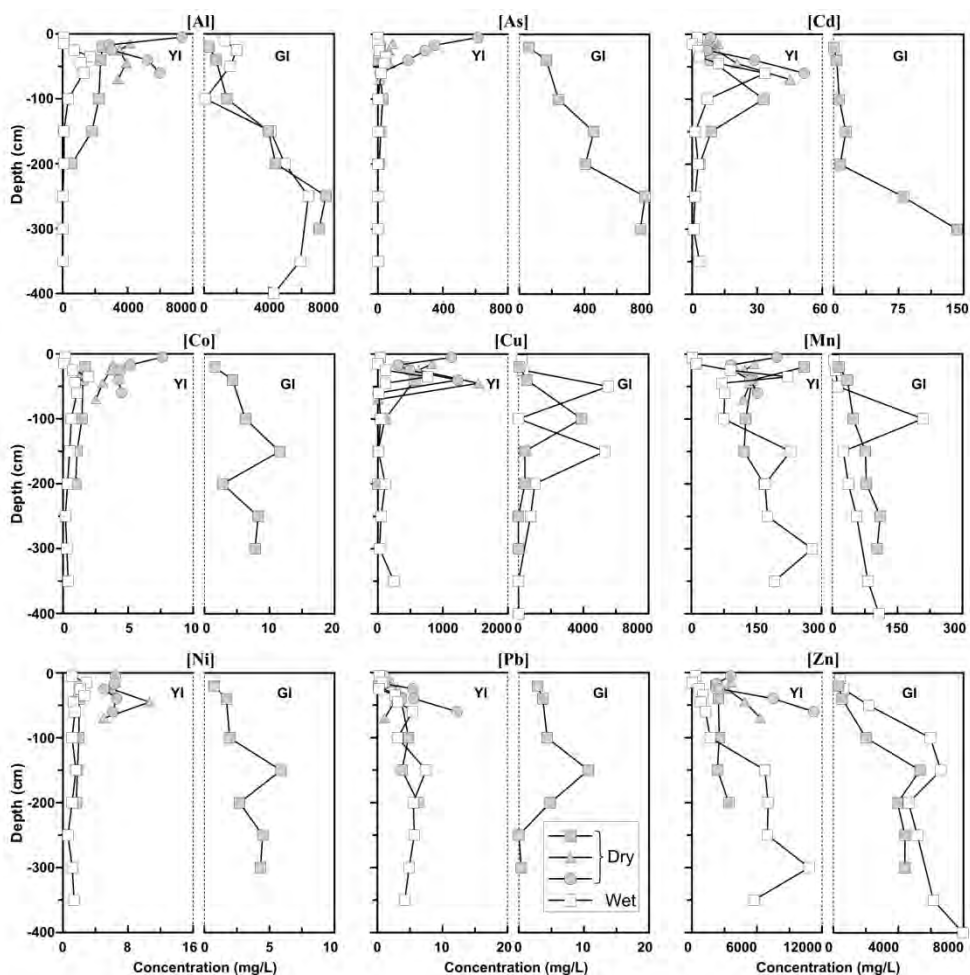
Fig. 3.8. Vertical profiles for pore-water Al, As, Cd, Co, Cu, Mn, Ni, Pb and Zn concentrations in the YI and GI. Data for As, Cd, Co, Ni and Pb are unavailable for the GI during wet season. In dry season, closed symbols correspond to the samplings of May 2005 (circles), June 2005 (triangles) and May 2010 (squares).

Conversely, the pore-water pH in the vadose zone of the GI remains highly acidic during wet seasons, with values as low as 0.49 (Fig. 3.7a); and Eh values of up to 466 mV (Fig. 3.7b). Sulfate and Fe concentrations are of up to 269 g/L and 79.1 g/L, respectively (Fig. 3.7c,d). The pH is so acidic that pore-waters remain strongly undersaturated with respect to any secondary oxidation products (Table A2 in the annex), which keeps in solution the pollutant load. Indeed, concentrations of other dissolved elements in the oxidation zone are

also slightly higher in wet period (Fig. 3.8). The sulfur-iron pε-pH diagram shows that pore-solutions lie in the stability field of dissolved species (Fig. 3.9). Geochemical modeling is again in agreement with the mineralogical observations. The lack of precipitation of secondary Fe^{3+} phases together with the dissolution of the evaporitic salts during the first rainfall events explain that solute concentrations in the vadose zone of the GI during wet seasons are higher than during dry seasons, in contrast to the observations for the YI. According to the geochemical calculations, pore-waters become so loaded with contaminants that are also supersaturated with respect to some evaporitic sulfates (namely bilinite and copiapite; Table A2 in the annex).

However, neither of these evaporitic salts was identified by XRD on the surface of the studied impoundments. In fact, little evidence of the direct precipitation of bilinite and copiapite in the field exists and their presence has been reported to occur frequently by oxidation of other previously-precipitated Fe^{2+} sulfates (Bigham and Nordstrom, 2000). The identified sulfate salts, i.e. mainly rozenite, szomolnokite, melanterite and hexahydrite, precipitate from extreme waters that do not persist for long without evaporating (Hammarstrom et al., 2005). To reproduce the evolution of pore-solutions from the shallowest part of the tailings materials during evaporation until almost total dryness, some geochemical calculations were performed using as starting solutions the ones corresponding to the oxidized zone of both impoundments. The observed mineralogy is fully consistent, in type of mineral phases and relative abundance, with the results of these geochemical simulations (Table A3 in the annex).

The occurrence of these water-soluble precipitates during the dry season in both impoundments and also during the wet season in the GI is consistent with the sequential extraction results. According to the extraction data, these iron sulfate salts also act as temporary sinks for other minor elements such as Cd, Co, Zn, Ni, Cu and Mn. These divalent elements have been reported to substitute Fe^{2+} in the structure of these minerals (e.g. Jamieson et al., 1999; Jambor et al., 2000; and references therein). Since all the detected secondary sulfate salts are readily soluble, they must play an alternating role as sinks (during evaporation) and secondary sources (during rainfall events) for the dissolved elements present in the pore-waters.

72
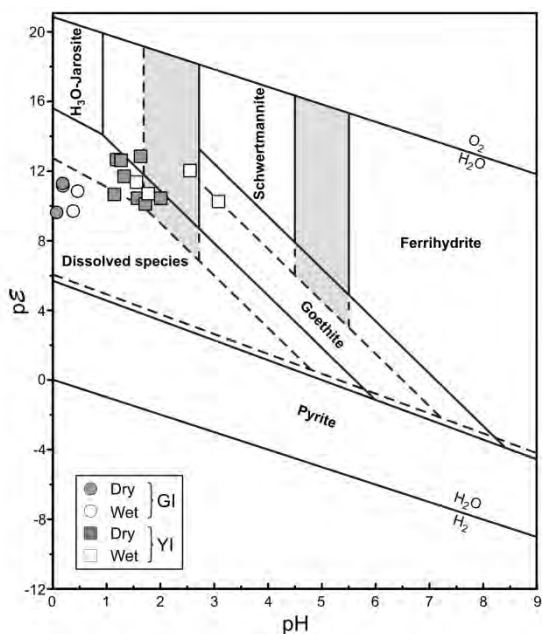
Fig. 3.9. Eh and pH projection into a sulfur-iron pε-pH diagram for the pore-water solutions of the oxidation zone of the YI and GI. The pε-pH diagram is for the system Fe-S-O-H at 25ºC and 1 bar pressure; assuming pε = Eh(mv)/59.2 and two extreme conditions: average pore-water composition for the wet season of the YI (log activities of Fe^{2+} = -3.41 and SO_4^{2-} = -1.72; solid line) and for the wet season of the GI (log activities of Fe^{2+} = -1.61 and SO_4^{2-} = -0.06; dashed line). Darker areas show possible expansion of jarosite and ferrihydrite fields according to Bigham et al. (1996).

In the saturated zone of both impoundments, the differences observed in the pore-water chemistry between wet and dry periods are much weaker, i.e. the seasonal changes affect at a less extent than in the shallowest part. Pore-water pH increases with depth, reaching values of up to 3.84 and 3.70 for the YI and GI, respectively (Fig. 3.7a); and the Eh decreases, reaching values of up to 206 mV and 228 mV for the YI and GI, respectively (Fig. 3.7b). Maximum concentrations in the deepest part (from 200 cm depth) of the YI are generally significantly lower than in the GI (Figs. 3.7 and 3.8). Moreover, these concentrations in the YI are much lower than in the oxidation and transition zones, chiefly during the dry period. Zinc is the only element that shows a different behavior in the saturated zone of the YI since its concentration greatly increases in depth in both seasonal periods (Fig. 3.8). This increase could be

due to the limited affinity of divalent cations for secondary Fe^{3+} oxyhydroxysulfates at such high concentrations (Caraballo et al., 2009). In fact, the remaining divalent cations such as Cd, Co, Ni, Cu and Mn seem to be also weakly adsorbed onto the Fe^{3+} phases in the oxidation front. Although these elements display lower concentrations than Zn and are retained in the oxidized zone during the wet season, they are again mobilized at low pH towards the tailings surface to form the evaporitic salts in dry periods. In contrast, As does not show any mobilization towards the surface of the tailings, which is probably due to its strong adsorption to secondary Fe^{3+} oxyhydroxysulfates in the low pH oxidation zone (Asta et al., 2010). This would explain the low As concentrations found in the evaporitic salts. Unlike in the YI (except for Zn), the concentrations of most of these elements in the deepest zones of the GI are maintained or even increased in depth (Figs. 3.7 and 3.8). The increase in the Zn concentration with depth in both impoundments could be also due to the fact that sphalerite dissolution kinetics is non-oxidative at the pH range measured in the tailings (Acero et al., 2007b).

In both impoundments, Fe^{2+} percentages with respect to total Fe in the deepest zones are about 95%. In this permanently wet hydrological zone, no oxidation of Fe^{2+} seems to take place due to the depletion of oxygen, which would prevent from precipitation of secondary iron phases to occur. According to geochemical calculations, only potential precipitation of gypsum, jurbanite and anglesite was possible along the entire depth profile, the pore-waters being undersaturated in the rest of phases (Table A2 in the annex).

3.4. CONCLUSIONS

The mineralogical and geochemical study of the Monte Romero mine tailings (IPB) allows for the development of a schematic oxidation model to explain the contrasting evolution of both impoundments. The extreme seasonal variations in the region determine the existence of two alternating flow and transport directions; upward and downward flow of water and solutes according to evaporation and rainfall periods, respectively. In both impoundments, the elements liberated by sulfide oxidation are mobile under acid conditions and transported to the tailings surface via capillarity in the dry-

74

warm season; where concentration by evaporation leads to the supersaturation with respect to readily soluble sulfate salts that temporarily retain trace elements such as Cd, Co, Zn, Ni, Cu and Mn. However, rainfall during the wet season washes out these salts and the contaminants are again released to the surface runoff and groundwaters.

In the vadose zone of the YI, the increase of pore-water pH to values around 3 by dilution after rainfall events causes supersaturation with respect to different secondary Fe^{3+} products resulting from pyrite oxidation such as jarosite, goethite or schwertmannite. The precipitation of these secondary phases would probably be responsible for the yellowish color of the oxidation front of this impoundment. Moreover, this upper level is clearly depleted in sulfides due to oxidation and relatively enriched in relict minerals such as clay minerals, quartz and barite. Precipitation of Fe^{3+} oxyhydroxysulfates together with sorption of trace elements onto the secondary phases in the oxidation front of the YI appears to reduce the pollutant load in wet seasons with respect to dry seasons. With the exception of Zn, contaminants percolating down to the water table also decrease.

In the GI, secondary oxidation products do not seem to appear in detectable amounts in the unsaturated zone. Pore-water pH is extremely acidic during both seasons and, thus, the solutions remain undersaturated throughout the year with respect to secondary Fe^{3+} oxyhydroxysulfates. The elements are kept in solution even during wet periods when their dissolved concentrations greatly increase by dissolution of evaporitic sulfate salts with the first rainfall events. The lack of precipitation of ferric phases could explain the absence of a yellowish oxidized level in the shallowest part of these tailings and, hence, the increase of the solute load percolating towards the water table.

Under identical climate conditions, the different weathering pattern observed in both impoundments is due to the contrasting mineralogical composition of the mine tailings. The mining sludge from the flotation process that was deposited in the first 50 cm of the GI contains much higher amounts of pyrite (approx. 80 wt%) than those observed in the YI (approx. 30 wt%). The higher pyrite percentage in the upper part of the GI implies a higher degree of oxidation and, hence, production of leachates with lower pH and

75

higher dissolved contaminant loads throughout the entire year. The acidity keeps the iron dissolved in the pore-water in reduced state. Even though oxidation is taking place, the ferric iron produced is rapidly reduced by pyrite dissolution, so no oxidized secondary minerals can form. Given that elements are not retained by precipitation of secondary Fe^{3+} oxyhydroxysulfates in the GI, most of the pollution can be evacuated by meteoric waters and affect to the surface and groundwater at a greater extent than the YI. In spite of this, the GI apparently seems much less weathered than the adjacent yellow one, and evidences the need of in depth studies prior to restoration decisions.

CAPÍTULO 4. FORMATION OF A HARDPAN IN THE CO-DISPOSAL OF FLY ASH AND SULFIDE MINE TAILINGS AND ITS INFLUENCE ON THE GENERATION OF ACID MINE DRAINAGE

Dino Quispe, Rafael Pérez-López, Patricia Acero, Carlos Ayora, José Miguel Nieto, Rémi Tucoulou. Formation of a hardpan in the co-disposal of fly ash and sulfide mine tailings and its influence on the generation of acid mine drainage. Chemical Geology 355 (2013) 45-55.

Abstract

Pilot-scale field experiments were conducted to test a strategy for the treatment of acid mine drainage by addition of an alkaline cover of coal combustion fly ash on two sulfide mine tailings impoundments (Iberian Pyrite Belt, SW Spain). During the pilot-scale treatment, calcium-rich alkaline solutions from fly ash interacted with metal-rich acidic solutions from mine tailings, leading to the massive precipitation of newly-formed phases mainly in the fly ash close to the interface between both materials. Over time, the interaction between fly ash and pyrite sludge promoted the formation of a chemically cemented zone or hardpan, which was analyzed at high spatial resolution by micro-X-ray diffraction (μ-XRD) and micro-X-ray fluorescence (μ-XRF) based on synchrotron radiation. These micro-characterization techniques extensively identified poorly-crystalline Fe oxyhydroxysulfates, jarosite and gypsum as newly-formed phases in the hardpan, and gypsum in the fly ash. As deduced from Principal Component Analysis of the fluorescence intensity data, these phases seem to exert a significant mineralogical control on element mobility; in particular, jarosite showed high affinity for As, whereas poorly-crystalline Fe-rich assemblages selectively concentrated Mn, Ni and Pb. Sequential extractions indicated that the application of a fly ash cover significantly reduced the bioavailability of most of the elements by modification of their chemical speciation into less mobile forms under typical oxidizing conditions. As an additional advantage, the development of the hardpan hindered the penetration of oxidizing agents to sulfide mine tailings. This effect significantly reduced the sulfide oxidation rates, therefore attenuating the release of potentially pollutant elements to the environment.

4.1. INTRODUCTION

Flotation processing of sulfide ores for obtaining base metals produces tailings consisting of fine-grained particles less than 100 µm of residual sulfides (mainly pyrite) and silicates that are stored in impoundments and, if not managed properly, can pose huge environmental problems. Exposure of sulfides to air and water leads to the release of acidic leachates with high concentrations of sulfate, iron and other metals, known as Acid Mine Drainage (AMD). The tailings impoundments are an almost inexhaustible source of AMD by sulfide oxidation, which represents the main environmental challenge facing the mining industry worldwide. In mine tailings, both free oxygen diffusion and large surface area due to micrometer-sized sulfides are factors that accelerate the oxidation process.

In order to reduce the environmental impact of mine tailings, several remediation strategies have been designed. Probably, the most common chemical treatment involves the addition and mixing of an alkaline reagent with the mining sludge to promote AMD neutralization, and consequently, metal removal by precipitation, co-precipitation or sorption (e.g. Nicholson et al., 1988, 1990; Mylona et al., 2000). In addition, this treatment strategy might decrease the sulfide oxidation rates due to the coating of grains by secondary ferric phases (Lapakko et al., 1997; Holmström et al., 1999). Unfortunately, this mixing is only feasible in active mining but not for abandoned tailings. A second remediation option is the physical treatment, which consists in the application of synthetic sealants on the tailings to prevent oxygen ingress and water infiltration (e.g. Farah et al., 1997; Romano et al., 2003). These cover systems minimize waste oxidation and, hence, AMD generation.

Finally, a third group of remediation strategies, which combines aspects of the physical and chemical strategies, is based on the self-isolation of the mining waste by inducing the formation of a cemented layer by adding an alkaline cover (e.g. Chermak and Runnells, 1997). The sudden change of pH

in the interface between both materials causes the local precipitation of cementing phases and the formation of a hardpan. These tightly cemented zones may act as low-permeability barriers towards the migration of infiltrating water and atmospheric oxygen. In addition, the acid-base chemical reactions forming the hardpan neutralize acidity and retain contaminants from the solution. This remediation is inspired in attenuation processes that occur naturally in inactive sulfide-rich mine tailings, where the natural formation of cemented layers or hardpans significantly decreases contaminant mobility by preferential precipitation of sulfates and oxyhydroxides (e.g. Blowes et al., 1991; McGregor and Blowes, 2002; Alakangas and Öhlander, 2006; Lottermoser and Ashley, 2006; Graupner et al., 2007; Kohfahl et al., 2011).

Limestone is the most commonly used additive to mining sulfide residues for their chemical neutralization. Alternatively, fly ash from coal combustion plants has also potential applications as acidity buffer. The advantages of using fly ash additives include that they are widely available and generally very inexpensive in comparison with limestone. Consequently, fly ash is currently receiving considerable attention as chemical treatment by mixing with metal-contaminated soils or mining wastes (e.g. Dermatas and Meng, 2003; Wang et al., 2006; Polat et al., 2007). In addition to chemical neutralizer, Pérez-López et al. (2007a) showed in the laboratory that a fly ash cover may be also efficient in the formation of a physical barrier to prevent the progress of tailings oxidation. This is due to the fact that the alkalinity supplied first by the lime and then by the silicate glass present in the fly ash may induce a reaction front and the development of a hardpan. In addition, the precipitation of a coating of iron oxyhydroxides on the surfaces of pyrite grains may prevent further oxidation (Pérez-López et al., 2007c). The results obtained in these foregoing laboratory experiments were so encouraging that fully justified the need for their upscaling to pilot field tests, prior to a future full-scale treatment. Such treatment upscaling is the main overall goal of the work presented in this paper.

The pilot-scale field experiments were conducted in two abandoned sulfide mine tailings impoundments from the Iberian Pyrite Belt (IPB, SW Spain), one of the largest sulfide-mining provinces in the world (Sáez et al., 1999). In each of these impounds, which show different mineralogical

and geochemical features, the weathering processes observed in vertical profiles of the untreated tailings were compared with those of tailings covered with fly ash. The main objective of this study is to provide a better knowledge of the effect of fly ash addition on the weathering of mine tailings impoundments. This information will be obtained by means of: (i) assessment of contaminant mobility using sequential extractions; (ii) characterization of the newly-formed precipitates in the interface between fly ash and mine tailings through synchrotron radiation-based X-ray microanalysis; and (iii) in-situ monitoring of the atmospheric oxygen access to the unsaturated zone of both impoundments.

4.2. MATERIALS AND METHODS

4.2.1. Study area

The present study was carried out at the tailings impoundments of the Monte Romero abandoned mining district in the IPB. The mine exploited from 1970 to 1978 massive sulfide ores that were processed by flotation to obtain copper, zinc and lead concentrates. The mining waste from flotation process was stored in two adjacent impoundments (Fig. 4.1). The semi-arid climate in this region, i.e. alternating humidity and high to moderate temperatures, prompts an oscillating water table between the first 40-70 cm and an active weathering of sulfides. Stored flotation tailings are made up of muscovite and clinochlore (40 wt%), pyrite (30%), quartz (20%), gypsum (5%), sphalerite (<5%) and barite (<5%). In one of the impoundments, the first 50 cm averages 80 wt% pyrite and contains extremely acidic pore-water (pH < 0.5) during the entire year, which keeps in solution the pollutant load. Hence, no precipitation of secondary Fe^{3+} phases takes place in the oxidation zone of this impoundment, which from now on will be called grayish impoundment (GI). The second one averages up to 30 wt% pyrite and has an additional 20-25 cm thick yellowish oxidation layer at the top consisting of 60 wt% clay minerals, 25% quartz, 10% H_3O-jarosite and abundant poorly crystalline Fe^{3+} oxyhydroxysulfates. Within the latter, the pore-water pH increases to 3.0 during rainy periods, causing supersaturation and the precipitation of the secondary Fe^{3+} phases in the oxidation front. From now on

this will be called yellowish impoundment (YI). Full details of the oxidation pattern of both impoundments can be found in Quispe et al. (2013).
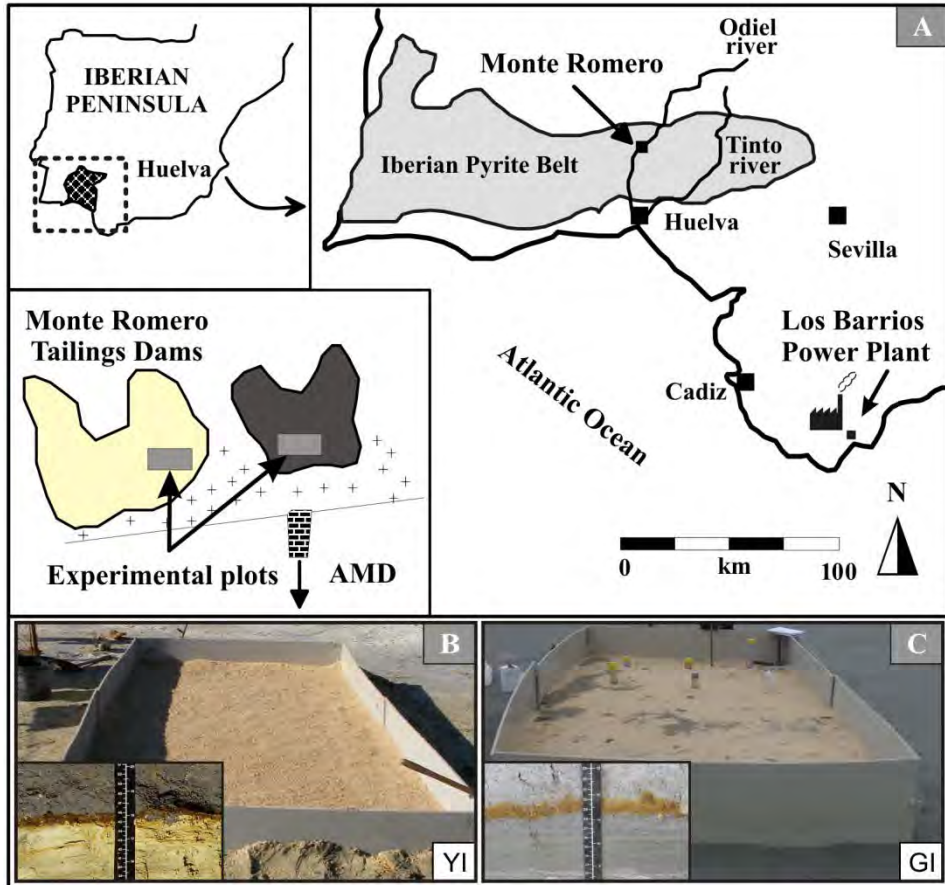
Fig. 4.1. (a) Map of the Monte Romero mine area (IPB) and plan view of the two mine tailings impoundments. Field pictures of the fly ash-amended experimental plots on the YI (b) and GI (c). The figure also shows a detail of the interface between fly ash and mine tailings of each experimental plot.

4.2.2. Pilot-scale treatment system

An 8 m² experimental plot (4 m x 2 m) was installed in each of the two tailings impoundments in November 2008. Both plots were surrounded with polyethylene sheets down to a depth of 1 m to avoid lateral groundwater circulation, and were covered with a 15 cm top layer of a mixture of 10 wt%

84

fly ash and 90 wt% inert quartz sand as a drain (Fig. 4.1). The fly ash used is a by-product from coal combustion at the Los Barrios power plant located in Cádiz (S Spain; Fig. 4.1). Pérez-López et al. (2007a,c) reported that Los Barrios fly ash is comprised of spherical particles whose mineralogical composition contains mullite (20.8 wt%), quartz (4.5%), lime (4.1%), magnetite (<1%), and mainly a Ca-aluminosilicate glass phase (66.4%). The presence of high alkali concentration contained in the most soluble phases (lime and glass matrix) accounts for the high acid neutralizing potential of the fly ash.

4.2.3. Sampling and preparation

Solid samples from both tailings were collected in two field sampling campaigns; one during the dry season (September 2009) and the other during the rainy season (March 2010). For each sampling, two core samples were taken by means of 60 cm-long polyethylene tubes, one inside and the other outside of each experimental plot. In the laboratory, subsamples of interest were selected, dried at 30 ºC, disaggregated, homogenized and subjected to conventional geochemical and mineralogical analysis. Sampling and conventional analysis of both mine tailings without treatment were previously described in Quispe et al. (2013). In addition, several undisturbed samples were taken in March 2010 from the interface between fly ash and mine tailings. These solid fragments were embedded in epoxy resin to be studied by conventional microscopy techniques and cut into slices of 2-3 mm thickness for synchrotron analysis.

4.2.4. Analytical methods

4.2.4.1. Conventional geochemical and mineralogical analysis

Aqua regia digestion (3:1 HCl-HNO$_3$) was performed to obtain a pseudo-total estimation of element contents, which can be considered as a measure of the maximum potential hazard under long-term weathering or extreme environmental regimes (McGrath and Cunliffe, 1985). In addition, the Community Bureau of Reference (BCR) sequential extraction scheme was carried out to study the mobility of elements; full details can be found elsewhere (Rauret et al., 1999; Sahuquillo et al., 1999). Following the BCR-

85

procedure, elements are speciated into three fractions (Table 4.1 in the Chapter 2): easily-soluble fraction (F1; exchangeable and associated with phases soluble in water or under slightly acidic conditions), reducible fraction (F2; bound to Fe-Mn oxyhydroxides) and oxidizable fraction (F3; bound to sulfides and organic matter). The addition of a fourth step with aqua regia allowed to determine the residual fraction (F4; non-mobile elements strongly bound to crystalline structures of non-silicate minerals). Siliceous material remained undigested after extraction.

Table 4.1. BCR-sequential extraction procedure used for speciation.

Step	Fractions	Extractant (1 g of dry solid)	Shaking time and temperature
F1	Water/acid soluble and exchangeable	40 mL of 0.11 M CH_3COOH	16 h at room temperature (RT)
F2	Reducible	40 mL of 0.5 M $HONH_2HCl$ (pH 2)	16 h at RT
F3	Oxidizable	10 mL of 8.8 M H_2O_2 (pH 2) + 10 mL of 8.8 M H_2O_2 (pH 2), add 50 mL of 1 M $NH_4C_2H_3O_2$ (pH	1 h at RT and 1 h a 85º C, 1 h at 85º C and 16 h at RT
F4	Residual *	10 mL of aqua regia 3:1 (12 M HCl : 15.8 M HNO_3)	Heating on hot plate to dryness

*Digestion of the residual material is not step of the BCR protocol.

Extractants of the geochemical studies were analyzed by inductively coupled plasma-atomic emission spectroscopy (ICP-AES; Thermo Jarrell Ash) and inductively coupled plasma-mass spectroscopy (ICP-MS; Thermo X-Series II) for determination of major and trace elements, respectively. Calibration with sets of standards was performed when the regression coefficient exceeded 0.999. Three laboratory standards were analyzed with every 10 samples to check for accuracy. Furthermore, dilutions from 1:2 to 1:100 were performed to ensure that the concentration of the samples was within the concentration range of the standards. The average measurement error was less than 5%. In addition, quality control of the extraction procedures and reproducibility of results were performed by calculating the recovery as the sum of the four BCR fractions divided by the amount of pseudo-total elements released by aqua regia digestion, expressed as percentage. A very good agreement between the sum of concentrations determined in each sequential extraction step and the pseudo-

86

total digestion by aqua regia was achieved with average recoveries ranging from 85% for Cd to 104% for Ca.

The mineralogical characterization of the samples was carried out by conventional X-ray diffraction (XRD; powder method) using a Bruker diffractometer (model D8 Advanced). Working conditions were slit fixed at 12 mm, Cu Kα monochromatic radiation, 30 mA and 40 kV. Samples were run at a speed of 0.5º 2θ/min (3-65º). Furthermore, carbon-coated polished sections were observed under a JEOL JSM 5410 scanning electron microscope with an energy dispersive system (SEM-EDS; JEOL JSM-5410).

4.2.4.2. Synchrotron-based μ-XRF and μ-XRD techniques

Analyses of micro-X-ray fluorescence (μ-XRF) and micro-X-ray diffraction (μ-XRD) based on synchrotron radiation were performed using the ID18F beamline at the European Synchrotron Radiation Facility in Grenoble (ESRF, France). The applicability of the ID18F beamline to study the element mobility during sulfide oxidation processes has been demonstrated in previous studies (Carbone et al., 2011; 2012). This beamline is a high-energy multi-technique X-ray microscope. Its double-crystal Si-monochromator offers a tunable energy in the 6-28 keV range for optimal excitation conditions for a broad range of elements (Somogyi et al., 2001). In this experiment, the excitation energy was fixed at 28 keV, a wavelength of 0.44279 Å was selected and the beam was focused to 8 μm horizontal × 1.8 μm vertical. A 2-dimensional CCD based X-ray detector (refined detector distance 112.1131 mm) was used to collect X-ray diffraction patterns in transmission mode. The X-ray fluorescence spectra were detected with a Si(Li) detector.

Sample sections were mounted so that the vertical direction was perpendicular to the contact between fly ash and mine tailings. Two-dimensional (2D) maps around the contact were acquired by raster scanning approx. 20 mm (V) x 2.8 mm (H) areas. The layers were laterally homogenous and, hence, three cross-band lines were sufficient for complete characterization. These vertical lines were raster-scanned point-by-point at high spatial resolution with a size-step of around 85 μm, which is congruent with the grain sizes observed by SEM-EDS (Fig. 4.2). The acquisition times were 1 s and 30 s

87

for XRD and XRF measurements, respectively. A total of 663 and 693 analysis points were collected in the samples of the YI and GI, respectively. Debye-Scherrer diffraction rings of the 2D-XRD patterns were unwrapped and integrated versus the azimuthal angle to produce 1D diffraction patterns (ESRF package Fit2D; Hammersley et al., 1996). On the other hand, the XRF spectrum of each pixel of the 2D images was treated with PyMca software and elemental maps were obtained through a batch treatment (Solé et al., 2007).

Multivariate statistical methods were used for the reduction of the μ-XRF data and the extraction of useful information for the metal mobility assessment in both experimental plots. Thus, the large databases of element intensities obtained in each XRF-map were processed by Principal Component Analysis (PCA) with the help of XLSTAT- Pro v7.5.2, an add-on of Microsoft Excel. Pearson correlation coefficient was used as index of similarity. After testing different representation forms, the use of plots showing the loadings of the various geochemical variables on the two first principal components (PC1 and PC2) was considered the most informative and simplest way to display the PCA results.

4.2.4.3. Pore-gas

During the transition from wet to dry season (June 2010), oxygen concentrations in pore-gas inside and outside both fly ash-amended experimental plots were in-situ analyzed in vertical profiles of increasing depth up to water saturation at 10 cm intervals using a portable gas-meter ANAGAS CD98 (Environmental Instruments, Leamington Spa, England) coupled to a steel-rod through a vacuum system. The sensitivity ranges from 0% to 30% ± 0.1% for O_2 concentration. The measurement device includes an integral pump for facilitating the gas circulation.

4.3. RESULTS AND DISCUSSION

Seasonal variations in the IPB correspond to a climate of Mediterranean type, i.e. wet-rainy winters and dry-warm summers, which causes an alternating downward and upward flux of water and solutes according to precipitation and evaporation periods, respectively. In the experimental plots, alkaline solutions

88

interact with acidic solutions at the contact between fly ash and mine tailings. As a result, laterally continuous red-brown hardpans were developed during the operation period (Fig. 4.1). The hardpan is mostly developed inside the fly ash boundary, suggesting that it grows induced by capillary upflow during the dry season. Under SEM-EDS inspection, Fe oxyhydroxysulfates and gypsum occur as microbotryoidal masses and massive aggregates of tabular crystals, respectively, strongly cementing to the rest of minerals and fly ash particles (Fig. 4.2a,b,c). Gypsum also forms within the fly ash levels as massive cement (Fig. 4.2d).
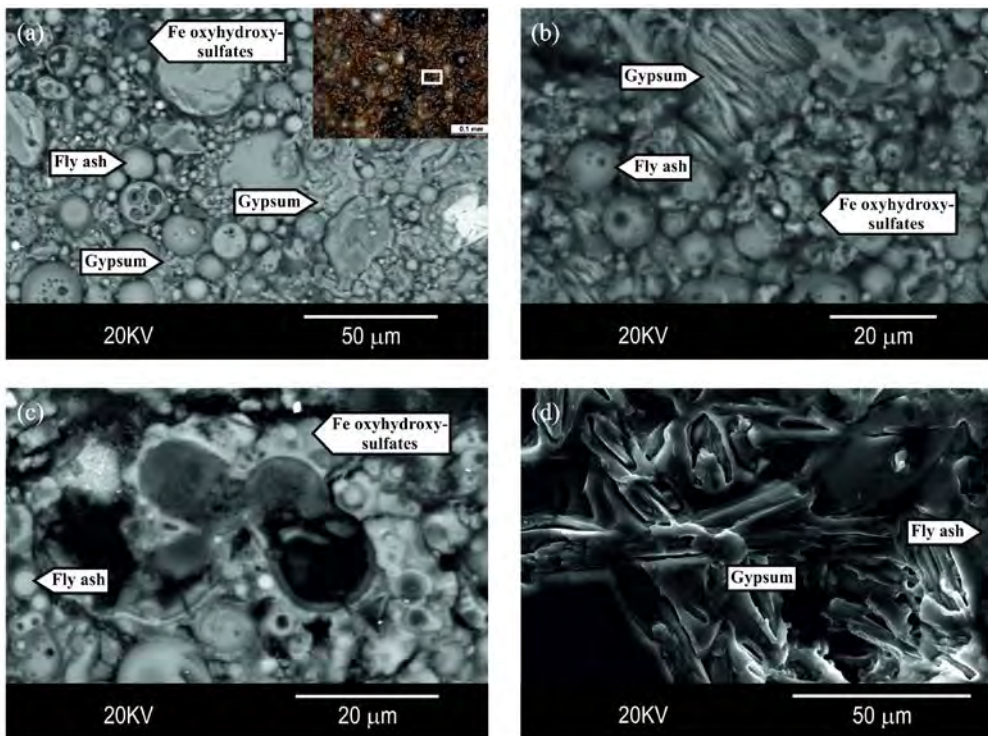
Fig. 4.2. SEM images of Fe oxyhydroxysulfates and gypsum in the hardpan (a,b,c) and gypsum in the fly ash (d). Note the high grade of compaction of particles in both levels. Aggregates of Fe oxyhydroxysulfates occur as pore-filling cement, which is better appreciable by their reddish color in reflected-light optical microscope images (a).

4.3.1. Influence of fly ash on elemental mobility

Element distributions in the fractions of the sequential extraction are given in Tables A1, A4 and A5 of the annex, and percentages are plotted in

Figs. 4.3, 4.4 and 4.5. This paper only shows an overview on results concerning the oxidation of both untreated impoundments; for more information the reader is referred to Quispe et al. (2013). The mineral assemblages that play an active role in the oxidation of both impoundments without treatment include evaporitic sulfate salts, secondary Fe^{3+} oxyhydroxysulfates and sulfides (mainly pyrite), which can be traced from the contents of S and Fe in F1, F2 and F3, respectively (Fig. 4.3). As expected from the mineralogical stratigraphy, soluble sulfate salts are mainly located in the shallowest part of both tailings during the dry season due to the combined effect of capillary rise and precipitation by evaporation; while the content significantly decreases by dissolution during the wet season. Secondary Fe^{3+} oxyhydroxysulfates occur exclusively in the yellowish oxidation layer of the YI (from 0 to 20-25 cm; Fig. 4.3a,b). On the other hand, sulfide minerals are present in the unoxidized zone of the YI (from 20-25 to 350 cm) and throughout the weathering profile of the GI (from 0 to 400 cm). It is worth noting the nearly-total consumption of sulfides in the oxidation front of the YI and the absence of secondary Fe^{3+} phases in the GI (Fig. 4.3c,d).

Fly ash levels of both impoundments contain much higher pseudo-total concentrations of Ca and, to a lesser extent, of Al, Ni and Mn, than untreated mine tailings (Tables A4 and A5 in the annex). Most of the calcium is leached in the easily-soluble fraction (average of 71% for the two levels throughout the year) (Figs. 4.4 and 4.5). The remaining elements display a lower mobility in the environment, with average percentages in the F1 of 6% for Al, and 17% for Ni and Mn. Fly ash levels also show minor contents of other elements, though with high average percentages in the easily-soluble fraction of e.g. Cd (87%), S (84%) and Zn (34%). However, the use of this by-product must not significantly increase contents of these elements already existing in much higher concentration in the leachates of the pyrite sludge (Tables A4 and A5 in the annex).

The zone of interface between fly ash and mine tailings in both experimental plots is locally favorable for the precipitation of elements leached from both materials. Just considering the pseudo-total content, both hardpans massively accumulate As, Fe and S compared to fly ash, and Ca, Mn and Ni compared to mine tailings (Tables A4 and A5 in the annex). Among these

elements, Fe is the main component of the newly-formed phases in the cementation zone. Furthermore, the addition of fly ash affects the dynamic of the mobile fractions involved in the weathering of the mining sludge. In comparison with the untreated mine tailings, there is a significant decrease in the S and, mainly, Fe content associated with soluble sulfate salts in the experimental plots. This decline is much more evident in the shallowest part of both impoundments and during the dry period. Thus, the average content in the F1 from 0 to -15 cm decreases from 81 to 21% for S and from 29 to 3% for Fe in the YI (Fig. 4.3a,b), and from 7 to 3% for S and from 8 to 5% for Fe in the GI (Fig. 4.3c,d).
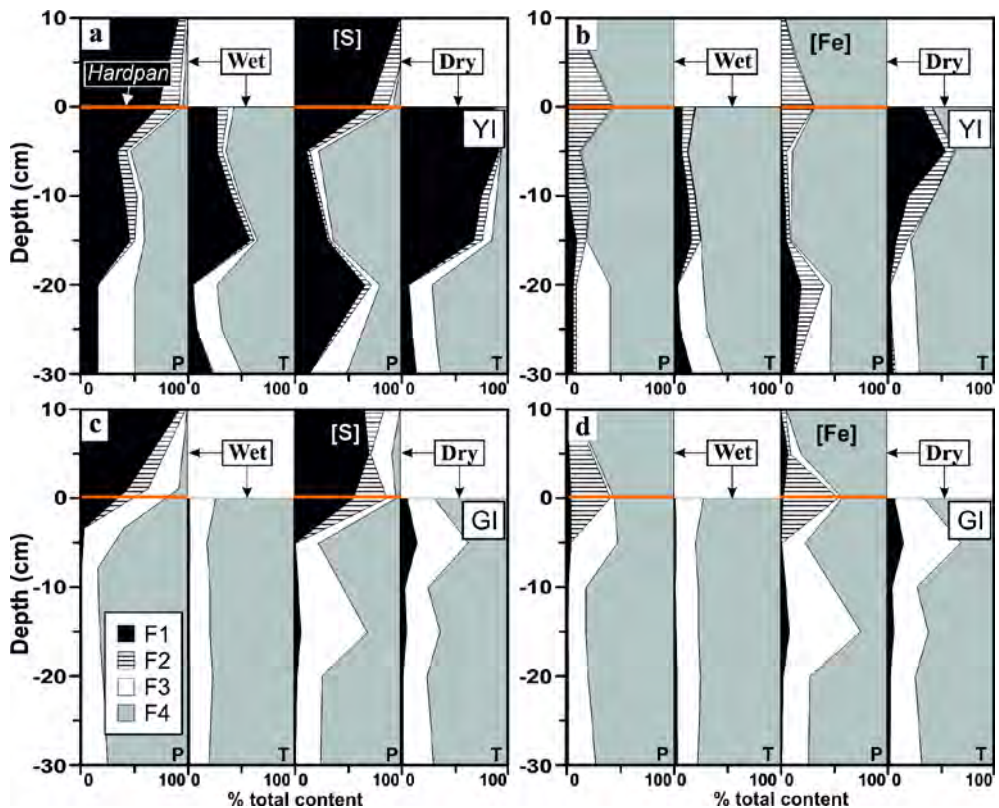
Fig. 4.3. Vertical profiles for the S and Fe percentages extracted in the sequential extraction, both in the experimental plot (P) and in the unreacted tailings (T) of the YI (a,b) and GI (c,d) during the wet and the dry season.

In contrast with this decrease in the easily-soluble fraction, the fly ash amendment involves a generalized increase in the S and Fe content associated with Fe^{3+} oxyhydroxysulfates, especially in the hardpans, with values of up to 18-31% for S and 30-52% for Fe bound to the F2 (Fig. 4.3). These percentages are significantly higher than the ones in the rest of the vertical profile both in the treated and in the untreated impoundments. In the YI, the high contents of secondary Fe^{3+} oxyhydroxysulfates in the shallowest 20 cm part of the untreated mine tailings are responsible for the leaching of up to 5-10% for S and Fe in the F2. Consequently, the increase of this fraction in this zone of the fly ash-amended experimental plot is partially masked. This increase is however specially noticeable in the unoxidized zone of the YI, whose contents pass from <1% up to 3% for S and 11% for Fe in the dry period (Fig. 4.3a,b). On the other hand, the lack of weathering precipitates in the untreated mine tailings of the GI explains the low contents of S and Fe leached in the F2 along the entire weathering profile over all the year (<1%). However, although these percentages do not exceed 1% in the experimental plot, the relative values increase almost double in comparison to the untreated sludge (Fig. 4.3c,d).

Therefore, the result of the fly ash amendment is a redistribution of mobile fractions in the mine tailings: the most bioavailable fraction (F1) decreases together with an increase in a more stable fraction (F2), especially in the hardpan developed in the interface between the fly ash and the mine sludge. This is likely due to the solubilization of sulfate salts followed by a neutralization of the subsequent acidic pore-waters from mining sludge weathering. Such pH increase can account for a fast oxidation, a decrease in the solubility of Fe, and the massive precipitation as secondary oxyhydroxides and/or oxyhydroxysulfates. The observed precipitation of newly-formed phases in the chemically cemented zone occurs in the fly ash part due to a higher porosity than in the mining sludge. This is also indicative of the neutralization process taking place mainly after deeper water rises by evaporation during the dry-warm period. While in the experimental plot of the YI hardpan is located just in the contact, it is important to note that in the GI this rigid crust is developed approx. 1 cm above it (Fig. 4.6). A possible explanation is that the pore-water in the GI is extremely more acidic than in the YI. Accordingly,

upward flow of solutions in the GI requires a longer contact time in the fly ash level to achieve the optimum pH for precipitation of secondary phases.
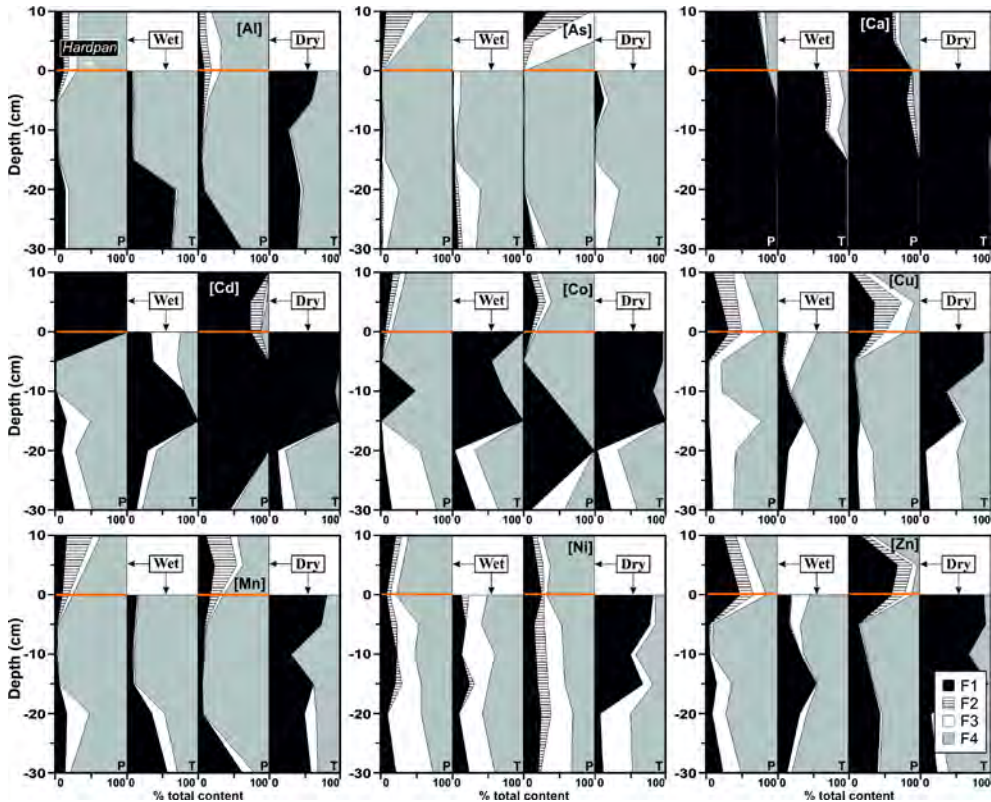
Fig. 4.4. Vertical profiles for Al, As, Ca, Cd, Co, Cu, Mn, Ni and Zn percentages extracted in the sequential extraction, both in the experimental plot (P) and in the unreacted tailings (T) of the YI during the wet and the dry season.

Regarding the fraction bound to sulfides, the percentages of S and Fe extracted in the F3 both in the unoxidized zone of the YI and in the entire profile of the GI are around 25%. These values are roughly similar to those of the experimental plots of both impoundments throughout the year (Fig. 4.3). These findings suggest that sulfide minerals, which are the source of contaminant release, remain apparently unreacted after fly ash treatment. However, this interpretation should be considered with caution because of the short duration of the study in comparison with the dissolution rates of these phases.

93
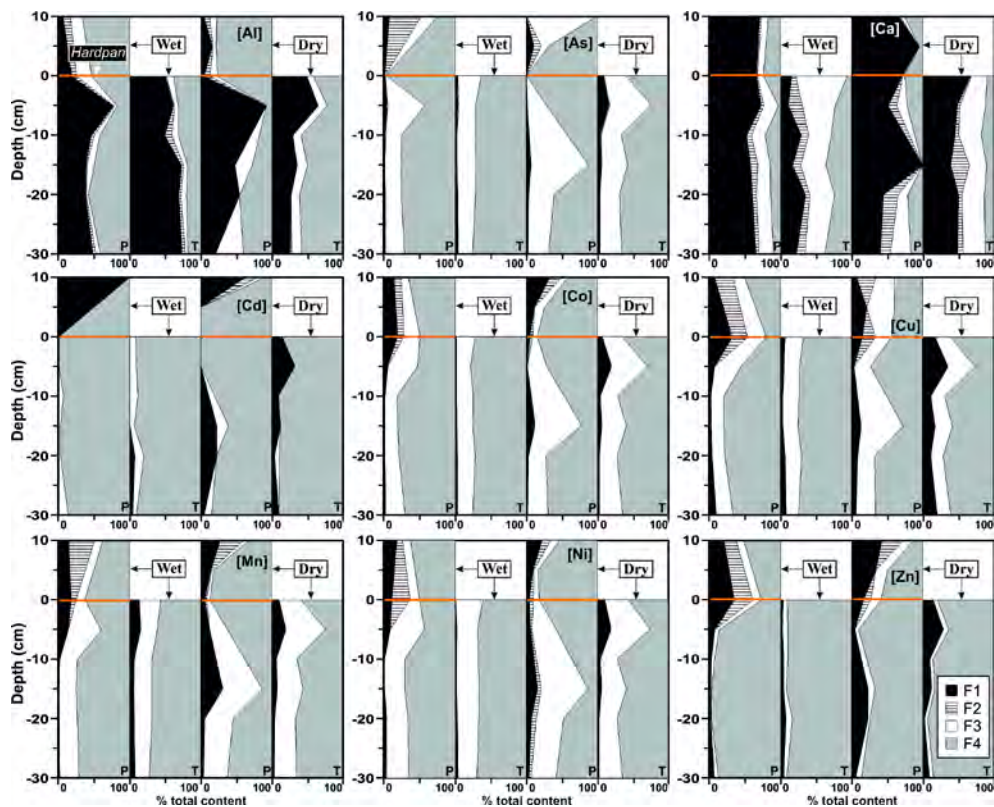
Fig. 4.5. Vertical profiles for Al, As, Ca, Cd, Co, Cu, Mn, Ni and Zn percentages extracted in the sequential extraction, both in the experimental plot (P) and in the unreacted tailings (T) of the GI during the wet and the dry season.

Concerning the mobility of the remaining elements, the most active fraction in both impoundments is the one associated with evaporite salts. During the dry season, the relative and absolute contents of most elements in the shallower 15 cm part of both impoundments decrease significantly in the fly ash-amended experimental plots compared to the untreated mine tailings. Thus, the average percentages of contaminants associated with evaporitic salts in the oxidation front of the YI decrease from 94 to 68% for Co, 87 to 24% for Zn, 70 to 18% for Ni, 68 to 11% for Cu, 62 to 7% for Mn, 48 to 6% for Al and 4 to values below detection limit for As (Fig. 4.4). Furthermore, the decline in the upper level of the GI occurs from 21 to 8% for Cu, 16 to 13% for Zn, 9 to 6% for Co and 8 to 3% for As (Fig. 4.5). For some elements, these decreases are even clearer for absolute contents (Tables A4 and A5 in the

94

annex). Indeed, in the case of Cd in the YI and Al, Cd, Mn and Ni in the GI, although the percentages are kept or even increased within the experimental plots, the absolute concentrations notably diminish with treatment. Towards deeper zones in the dry season and along the whole profile in the wet season, the decrease in mobility is less evident in both impoundments.

4.3.2. Newly-formed phases in the reaction zone

Synchrotron radiation-based micro-characterization techniques were applied to identify the newly-formed phases potentially controlling the contaminant mobility in the reaction zone of both fly ash experimental plots. As already noted, conventional laboratory X-ray sources were used to conduct measurements. However, Cu-Kα XRD patterns of the samples showed only reflections of the minerals of the raw initial substrate (Fig. 4.6). The relatively high background signal and reduced peak intensities in the conventional patterns must be likely due to the amorphous nature of the fly ash glass and the cryptocrystalline size of the newly-formed phases, respectively. Except a small peak at around 11.7° 2θ that could correspond to gypsum, there were no well-defined peaks that allowed the accurate identification of newly-formed phases. Otherwise, μ-XRF-XRD mapping through synchrotron light was very accurate in the mineral identification due to the high energy and spatial resolution.
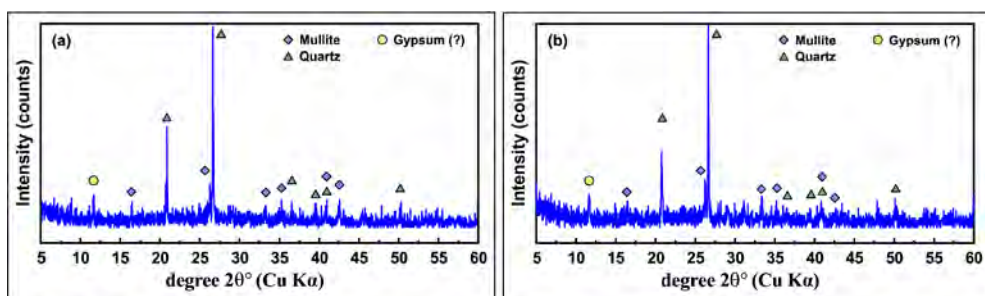
Fig. 4.6. Conventional Cu Kα XRD spectra of the bulk sample of the hardpan zone in both impoundments: (a) YI and (b) GI.

Fig. 4.7 shows the micro-section studied by μ-XRF in the hardpan developed in the contact between fly ash and mine tailings of each

95

experimental plot. A typical X-ray fluorescence spectrum is shown in Fig. 4.7a. The μ-XRF maps confirm that Fe is preferentially accumulated in the hardpan of both experimental plots. From these maps, high Fe intensities are found not only in the hardpan but also in the mine tailings of the GI; high S intensities occur both in the mine tailings and in the hardpan, and at a less extent in the fly ash of both experimental plots; and high Ca intensities appear both in the fly ash and in the hardpan of both experimental plots (Fig. 4.7b,c). Mineral identification of newly-formed precipitates was made by analyzing relationships through PCA among the fluorescence intensity of elements in the 663 and 693 spectra of μ-XRF of the YI and GI, respectively, along with representative μ-XRD patterns of each zone (mine tailings, fly ash and hardpan). Note that spectra of μ-XRD are characterized by a good signal-to-noise ratio (Fig. 4.8) in relation to conventional XRD spectra (Fig. 4.6).

PCA analyses applied to the levels of mine tailings and fly ash in both experimental plots allow identifying the phases responsible for the release of elements to solution during weathering. Thus, in the zone of mine tailings of the YI, the two first principal components account for 60.43% of the total variance in the data. In this zone, Fe is the predominant element and its spatial distribution in the μ-XRF map is highly correlated with Cu (R^2 = 0.78), Zn (R^2 = 0.71), Pb (R^2 = 0.69) and As (R^2 = 0.64). In fact, these elements are strongly grouped with positive loading upon the first principal component axis (Fig. 4.8a). However, μ-XRD spectra reveal only the presence of H_3O-jarosite, quartz and muscovite. The lack of correlation between S and Fe intensities suggests that H_3O-jarosite appears as a minor constituent and may not be responsible for the control of the mobility of Fe in the mine tailings. The group associated with Fe in the PCA may correspond to the abundant occurrence of poorly-crystalline secondary oxyhydroxysulfates (undetectable by XRD) predefined by Quispe et al. (2013), which may contain most of these elements in the oxidation front of the YI. The contribution of this type of relatively amorphous iron precipitates to the diffraction effects could be minor and masked by well-crystallized minerals even with synchrotron radiation (Shimizu et al., 2011).
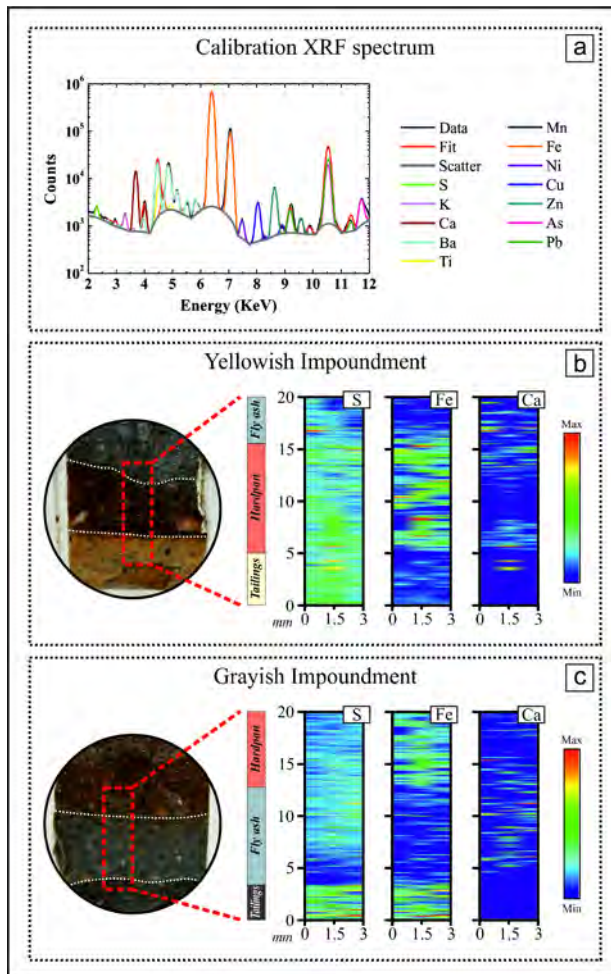
Fig. 4.7. Micro cross-sections analyzed in the samples of the interface between fly ash and mine tailings by synchrotron-based μ-XRF: (a) calibration spectrum fitted with PyMca software. Elemental micro-distribution maps for S, Fe and Ca in the YI (b) and GI (c). For interpretation of colors, the reader is referred to the web version of this paper.

On the other hand, the analysis of the mine tailings of the GI showed that the two first principal components account for 51.66% of the total variance in the data. Sulfur and iron are the predominant elements in this zone and their spatial correlation in the μ-XRF map is evident (R^2 = 0.77). This is in agreement with the elevated amount of pyrite (up to 80%) in this mining waste, as also pointed out by the μ-XRD spectra (Fig. 4.8a). The fact that S and Fe appear in the same quadrant of the PCA along with Cu, As, Pb and Zn

97

may imply that pyrite and other minor sulfides control the release by oxidation of these elements. Indeed, the presence of sphalerite, chalcopyrite and galena was reported in earlier studies (Acero et al., 2007).

In the two fly ash levels, the sum of both principal components accounts for 73.71% and 55.26% of the total variance of the data for the YI and GI, respectively. The main elements are grouped into two well-defined areas in the PCA (Fig. 4.8b). Most of them (Fe, Mn, Ni, Pb, As, Zn and Cu) are grouped along the first principal component axis, suggesting that their potential release is controlled by the same phase. Among the crystalline phases identified by μ-XRD, only magnetite may contain some of these elements but its presence is largely insignificant. As stated before, fly ash is mostly made up of a glass matrix whose relatively rapid dissolution must be source of alkaline solutions containing not only these minor elements but also S and, mainly, Ca (Pérez-López et al., 2009; Quispe et al., 2012). However, S and Ca are highly mobile in solution and their concentrations became so high that the leachates are supersaturated with respect to gypsum, which precipitates according to the μ-XRD spectra and accounts for their association in a separate group closer to the second principal component axis in the PCA (Fig. 4.8b). This is also in agreement with the SEM-EDS observations.

The plot of the two first principal components in the hardpan of both impoundments accounts for 63.58% for YI and 58.90% for GI of the total variance in the data. Both components define associations that are consistent with the μ-XRD spectra. The newly-formed crystalline minerals that massively precipitate in the reaction zone are gypsum and jarosite, which may explain the groupings of S-Ca and S-As in the PCA, respectively (Fig. 4.8c). Unlike the jarosite present in the mine sludge of the YI, the newly-formed jarosite in the hardpan appears to strongly control As mobility. The preferential Fe precipitation in this zone must occur as a newly-formed phase of poorly-crystalline nature again not detectable by XRD (Fig. 4.8c), which may correspond to the Fe oxyhydroxysulfates extracted in the F2 of the sequential extraction. These poorly-crystalline Fe-rich aggregates must be present in higher amounts than jarosite, which would explain that Fe is not grouped with S o As in the PCA. In addition, the spatial distribution of Fe is highly correlated with Mn (R^2 = 0.93 for the YI and 0.84 for the GI), Ni (R^2 = 0.62

for the YI and 0.58 for the GI) and Pb (R^2 = 0.58 for the YI and 0.66 for the GI). Accordingly, this coupling suggests that the phase responsible for Fe removal is also responsible for the removal of these elements in the reaction zone.

The plot of the first and third or fourth principal component in the hardpan of both experimental plots also accounts for high total variance in the data, similar to that observed between the first two factors (data not shown). In these plots, it is certainly observed that S is associated more closely with the Fe group and just midway between Ca and As. This clearly confirms the existence of gypsum and jarosite, which control Ca and As respectively, and the presence of S in the poorly-crystalline Fe oxyhydroxysulfates.

The newly-formed phases identified by synchrotron in the hardpan and their role in the element retention are fully consistent with the SEM-EDS results and with the preferential accumulation of As, Ca, Fe, Mn, Ni and S that was previously defined from the pseudo-total concentrations. Jarosite was not found as euhedral crystals under microscope probably because it occurs as microcrystalline cement along with the remaining amorphous Fe-rich phases. Arsenic immobilization by jarosite is especially significant, since this element is extracted in the residual fraction of the sequential extraction and, therefore, it can be considered relatively immobile under usual environmental conditions (Tables A4 and A5 in the annex). This suggests that jarosite has a high crystallinity and As is structurally incorporated into the crystalline lattice, possibly as AsO_4 replacing to SO_4 (Paktunc and Dutrizac, 2003). Well-crystallized jarosite, as revealed by relatively strong XRD peaks, could become highly insoluble and survive to the reducible step of the sequential extraction (Martínez-Sánchez et al., 2008; Hayes et al., 2009).

Metals such as Mn and Ni are associated with Fe oxyhydroxysulfates in the hardpan and, therefore, their mobility is also restricted under the oxidizing conditions typical of these environments. The association of Pb with Fe oxyhydroxysulfates according to the μ-XRF observations is also consistent with those found in natural cemented layers (Alakangas and Öhlander, 2006). On the other hand, elements such as Zn and Cu are not locally accumulated in the hardpan relatively to the fly ash or to the mining sludge according to their

pseudo-total contents. Thus, the newly-formed phases in this zone must weakly control the mobility of these elements. In fact, although close to the oxyhydroxysulfates group in the PCA (Fig. 4.8c), Fe is much less correlated to Zn and Cu ($R^2 < 0.50$) than to other elements.
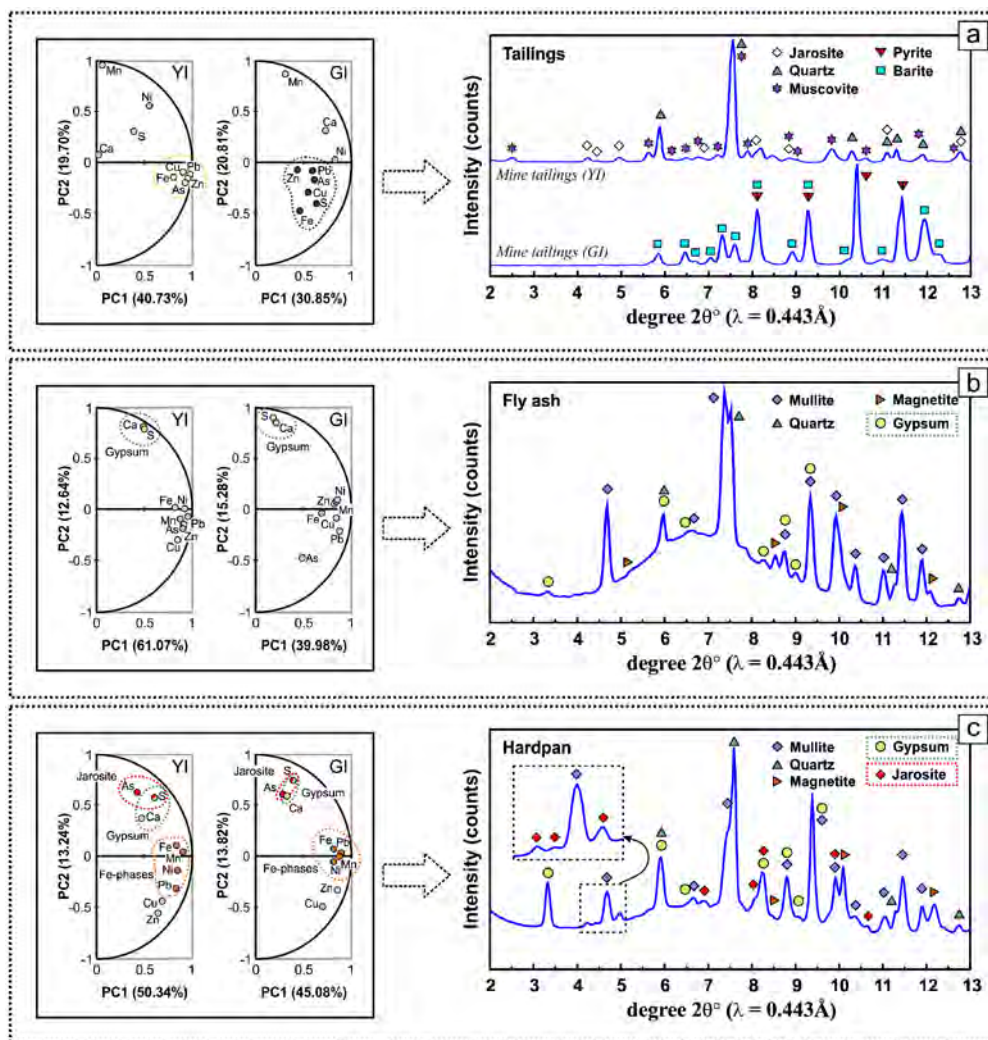
Fig. 4.8. Projections of the element intensities obtained by μ-XRF mapping on a plot of the two first principal components from the PCA results and synchrotron-based μ-XRD spectra integrated with Fit2D package. Similar μ-XRD spectra were obtained for all analysis points of the scan 2D maps within each zone, i.e. mine tailings in the YI and in the GI (a), and fly ash (b) and hardpan (c) in both impoundments and, thus, only a representative example is shown.

100

4.3.3. Impact of hardpan on oxygen diffusivity

The water table was located during sampling at depths of 40 cm and 60 cm in the YI and GI, respectively (Fig. 4.9). In the unsaturated zone of both tailings without treatment, pore-gas oxygen concentrations decrease from 20% at the surface (atmospheric conditions) until complete exhaustion at the water table depth due to sulfide oxidation. Measurements were performed close to the dry season and, therefore, sulfide surfaces are almost water-free and available for oxidation. Consequently, oxygen is rapidly depleted in the first centimeters especially in the GI, which displays higher pyrite percentages in this shallowest part. This trend is different in both fly ash-amended plots. Whereas pore-gas oxygen concentrations in the fly ash levels are typical of atmospheric conditions, they are around 11-12% in the mine tailings just below the hardpan, approx. 50% less than in the untreated mine tailings at the same depth (Fig. 4.9). The fly ash cover contains 90 wt% of quartz sand and, despite gypsum precipitation in the pores, a priori must not be a barrier to oxygen diffusion. In addition, no oxygen-consuming reactions were identified in the fly ash. It is therefore reasonable to assume that the partial depletion of oxygen in the pore-gas is due to this chemically cemented zone. Thus, the development of the hardpan partially isolates the mine tailings from the weathering.

Below the hardpans, oxygen concentrations also decrease slightly but always show higher values for the equivalent depths outside the treatment (Fig. 4.9). In fact, unlike in both untreated mine tailings, pore-gas oxygen is not completely consumed at the water table depth (ca. 3% in the YI and 6% in the GI). This could be attributed to the fast precipitation of Fe oxyhydroxysulfates over the sulfide grains induced by the alkaline conditions, process known as microencapsulation. These Fe-bearing phases, which rapidly grow in thickness, would prevent oxidizing agents from reaching the surfaces and, thus, would attenuate pyrite oxidative dissolution (Pérez-López et al., 2007c). The coating formation on pyrite grains in the current study is congruent with the increase in the F2 and the unreacted maintenance of the F3 of the sequential extraction during the fly ash treatment. The microencapsulation process seems to operate over shorter time scales than the hardpan formation. At pilot-scale field experiments, although the hardpan is forming on both fly ash-amended plots,

it still seems to be too narrow to completely prevent oxygen diffusion. However, the oxygen accessing the system is consumed to a lesser extent that without any treatment because sulfides are probably undergoing microencapsulation.
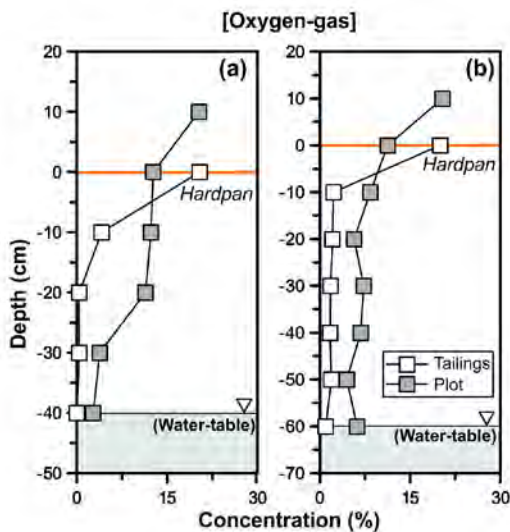
Fig. 4.9. Vertical profiles for pore-gas oxygen concentration, both inside and outside each experimental plot, in the YI (a) and GI (b).

4.4. CONCLUSIONS

This paper describes pilot-scale experiments to evaluate the performance of a cover of coal combustion fly ash to mitigate acid mine drainage being generated by two sulfide mine tailings impoundments at the Monte Romero mining district (SW Spain, Iberian Pyrite Belt). Sequential extraction results showed that the fly ash cover was effective in reducing element mobility and the potential associated pollution. Water-soluble elements (mainly S, Fe and Ca) were locally accumulated by preferential precipitation in the interface zone between fly ash and mine tailings. The high abundance of newly-formed phases and the intense cementation produced in this interface by the formation of a relatively hard crust or hardpan, significantly reduced the permeability and self-isolated materials from one another.

Micro-X-ray fluorescence (µ-XRF) and micro-X-ray diffraction (µ-XRD) were used to reveal spatially resolved information about geochemical and

102

mineralogical characteristics of the newly-formed precipitates. Poorly-crystalline oxyhydroxysulfates, jarosite and gypsum were the most important cementing agents in the hardpan, and high amounts of gypsum also occurred in the fly ash layer. The hardpan acted as a sink for other minor dissolved elements. Thus, the spatial distribution of poorly-crystalline Fe oxyhydroxysulfates was highly correlated to Mn, Ni and Pb, which indicated that this phase also controlled the uptake of these metals in solution; whereas jarosite seems to be responsible for arsenic immobilization. The decrease in porosity in the chemically cemented zone also acted as a physical barrier to the weathering agents. In addition, the Fe-bearing precipitates presumably formed a coating over the sulfide grains, which is known as microencapsulation.

As a conclusion, the development of the hardpan decreased the oxygen diffusion to the surface of sulfide grains, which minimized oxidation and thus production of acid mine water. In addition, the precipitation of secondary phases caused the decrease in metal mobility in both tailing piles, i.e., metals passed from being contained in the available fraction of mine wastes to being in the reducible fraction (more-stable in oxidizing conditions), or even in the residual fraction. Although some metals such as Cu and Zn were weakly retained by newly-formed phases, their mobility also decreased as a consequence of the isolation of sulfides to oxidation. This mechanism of inhibition, along with the sulfide microencapsulation previously observed in laboratory experiments (Pérez-López et al. 2007a,c), strongly recommends the use of fly ash in a cover on tailings impoundments as an effective treatment strategy to inhibit weathering process, and hence, release of contaminants into the environment.

CAPÍTULO 5. CONCLUSIONES

CONCLUSIONES GENERALES

El depósito de determinados residuos derivados de la actividad minera y de la industria energética puede suponer un riesgo potencial para el medioambiente y la salud humana. En numerosas ocasiones, no se realiza una correcta caracterización preventiva del potencial de contaminación y, mucho menos, no se establece ninguna medida para impedir su meteorización. Es de especial interés mencionar los elevados volúmenes de residuos producidos en la flotación de menas metálicas o carbón, así como aquellos generados en la combustión del carbón en centrales térmicas. Por un lado, los residuos de flotación se depositan en balsas mineras, las cuales están constituidas en gran parte por partículas de sulfuros cuya oxidación produce un lixiviado extremadamente ácido y elevada carga de contaminantes, denominado drenaje ácido de mina (AMD). Por otro lado, los residuos de la combustión del carbón (cenizas volantes y cenizas de fondo) son fuertemente alcalinos y a menudo se almacenan expuestos a meteorización en las proximidades de las centrales térmicas y/o se reciclan como material de construcción sin ningún control de los contenidos tóxicos.

El principal propósito de esta Tesis Doctoral es caracterizar el comportamiento de las balsas mineras de flotación y los residuos de combustión del carbón como fuente de contaminantes bajo diferentes escenarios de meteorización. La idea final sería aprovechar el carácter alcalino de los residuos de combustión del carbón para mitigar la contaminación ácida generada por las balsas de flotación mediante experiencias a escala piloto de campo en una de las principales regiones productoras de AMD, la Faja Pirítica Ibérica (FPI). La utilización de un residuo para neutralizar a otro residuo reduciría los costes de tratamiento. A este respecto, las principales conclusiones de este trabajo en orden de desarrollo se presentan a continuación.

La primera parte de esta Tesis estudia el potencial de impacto para el medioambiente y la salud humana, derivado del almacenamiento, transporte y el posible uso como material de construcción, de los sub-productos de combustión de carbón en la central térmica de Santa Catarina (Brasil). Los resultados se publicaron en el artículo: **Changes in mobility of hazardous elements during coal combustion in Santa Catarina power plant (Brazil)** (Fuel 94 (2012) 495-503). Las conclusiones de este trabajo fueron:

-   Basado en el análisis químico total, aproximadamente el 100% de los elementos trazas existentes en el carbón se transfieren a las cenizas residuales durante el proceso de combustión.

-   La emisión de contaminantes volátiles a la atmósfera en la central térmica es prácticamente nula. Aunque se produce la volatilización de los elementos en la caldera de combustión, la mayoría condensan y se depositan sobre las partículas de cenizas volantes.

-   Sin embargo, la combustión del carbón altera la movilidad de los elementos trazas. Las cenizas residuales presentan concentraciones más altas de la mayoría de los elementos que el carbón original en la fracción de metales fácilmente soluble en agua; es decir, los contaminantes más tóxicos para el medioambiente.

-   Este trabajo propone una metodología para evaluar el riesgo ambiental de contaminación de la central térmica. Las cantidades totales de contaminantes móviles asociados a los residuos de combustión producidos anualmente son aproximadamente: 2551 t de Al, 1495 t de Fe, 152 t de Mn, 19 t de As, 11 t de Zn, 8.1 t de Cr, 6.0 t de Cu, 1.6 t de U, 1.5 t de Pb y 20 kg de Th.

-   La fracción fácilmente soluble contiene alrededor del 65% de Mn; 30-40% de Zn, Cr, Al y U; 25% de Cu; 10% de Fe y As; y 1% de Pb. Es por tanto recomendable la implementación de medidas de control de las impurezas tóxicas presentes en estos residuos antes de su almacenamiento o reutilización como material de construcción.

La segunda parte de esta Tesis se centra en el estudio del modelo conceptual de oxidación y generación de AMD en dos balsas abandonadas de lodos piríticos en el distrito minero de Monte Romero (FPI). Los resultados se dieron a conocer mediante el artículo: **The role of mineralogy on element mobility in two sulfide mine tailings from the Iberian Pyrite Belt (SW Spain)** (Chemical Geology 345 (2013) 119-129). Las conclusiones de este trabajo fueron:

- La meteorización se produce bajo un clima semiárido, lo cual determina la existencia de dos direcciones alternantes de flujo y transporte de agua y solutos: ascendente y descendente de acuerdo a periodos de evaporación y lluvias, respectivamente.

- Los elementos liberados por la oxidación de los sulfuros son móviles en condiciones ácidas y se transportan a la superficie de ambas balsas por capilaridad en la estación seca; donde se concentran por evaporación y precipitan como sales sulfatadas solubles que retienen temporalmente Cd, Co, Zn, Ni, Cu y Mn. Sin embargo, las lluvias durante la estación húmeda lavan estas sales y los contaminantes se liberan de nuevo en solución.

- El lodo minero de ambas balsas se diferencia en el contenido de pirita que presentan en los primeros 50 cm; una balsa contiene aproximadamente un 30% (balsa amarilla) y la otra aproximadamente un 80% (balsa gris).

- En la zona superficial de la balsa amarilla, el aumento del pH del agua de poro a un valor aproximado de 3 por la dilución durante los eventos de lluvia provoca la sobresaturación y precipitación de productos secundarios de Fe^{3+} (jarosita, goethita o schwertmannita). Estas fases son responsables del color amarillento de la zona superficial de esta balsa. Además, este nivel superior está empobrecido en sulfuros debido a los procesos de oxidación que los ha consumido. La precipitación de oxihidroxisulfatos de Fe^{3+} junto con la coprecipitación y adsorción de elementos trazas parece reducir la carga contaminante durante periodos húmedos con respecto a periodos secos.

- En la balsa gris, no precipitan productos secundarios de la oxidación debido a que el pH del agua de poro es extremadamente ácido durante ambas estaciones. Las soluciones permanecen subsaturadas en oxihidroxisulfatos de Fe^{3+} durante todo el año y los elementos se mantienen en solución. La falta de precipitación de fases de hierro explicaría la ausencia del nivel oxidado amarillento en la parte superficial y, por tanto, el incremento de la carga contaminante que se lixivia hacia el nivel freático.

- El proceso de la oxidación en ambas balsas es diferente incluso bajo condiciones climáticas idénticas debido a que está controlado por el contenido superficial de pirita. El mayor porcentaje de pirita en la balsa gris implica un mayor grado de oxidación y, por lo tanto, la producción de lixiviados con pH más bajos y mayor carga de contaminantes durante todo el año.

- A pesar de su aspecto aparentemente no oxidado, la balsa gris no retiene el contenido de contaminantes por precipitación de oxhidroxisulfatos de Fe^{3+} y, por tanto, su carga contaminante puede ser evacuada por las aguas meteóricas y afectar al medioambiente en una mayor magnitud que la carga producida en la balsa amarilla.

La tercera parte de la Tesis muestra los resultados de la implantación de dos parcelas experimentales a escala piloto de campo para el tratamiento del AMD producido por las dos balsas de lodo minero de Monte Romero usando una cubierta de cenizas volantes generadas por combustión del carbón. Los resultados se publicaron en el artículo: **Formation of a hardpan in the co-disposal of fly ash and sulfide mine tailings and its influence on the generation of acid mine drainage** (Chemical Geology 355 (2013) 45-55). Las conclusiones de este trabajo fueron:

- Mediante el método de extracciones secuenciales se puede comprobar que el uso de la cubierta de cenizas volantes es eficaz reduciendo la movilidad de los elementos y el potencial de contaminación asociado a los lodos piríticos.

110

- La fracción de elementos solubles en agua (principalmente S, Fe y Ca) precipita localmente en la interfase entre las cenizas volantes y el lodo minero. Con el tiempo, la intensa cementación por la precipitación preferencial de fases neoformadas promueve el desarrollo de una costra dura o hardpan, lo que reduce significativamente la permeabilidad y autosella al lodo minero.

- Oxihidroxisulfatos pobremente cristalinos, jarosita y yeso son los principales agentes cementantes en el hardpan. Además, el yeso precipita masivamente en la capa de cenizas volantes. El hardpan actúa como sumidero de otros elementos disueltos tales como As, Mn, Ni y Pb. Estos resultados se obtuvieron mediante la caracterización química y mineralógica del hardpan usando micro-fluorescencia y micro-difracción de rayos X con radiación sincrotrón.

- La formación del hardpan actúa como una barrera física a los agentes meteorizantes y, por tanto, reduce los procesos de oxidación de sulfuros y la liberación de contaminantes al medioambiente circundante.

BIBLIOGRAFÍA

BIBLIOGRAFÍA

Acero, P., Ayora, C., Carrera, J. (2007a). Coupled thermal, hydraulic and geochemical evolution of pyritic tailings in unsaturated column experiments. Geochimica et Cosmochimica Acta 71, 5325-5338.

Acero, P., Ayora, C., Carrera, J., Saaltink, M.W., Olivella, S. (2009). Multiphase flow and reactive transport model in vadose tailings. Applied Geochemistry 24, 1238-1250.

Acero, P., Cama, J., Ayora, C. (2007b). Sphalerite dissolution kinetics in acidic environment. Applied Geochemistry 22, 1872-1883.

Akcil, A., Koldas, S., (2006). Acid Mine Drainage (AMD): causes, treatment and case studies. Journal of Cleaner Production 14(12-13), 1139-1145.

Anderson, M., Elliott, M., Hickson, C. (2001). Factory Scale Proving Trials Using Combined Mixtuesof Three By-Product Wastes (Including Incinerated Sewage Sludge Ash) in Clay Buildings Bricks. International Workshop on Novel Products from Combustion Residues: Opportunities and Limitations. Morella (Spain) 7th June 325-334.

Andres, A., Ortiz, I., Viguri, J.R., Irabien, A. (1995). Long-term Behaviour of Toxic Metals in Stabilized Steel Foundry Dusts. Journal of Hazardous Materials 40, 31-42.

Asta, M.P., Ayora, C., Román-Ross, G., Cama, J., Acero, P., Gault, A.G., Charnock, J. M., Bardelli, F. (2010). Natural attenuation of arsenic in the Tinto Santa Rosa acid stream (Iberian Pyritic Belt, SW Spain): The role of iron precipitates. Chemical Geology 271, 1-12.

Ball, J.W., Nordstrom, D.K. (1991). User's manual for WATEQ4F, with revised thermodynamic data base and test cases for calculating speciation of major, trace, and redox elements in natural waters. US Geological Survey Open-File p. 91-183.

Banks, D., Younger, P.L., Arnesen, R.T., Iversen, E.R., Banks, S.B. (1997). Mine-water chemistry: the good, the bad and the ugly. Environmental Geology 32, 157–174.

Bernd, G.L. (2007). Mine Wastes: Characterization, Treatment, Environmental Impacts. Springer Berlin Heidelberg New York 2º Ed.

Bigham, J.M., Nordstrom, D.K. (2000). Iron and aluminum hydroxysulfates from acid sulfate waters, in: Alpers, C.N., Jambor, J.L., Nordstrom, D.K. (Eds.), Sulfate Minerals: Crystallography, Geochemistry, and Environmental Significance. Reviews in Mineralogy and Geochemistry, Mineralogical society of America, Chantilly, Virginia 40, 351-403.

Bigham, J.M., Schwertmann, U., Traina, S.J., Winland, R.L., Wilf, M. (1996). Schwertmannite and the chemical modeling of iron in acid sulfate waters. Geochimica et Cosmochimica Acta 60, 2111-2121.

Blowes, D.W., Jambor., J.L. (1990). The pore-water geochemistry and the mineralogy of the vadose zone of sulfide tailings, Waite Amulet, Quebec, Canada. Applied Geochemistry 5, 327-346.

Blowes, D.W., Ptacek, C.J., Benner, S.G., McRae, C.W.T., Bennett, T.A., Puls, R.W. (2000). Treatment of inorganic contaminants using permeable reactive barriers. Journal of Contaminant Hydrology. 45, 123-137.

Blowes, D.W., Ptacek, C.J., Jambor, J.L., Weisner, C.G. (2004). The geochemistry of acid mine drainage. In: Lollar, B.S., Holland, H.D., Turekian, K.K. (Eds.): Treatise on Geochemistry. Environmental Geochemistry 9, 149-204.

Blowes, D.W., Reardon, E.J., Jambor, J.L., Cherry J.A. (1991). The formation and potential importance of cemented layers in inactive sulfide mine tailings. Geochimica et Cosmochimica Acta 55, 965-978.

Brown, M., Barley, B., Wood, H. (2002). Minewater treatment: technology, application and policy. International Water Association Publishing.

Buckley, A.N., Woods, R.W. (1987). The surface oxidation of pyrite. Applied Surface Science 27, 437-452.

Cánovas, C.R., Olias, M., Nieto, J.M., Sarmiento, A.M., Ceron, J.C. (2007). Hydrogeochemical characteristics of the Tinto and Odiel Rivers (SW Spain). Factors controlling metal contents. Science of the Total Environment 373(1), 363-382.

Caraballo, M.A., Macías, F., Rötting, T.S., Nieto, J.M., Ayora, C. (2011). Long term remediation of highly polluted acid mine drainage: A sustainable approach to restore the environmental quality of the Odiel river basin. Environmental Pollution 159, 3613-3619.

Caraballo, M.A., Rötting, T.S., Macías, F., Nieto, J.M., Ayora, C. (2009). Field multi-step limestone and MgO passive system to treat acid mine drainage with high metal concentrations. Applied Geochemistry 24, 2301-2311.

Carbone, C., Marescotti, P., Lucchetti G., Martinelli, A., Basso, R., Cauzid, J. (2012). Migration of selected elements of environmental concern from unaltered pyrite-rich mineralizations to Fe-rich alteration crusts. Journal of Geochemical Exploration 114, 109-117.

Carbone, C., Marescotti, P., Lucchetti, G., Cauzid, J., Chalmin, E. (2011). Application of synchrotron radiation-based techniques (μ-XRD, μ-XRD, and μ-XANES) to study Fe-rich hardpans within waste-rock dump. Neues Jahrbuch für Mineralogie 188, 21-30.

Chermak, J.A., Runnells, D.D. (1997). Development of chemical caps in acid rock drainage environments. Mining Engineering (Littleton, Colorado) 49(6), 93-97.

Clarke, L.B. (1993). The fate of trace elements during coal combustion and gasification: an overview. Fuel 72, 731-736.

Crawford, R., Ralston, J. (1988). The influence of particle size and contact angle in mineral flotation. International Journal of Minerals Processing 23, 1-24.

Crozier, R.D. (1992). Flotation: Theory, Reagents and Testing, Pergamon Press, Oxford.

Delany, J., Lundeen, S. (1990). The LLNL thermodynamic database. Tech. Rep. Technical Report UCRL-21658, Lawrence Livermore National Laboratory.

Delgado, J., Sarmiento, A.M., Condesso de Melo, M.T., Nieto, J.M. (2009). Environmental impact of mining activities in the Southern sector of the

Guadiana basin (SW of the Iberian Peninsula). Water, Air, and Soil Pollution 199, 323-341.

Dermatas, D., Meng, X. (2003). Utilization of fly ash for stabilization/solidification of heavy metal contaminated soils. Engineering Geology 70(3-4), 377-394.

Dold, B., Fontboté, L. (2001). Element cycling and secondary mineralogy in porphyry copper tailings as a function of climate, primary mineralogy, and mineral processing. Journal of Geochemical Exploration 74, 3-55.

Dold, B., Fontboté, L. (2002). A mineralogical and geochemical study of element mobility in sulfide mine tailings of Fe oxide Cu-Au deposits from the Punta del Cobre belt, northern Chile. Chemical Geology. 189, 135-163.

ECOBA (2011). European association for Use of The By-products of Coal-Fired Power-Stations. www.ecoba.com.

Evangelou, V.P. (1995). Pyrite Oxidation and its Control: Solution Chemistry, Surface Chemistry, Acid Mine Drainage (AMD), Molecular Oxidation Mechanisms, Microbial Role, Kinetics, Control, Ameliorates and Limitations, Microencapsulation. CRC Press, Boca Raton, FL.

Evangelou, V.P., Zhang, Y.L. (1995). A review: pyrite oxidation mechanisms and acid mine drainage prevention. Critical Reviews in Environmental Science and Technology 25(2), 141-199.

Farah, A., Hmidi, N., Moskalyk, R., Amaratunga, L.M., Tombalakian, A.S. (1997). Numerical modelling of the effectiveness of sealants in retarding acid mine drainage from mine waste rock. Canadian Metallurgical Quarterly 36(4), 241-250.

Fernández, A.M., Baeyens, B., Bradbury, M., Rivas, P. (2004). Analysis of the porewater chemical composition of a Spanish compacted bentonite used in an engineered barrier. Physics and Chemistry of the Earth Parts A/B/C 29, 105-118.

Fernández-Martínez, A., Cuello, G.J., Johnson, M.R., Bardelli, F., Román-Ross, G., Charlet, L., Turrillas, X. (2008). Arsenate Incorporation in

Gypsum Probed by Neutron, X-ray Scattering and Density Functional Theory Modeling. The journal of physical chemistry A 112, 5159-5166.

Fernández-Remolar, D., Gómez-Elvira, J., Gómez, F., Sebastián, E., Martín, J., Manfredi, J.A., Torres, J., González Kesler, C., Amils, R. (2004). The Tinto River, an extreme acidic environment under control of iron, as an analog of the Terra Meridiani hematite site of Mars. Planetary and Space Science 52, 239-248.

Finch, J.A., Dobby, G.S. (1990). Column Flotation, Pergamon Press, Oxford.

Ghosh, T. (1997). Fly Ash as Land Fill & Structural Fill Material within the Metropolitan Area of Calcutta. International Ash Symposium, Lexington, Kentucky 212-220.

Goñi, S., Lorenzo, P., Hernández, M.S. (1997). The role of the fly aluminous component on the durability of the portland fly ash pastes in sulfated medium. Part i-characterization of the solid phase, 4th CANMET (aci international conference on durability of concrete) Sidney, Australia.

Goodarzi, F. (2006). Characteristics and composition of fly ash from Canadian coal-fired power plants. Fuel 85, 1418-1427.

Graupner, T., Kassahun, A., Rammlmair, D., Meima, J.A., Kock, D., Furche, M., Fiege, A., Schippers, A., Melcher, F. (2007). Formation of sequences of cemented layers and hardpans within sulfide-bearing mine tailings (mine district Freiberg, Germany). Applied Geochemistry 22, 2486-2508.

Gunsinger, M.R., Ptacek, C.J., Blowes, D.W., Jambor, J.L., Moncur, M.C. (2006). Mechanisms controlling acid neutralization and metal mobility within a Ni-rich tailings impoundment. Applied Geochemistry 21, 1301-1321.

Gurgueira, S., Lawrence, J., Brent, C., Krishna, M., Gonzalez-Flecha, B. (2002). Rapid increases in the steady-state concentration of reactive oxygen species in the lungs and heart after particulate air pollution inhalation. Environmental Health Perspectives 110, 749-755.

Gurmendi, A.C. (2007). The Mineral Industry of Brazil. US Geological Survey Minerals Yearbook.

Hammarstrom, J.M., Seal, R.R., Meier, A.L., Kornfeld, J.M. (2005). Secondary sulfate minerals associated with acid drainage in the eastern US: recycling of metals and acidity in surficial environments. Chemical Geology 215, 407-431.

Hammermeister, A.M., Naeth, M.A., Chanasyk, D.S. (1998). Implications of fly ash application to soil for plant growth and feed quality. Environmental Technology 19, 143-152.

Hammersley, A.P., Svensson, S.O., Han, M., Fitch, A.N., Hausermann, D. (1996). Two-dimensional detector software: from real detector to idealised image or two-theta scan. High Pressure Research 14(4-6), 235-248.

Harris, M.C., Runge, K.C., Whiten, W.J., Morrison, R.D. (2002). JKSimFloat as a practical tool for flotation process design and optimisation, SME Mineral Processing Plant Design, Practice and Control Conference, Vancouver, Canada (Oct.) 461-478.

Hayes, S.M., White, S.A., Thompson, T.L., Maier, R.M., Chorover, J. (2009). Changes in lead and zinc lability during weathering-induced acidification of desert mine tailings: Coupling chemical and micro-scale analyses. Applied Geochemistry 24, 2234-2245.

Hedin, R.S., Nairn, R.W. Kleinmann, R.L.P. (1994). Passive treatment of coal mine drainage. US Bureau of Mines IC-9389, Washington, DC 2-35.

Höller, H., Wirsching, U. (1985). Zeolites formation from fly ash. Fortschritte der Mineralogie 63, 21-43.

Holmström, H., Ljungberg, J., Öhlander, B. (1999). Role of carbonates in mitigation of metal release from mining waste. Evidence from humidity cells tests. Environmental Geology 37(4), 267-280.

Holmström, H., Ohlander, B. (1999). Oxygen penetration and subsequent reactions in flooded sulfidic mine tailings: a study at Stekenjokk, northern Sweden. Applied Geochemistry 14, 747-759.

Hower, J.C., Robl, T.L., Anderson, C., Thomas, G.A., Sakulpitakphon, T., Mardon, S.M. (2005). Characteristics of coal combustion products (CCP's) from Kentucky power plants, with emphasis on mercury content. Fuel 84, 1338-1350.

IEA, International Energy Agency. IEA Statistics (2011). Oil, Gas, Coal and Electricity. Quarterly statistics, first quarter 2011.

Ives, K.J. (ed.) (1984). The Scientific Basis of Flotation, Martinus Nijoff Publishers, The Hague.

Jambor, J.L., Nordstrom, D.K., Alpers, C.N. (2000). Metalsulfate salts from sulfide mineral oxidation, in: Alpers, C.N., Jambor, J.L., Nordstrom, D.K. (Eds.), Sulfate Minerals: Crystallography, Geochemistry, and Environmental Significance. Reviews in Mineralogy and Geochemistry 40, 305-350.

Jamieson, H., Alpers, C., Nordstrom, D.K., Peterson, R. (1999). Substitution of zinc and other metals in iron-sulfate minerals at Iron Mountain, California, in: Goldsack, D., Belzile, N., Yearwood, P., Hall, G. (Eds.), Conference Proceedings Sudbury'99: Mining and the Environment II, vol. 1. Sudbury, Ontario, Canada p. 231-241.

Jarvis, S.T., Brooks, T.G. (1996). The use of PFA: Cement Pastes in The Stabilisation of Abundant Mineworkings. Waste Management 16(1-3), 135-144.

Johnson, N.W., Munro, P.D. (2002). Overview of Flotation Technology and Plant Practice for Complex Sulphide Ores, SME Mineral Processing Plant Design, Practice and Control Conference, Vancouver, Canada (Oct.) 1097-1123.

Johnson, R.H., Blowes, D.W., Robertson, W.D., Jambor, J.L. (2000). The hydrogeochemistry of the Nickel Rim mine tailings impoundment, Sudbury, Ontario. Journal of Contaminant Hydrology 41, 49–80.

Jurjovec, J., Ptacek, C.J., Blowes, D.W. (2002). Acid neutralization mechanisms and metal release in mine tailings: A laboratory column experiment. Geochimica et Cosmochimica Acta 66, 1511-1523.

Keith, C.N., Vaughan D.J. (2000). Mechanisms and rates of sulphide oxidation in relation to the problems of acid rock (mine) drainage. In: Cotter-Howells, J.D., Campbell, L.S., Valsami-Jones, E., Batchelder, M. (eds). Environmental mineralogy: microbial interactions, anthropogenic influences, contaminated land and waste management. Mineralogical Society, London. Mineralogical Society Series 9, 117–139.

121

Kepler, D.A., McCleary, E.C. (1994). Successive alkalinity producing systems (SAPS) for the treatment of acidic mine drainage. In: Proceedings of the International Land Reclamation and Mine Drainage Conference and the Third International Conference on the Abatement of Acidic Drainage, Pittsburgh, PA, April 1994 1, 195-204.

King, R.P. (1982). Principles of Flotation, South African Institute of Mining and Metallurgy, Johannesburg p. 267.

Kleinmann, R.L.P. (1990). Acid mine drainage in the United States. En: Proceedings of the First Midwestern Region Reclamation Conference.

Kohfahl, C., Graupner, T., Fetzer, C., Holzbecher, E., Pekdeger, A. (2011). The impact of hardpans and cemented layers on oxygen diffusivity in mining waste heaps: Diffusion experiments and modelling studies. The Science of the total environment 409(17), 3197-3205.

Kuyucak, N. (2001). Acid mine drainage: treatment options for mining effluents. Mining Environmental Management 9, 14–17.

Langmuir, D. (1997). Aqueous Environmental Geochemistry. Prentice-Hall, Upper Saddle River, NJ.

Lapakko, K., Antonson, D.A., Wagner, J.R. (1997). Mixing of limestone with finely-crushed acid producing rock. ICARD, Vancouver 1345-1360.

Laskowski, J.S., Poling, G.W. (1995). Processing of Hydrophobic Minerals and Fine Coal CIM, Montreal.

Laskowski, J.S., Ralston, J. (1992). Colloid Chemistry in Mineral Processing. Developments in Mineral Processing 12, 225.

Leblanc, M., Borrego, J., Elbaz-Poulichet, F. (2000). 4.500 year old mining pollution in Southwestern Spain: long-term implications for modern mining pollution. Economic Geology 95, 655-662.

Leja, J. (1982). Surface Chemistry of Froth Flotation, Plenum Press, New York.

Levandowski, J., Kalkreuth, W. (2008). Chemical and petrographical characterization of feed coal, fly ash and bottom ash from the Figueira Power Plant, Paraná, Brazil. International Journal of Coal Geology 77, 269-281.

Ljungberg, J., Ohlander, B. (2001). The geochemical dynamics of oxidising mine tailings at Laver, northern Sweden. Journal of Geochemical Exploration 74, 57-72.

Lottermoser, B.G., Ashley, P.M. (2006). Mobility and retention of trace elements in hardpan-cemented cassiterite tailings, north Queensland, Australia. Environmental Geology 50, 835-846.

Lowson, R.T. (1982). Aqueous oxidation of pyrite by molecular oxygen. Chemical Reviews 82, 461-497.

Luther, I.G.W. (1987) Pyrite oxidation and reduction: molecular orbital theory considerations. Geochimica et Cosmochimica Acta 51, 3193-3199.

Macías, F., Caraballo, M.A., Rötting, T.S., Pérez-López, R., Nieto, J.M., Ayora, C. (2012). From highly polluted Zn-rich acid mine drainage to non-metallic waters: Implementation of a multi-step alkaline passive treatment system to remediate metal pollution. Science of The Total Environment 433, 323-330.

Manz, O.E. (1997). Worldwide Production of Coal Ash and Utilization in Concrete and Other Products. Fuel 76, 691-696.

Martínez-Sánchez, M.J., Navarro, M.C., Pérez-Sirvent, C., Marimón, J., Vidal, J., García-Lorenzo, M.L., Bech, J. (2008). Assessment of the mobility of metals in a mining-impacted coastal area (Spain, Western Mediterranean). Journal of Geochemical Exploration 96(2-3), 171-182.

Martín-Ramos, J.D. (2004). Using XPowder: a software package for powder X-ray diffraction analysis. D.L. GR-1001/04; ISBN: 84-609-1497-6, Spain. http://www.xpowder.com (accessed 26.10.2011).

McGrath, S.P., Cunliffe, C.H. (1985). A simplified method for the extraction of the metals Fe, Zn, Ni, Pb, Cr, Co, Mn from soils and sewage sludges. Journal of the Science of Food and Agriculture 36, 794-798.

McGregor, R.G., Blowes, D.W. (2002). The physical, chemical and mineralogical properties of three cemented layers within sulfide-bearing mine tailings. Journal of Geochemical Exploration 76(3), 195-207.

McGregor, R.G., Blowes, D.W., Jambor, J.L., Robertson, W.D. (1998). The solid-phase controls on the mobility of heavy metals at the Copper Cliff

tailings area, Sudbury, Ontario, Canada. Journal of Contaminant Hydrology 33, 247-271.

Megía, A. (1998). Generadores de vapor para centrales térmicas. In: Lapuerta, M., Hernández, J.J. (Eds.): Tecnologías de la combustión. Universidad de Castilla-La Mancha, colección Ciencia y Tecnología P. 382.

Meij, R. (1995). The distribution of trace elements during the combustion of coal. In: Swaine DJ, Goodarzi F, editors. Environmental Aspects of Trace Elements in Coal, Dordrecht Netherlands: Kluwer Academic Publication p. 111-127.

Mylona, E., Xenidis, A., Paspaliaris, I. (2000). Inhibition of acid generation from sulphidic wastes by the addition of small amounts of limenstone. Minerals Engineering 13, 1161-1175.

Moncur, M.C., Ptacek, C.J., Blowes, D.W., Jambor, J.L. (2005). Release, transport and attenuation of metals from an old tailings impoundment. Applied Geochemistry 20, 639-659.

Mylona, E., Xenidis, A., Paspaliaris, I. (2000). Inhibition of acid generation from sulphidic wastes by the addition of small amounts of limestone. Minerals Engineering 13(10-11), 1161-1175.

Navarrete, B., Vilches, L.F., Cañadas, L., Salvador, L. (2004). Influence of start-ups with fuel oil on the operation of electrostatic precipitators in pulverised coal boilers. Environmental Progress 23, 29-38.

Nicholson, R.V., Gillham, R.W., Reardon, E.J. (1988). Pyrite oxidation in carbonate-buffered solution: 1. Experimental kinetics. Geochimica et Cosmochimica Acta 52(5), 1077-1085.

Nicholson, R.V., Gillham, R.W., Reardon, E.J. (1990). Pyrite oxidation in carbonate-buffered solution: 2. Rate control by oxide coatings. Geochimica et Cosmochimica Acta 54(2), 395-402.

Nocete, F., Sáez, R., Nieto, J.M., Cruz-Auñón, R., Cabrero, R., Alex, E., Bayona, M.R. (2005). Circulation of silicified oolitic limestone blades in South-Iberia (Spain and Portugal) during the third millennium B.C.: an expression of a core/periphery framework. Journal of Anthropological Archaeology 24, 62-81.

Nordstrom, D.K., Alpers, C.N. (1999). Geochemistry of acid mine waters. In: The Environmental Geochemistry of Mineral Deposits (eds. Plumlee, G.S., Logsdon, M.J.). Society of Economic Geologists Inc., Littleton, DC, vol. 6A p. 133–157.

Nordstrom, D.K., Wilde, F.D. (1998). Reduction-oxidation potential (electrode method). National field manual for the collection of water quality data, U.S. Geological Survey, Techniques of Water-Resources Investigations, book 9, chapter A6.5 p. 3-20.

Paktunc, D., Dutrizac, J.E. (2003). Characterization of arsenate-for-sulfate substitution in synthetic jarosite using X-ray diffraction and X-ray absorption spectroscopy. The Canadian Mineralogist. 41, 905-919.

Parker, G., Robertson, A. (1999). Acid Drainage. A critical review of acid generation from sulfide oxidation: Processes, treatment and control. Australian Minerals & Energy Environment Foundation, Occasional Paper nº. 11 p 227.

Parkhurst, D.L., Appelo, C.A.J. (2005). PHREEQC-2 version 2.12: A hydrochemical transport model. http://wwwbrr.cr.usgs.gov.

Parviainen, A. (2009). Tailings Mineralogy and Geochemistry at the Abandoned Haveri Au-Cu Mine, SW Finland. Mine Water Environ 28, 291-304.

Patterson, R.J., Frape, S.K., Dykes, L.S., McLeod, R.A. (1978). Coring and squeezing technique for detailed study of subsurface water chemistry. Canadian Journal of Earth Sciences 15, 162-169.

Penilla, R.P., Bustos, A.G., Elizalde, S.G. (2006). Immobilization of Cs, Cd, Pb and Cr by synthetic zeolites from Spanish low-calcium coal fly ash. Fuel 85, 823-832.

Pérez-López, R., Nieto, J.M., Álvarez-Valero, A.M., Almodóvar, G.R. (2007a). Mineralogy of the hardpan formation processes in the interface between sulfide-rich sludge and fly ash: Applications for acid mine drainage mitigation. American Mineralogist 92, 1966-1977.

Pérez-López, R., Nieto, J.M., Almodóvar, G.R. (2007b). Utilization of fly ash to improve the quality of the acid mine drainage generated by oxidation of

a sulphide-rich mining waste: Column experiments. Chemosphere 67, 1637-1646.

Pérez-López, R., Cama, J., Nieto, J.M., Ayora, C. (2007c). The iron-coating role on the oxidation kinetics of a pyritic sludge doped with fly ash. Geochimica et Cosmochimica Acta 71(8), 1921-1934.

Pérez-López, R., Álvarez-Valero, A.M., Nieto, J.M., Sáez, R., Matos, J.X. (2008). Use of sequential extraction procedure for assessing the environmental impact at regional scale of the São Domingos Mine (Iberian Pyrite Belt). Applied Geochemistry 23, 3452-3463.

Pérez-López, R., Cama, J., Nieto, J.M., Ayora, C., Saaltink, M.W. (2009). Attenuation of pyrite oxidation with a fly ash pre-barrier: Reactive transport modelling of column experiments. Applied Geochemistry 24(9), 1712-1723.

Petit, M.D., Rucandio, M.I. (1999). Sequential extractions for determination of cadmium distribution in coal fly ash, soil and sediment samples. Analytica Chimica Acta 401, 283-291.

Phipps, T.T., Fletcher, J.J., Fiske, W., Skousen, J.G. (1991). A methodology for evaluating the costs of alternative AMD treatment systems. In: Proceedings of the 12th Annual West Virginia Surface Mine Drainage Task Force Symposium.

Pickles, C.A., Mclean, A., Alcock, C.B., Nikolic, R.N. (1990). Plasma Recovery of Metal Values From Fly Ash. Canadian Metallurgical Quarterly 29(3), 193-200.

Pinedo Vara, I. (1963). Piritas de Huelva. Su Historia, Minería y Aprovechamiento, In: Summa, Madrid.

Pitzer, K.S. (1973). Thermodynamics of electrolytes. 1. Theoretical basis and general equations. Journal of Physical Chemistry 77, 268-277.

Polat, M., Guler, E., Lederman, E., Cohen, H. (2007). Neutralization of an extremely acidic sludge and stabilization of heavy metals in fly ash aggregates. Waste management 27(4), 482-489.

Potgieter-Vermaak, S.S., Potgieter, J.H., Monama, P., Van Grieken, R. (2006). Comparison of limestone, dolomite and fly ash as pre-treatment agents for acid mine drainage. Minerals Engineering 19, 454-462.

Queralt, I., Querol, X., López-Soler, A., Plana, F. (1997). Use of coal fly ash for Ceramics: a case study for a large Spanish power station. Fuel 76, 787-791.

Querol, X., Fernández-Turiel, J.L., LópezSoler, A. (1995). Trace element behaviour in a large power station. Fuel 74, 331-343.

Querol, X., Umaña, J.C., Alastuey, A., Bertrana, C., Lopez-Soler, A., Plana, F. (1999). Physicochemical Characterization of Spanish Fly Ashes. Energy Sources 21, 883-898.

Quispe, D., Pérez-López, R., Acero, P., Ayora, C., Nieto, J.M. (2013). The role of mineralogy on element mobility in two sulfide mine tailings from the Iberian Pyrite Belt (SW Spain). Chemical Geology 345, 119-129.

Quispe, D., Pérez-López, R., Silva, L.F.O., Nieto, J.M. (2012). Changes in mobility of hazardous elements during coal combustion in Santa Catarina power plant (Brazil) Fuel 94, 495-503.

Rao, S.R. (2004). Surface Chemistry of Froth Flotation, 2nd edition, Kluwer Academic/Plenum Publishers, New York.

Rauret, G., López-Sánchez, J.F., Sahuquillo, A., Rubio, R., Davidson, C., Ure, A.M., Quevauviller, Ph. (1999). Improvement of the BCR three step sequential extraction procedure prior to the certification of new sediment and soil reference materials. Journal of Environmental Monitoring 1, 57-61.

Reardon, E.J. (1988). Ion interaction parameters for aluminum sulfate and application to the prediction of metal sulfate solubility in binary salt systems. The Journal of Physical Chemistry 92, 6426-6431.

Reardon, E.J., Beckie, R.D. (1987). Modelling chemical-equilibria of acid-mine drainage - the FeSO4-H2SO4-H2O system. Geochimica et Cosmochimica Acta 51, 2355-2368.

Reardon, E.J., Moddle, P.M. (1985). Gas diffusion coefficient measurements on uranium mill tailings: implications to cover layer design. Uranium 2, 111-131.

Rice, C.A., Breit, G.N., Affolter, R.H., Bullock, J., Motooka J. (1997). Geochemical Analysis and Modeling of Coal Combustion Waste Leachate. International Ash Symposium, Lexington, Kentucky 231-238.

Rimstidt, J.D., Vaughan, D.J. (2003). Pyrite oxidation: A state-of-the-art assessment of the reaction mechanism. Geochimica et Cosmochimica Acta 67, 873-880

Rodier, J., Broutin, J.P., Chambon, P., Champsaur, H., Rodi, L. (1996). L'analyse de l'eau. Dunod, Paris.

Romano, C.G., Mayer, K.U., Jones, D.R., Ellerbroek, D.A., Blowes, D.W. (2003). Effectiveness of various cover scenarios on the rate of sulfide oxidation of mine tailings. Journal of Hydrology 271(1-4), 171-187.

Sáez, R., Pascual, E., Toscano, M., Almodóvar, G.R. (1999). The Iberian type of volcano-sedimentary massive sulphide deposits. Mineralium Deposita 34(5-6), 549-570.

Sahuquillo, A., Lopez-Sanchez, J.F., Rubio, R., Rauret, G., Thomas, R.P., Davidson, C.M., Ure, A.M. (1999). Use of a certified reference material for extractable trace metals to assess sources of uncertainty in the BCR three-stage sequential extraction procedure. Analytica Chimica Acta 382(3), 317-327.

Sáinz, A., Grande, J.A., de la Torre, M.L., Sánchez-Rodas, D. (2002). Characterisation of sequential leachate discharges of mining waste rock dumps in the Tinto and Odiel rivers. Journal of Environmental Management 64, 345-353.

Sarmiento, A.M., Nieto, J.M., Olías, M., Cánovas, C.R. (2009). Hydrochemical characteristics and seasonal influence on the pollution by acid mine drainage In the Odiel river Basin (SW Spain). Applied Geochemistry 24, 697-714.

Saylak, D., Viswanathan, R., Estakhri, C. (1997). Stabilization of Subgrade Soils Using Fly Ash. International Ash Symposium, Lexington, Kentucky 204-211.

Schippers, A., Sand, W. (1999). Bacterial leaching of metal sulfides proceeds by two indirect mechanisms via thiosulfate or via polysulfides and sulfur. Applied and Environmental Microbiology 65, 319-321.

Shimizu, M. Arai, Y., Sparks, D.L. (2011). Multiscale Assessment of Methylarsenic Reactivity in Soil. 2. Distribution and Speciation in Soil. Environmental science and technology 45(10), 4300-4306.

Silva, L.F.O., Moreno, T., Querol, X. (2009a). An introductory TEM study of Fe-nanominerals within coal fly ash. Science of the Total Environment 407, 4972-4974.

Silva, L.F.O., Oliveira, M.L.S., da Boit, K.M, Finkelman, R.B. (2009b). Characterization of Santa Catarina (Brazil) coal with respect to Human Health and Environmental Concerns. Environmental Geochemistry and Health 31, 475-485.

Silva, L.F.O., Ward, C., Hower, J., Izquierdo, M., Waanders, F., Oliveira, M., Li, Z., Hatch, R., Querol, X. (2010a). Mineralogy and Leaching Characteristics of Coal Ash from a Major Brazilian Power Plant. Coal Combustion and Gasification Products 2, 51-65.

Silva, L.F.O., da Boit, K. (2010b). Nanominerals and nanoparticles in feed coal and bottom ash: implications for human health effects. Environmental Monitoring and Assessment 174, 187-197.

Silva, L.F.O., Oliveira, M.L.S., Neace, E.R., O'Keefe, J.M.K., Henke, K.R., Hower, J.C. (2011). Nanominerals and ultrafine particles in sublimates from the Ruth Mullins coal fire, Perry County, Eastern Kentucky, USA. International Journal of Coal Geology 85, 237-245.

Skousen, J., Rose, A., Geidel, G., Foreman, J., Evans, R., Hellier, W. (1998). A Handbook of Technologies for the Avoidance and Remediation of Acid Mine Drainage. Acid Drainage Technology Initiative (ADTI). National Mine Land Reclamation Center, Morgantown, WV p. 131.

Smeda, A., Zyrnicki, W. (2002). Application of sequential extraction and the ICP-AES method for study of the partitioning of metals in fly ashes. Microchemical Journal 72, 9-16.

Smith, I.M. (1987). Trace elements from coal combustion: emissions, chap 2, Source of trace elements, IEACR/01 IEA Coal Research, London.

Solé, V.A., Papillon, E., Cotte, M., Walter, P.H., Susini, J. (2007). PyMca: a multiplatform code for the analysis of energy-dispersive X-ray spectra. Spectrochimica Acta Part B 62, 63-68.

Somogyi, A., Drakopoulos, M., Vincze, L., Vekemans, B., Camerani, C., Janssens, K., Snigirev, A. Adams, F. (2001). ID18F: a new micro-x-ray fluorescence end-station at the European Synchrotron Radiation Facility (ESRF): preliminary results. X-Ray Spectrometry 30(4), 242-252.

Spears, D.A., Lee, S. (2004). The geochemistry of leachates from coal ash. Geological Society, London, Special Publications 236, 619-639.

Stumm, W., Sulzberger, B. (1992). The cycling of iron in natural environments: Considerations based on laboratory studies of heterogeneous redox processes. Geochimica et Cosmochimica Acta 56, 3233-3257.

Tosca, N.J., McLennan, S.M., Clark, B.C., Grotzinger, J.P., Hurowitz, J.A., Knoll, A.H., Schroder, C., Squyres, S.W. (2005). Geochemical modeling of evaporation processes on Mars: Insight from the sedimentary record at Meridiani Planum. Earth and Planetary Science Letters 240, 122-148.

Trahar, W.J., Warren, L.J. (1976). The floatability of very fine particles - A review. International Journal of Mineral Processing 3(2), 103-131.

Turner, D., McCoy, D. (1990). Anoxic alkaline drain treatment system, a low cost acid mine drainage treatment alternative. In: Graves, D.H., DeVore, R.W. (Eds.): Symp. Surface Mining Hydrology, Sedimentology and Reclamation, Lexington, KY p. 73-75.

Ure, A.M., Quevauviller, P., Muntau, H., Griepink, B. (1993). Speciation of heavy metals in soils and sediments-an account of the improvement and harmonization of extraction techniques undertaken under the auspices of

the BCR of the Commission of the European Communities. International Journal of Environmental Analytical Chemistry 51, 135-151.

Valentim, B., Guerdes, A., Flores, D., Ward, C.R., Hower, J.C. (2009). Variations in fly ash composition with sampling location: Case study from a Portuguese power plant. Coal Combustion and Gasification Products 1, 14-24.

Vassilev, S.V., Tascón, J.M.D. (2003). Methods for Characterization of Inorganic and Mineral Matter in Coal: A Critical Overview. Energy and Fuels 17, 271-281.

Vassilev, S.V., Vassileva, C.G. (1996). Mineralogy of combustion wastes from coal-fired power stations. Fuel Processing Technology 47, 261-280.

Vassilev, S.V., Vassileva, C.G. (1996). Occurrence, abundance and origin of minerals in coals and coal ashes. Fuel Processing Technology 48, 85-106.

Vassilev, S.V., Vassileva, C.G. (2005). Methods for Characterization of Composition of Fly Ashes from Coal-Fired Power Stations: A Critical Overview. Energy and Fuels 19, 1084-1098.

Vassilev, S.V., Vassileva, C.G. (2007). A new approach for the classification of coal fly ashes based on their origin, composition, properties, and behaviour. Fuel 86, 1490-1512.

Vilches, L.F., Fernández-Pereira, C., Olivares del Valle, J., Rodríguez Piñero, M., Vale J. (2001). Development of New Fire-Products Made from Coal Fly Ash. The CEFYR Project. Progres Workshop on Novel Products from Combustion Residues. Morella 343-351.

Walton-Day, K. (2003) Passive and active treatment of mine drainage. In: Jambor, J.L., Blowes, D.W., Ritchie, A.I.M. (eds) Environmental aspects of mine wastes. Mineralogical Association of Canada, Nepean (Short course handbook) 31, 335-359.

Wang, H.L., Shang, J.Q., Kovac, V., Ho, K.S. (2006). Utilization of Atikokan coal fly ash in acid rock drainage control from Musselwhite Mine tailings. Canadian Geotechnical Journal 43(3), 229-243.

Ward, C.R., French, D., Jankowski, J., Dubikova, M., Li, Z., Riley, K.W. (2009). Element mobility from fresh and long-stored acidic fly ashes

associated with an Australian power station. International Journal of Coal Geology 80, 224-236.

Watzlaf, G.R. (1997). Passive treatment of acid mine drainage in down-flow limestone systems. En: Proceedings of the 14th Annual National Meeting of the American Society of Surface Mining and Reclamation p. 611-622.

Webster, J.G., Nordstrom, D.K., Smith, K.S. (1994). Transport and natural attenuation of Cu, Zn, As and Fe in the acid mine drainage of Leviathan and Bryant Creeks. In: Alpers, C.N., Blowes, D.W. (Eds.): Environmental geochemistry of sulfide oxidation. ACS Symposium series 550, 244-260.

Yan, J., Kirk, D.W., Jia, C.Q., Liu, X. (2007). Sorption of aqueous phosphorus onto bituminous and lignitous coal ashes. Journal of Hazardous Materials 148, 395-401.

Yılmaz, B., Olgun, A. (2008). Studies on cement and mortar containing low-calcium fly ash, limestone, and dolomitic limestone. Cement and Concrete Composites 30, 194-201.

Younger, P.L. (2002). A reducing and alkalinity-producing system (RAPS) for the passive treatment of acidic, aluminium-rich leachates emanating from revegetated colliery spoil materials at Bowden Close, County Durham. In: Proceedings of the Cl: aire Annual Project Conference, Imperial College, London, 11 April 2002, Paper 7 p. 21.

Younger, P.L., Banwart, S.A., Hedin, R.S. (2002). Mine Water - Hydrology, Pollution, Remediation. Kluwer Academic Publishers, Dordrecht. 5, p. 442

Yu, J.Y., Heo, B., Choi, I.K., Cho, J.P., Chang, H.W. (1999). Apparent solubilities of schwertmannite and ferrihydrite in natural stream waters polluted by mine drainage. Geochimica et Cosmochimica Acta 63, 3407-3416.

ANEXO I. TABLAS

Table A1. Results obtained for BCR sequential extraction [F1: water-soluble fraction, F2: reducible fraction, F3: oxidizable fraction, F4: residual fraction, and the Sum of the extraction steps] and agua regia digestion [PT: pseudo-total content] for the two mine tailings impoundments. Comparative results (% recovery) of BCR sequential extraction and aqua regia digestion are also shown.

Results for the yellowish impoundment:

Samples Depth (cm)	Step	Elements (mg/kg)									
		Al	As	Cd	Co	Cu	Fe	Mn	Ni	S	Zn
Dry season											
0	F1	5259	14.1	13.3	2.50	1084	13472	172	3.49	44001	4755
	F2	16.4	2.32	-	-	9.04	3164	0.35	-	850	23.2
	F3	71.5	17.1	0.10	-	20.9	478	0.93	0.14	637	41.4
	F4	2309	555	0.12	0.10	108	22767	38.7	0.60	4632	469
	Sum	7657	588	13.5	2.60	1223	39881	212	4.23	50119	5289
	Pseudo-total	7024	500	14.7	2.72	1204	40923	183	5.64	52308	6110
	% Recovery	109	118	91.8	95.8	102	97.5	115	75.0	95.8	86.6
-5	F1	4681	39.1	13.9	2.65	1151	17129	185	3.60	37869	5393
	F2	18.3	2.39	-	-	8.58	2189	0.41	-	671	16.2
	F3	143	21.0	-	-	4.13	602	1.92	0.41	466	20.2
	F4	3090	257	-	0.10	137	11112	67.5	0.62	2045	377
	Sum	7933	319	13.9	2.75	1301	31032	255	4.63	41051	5807
	Pseudo-total	8039	504	15.2	2.90	1311	37669	216	5.59	45474	6581
	% Recovery	98.7	63.3	91.3	94.8	99.2	82.4	118	82.8	90.3	88.2
-10	F1	1028	1.58	3.62	0.68	256	3566	47.4	0.95	11827	1523
	F2	28.0	2.36	-	-	11.8	4517	0.28	-	1171	17.3
	F3	93.2	5.25	0.11	-	20.7	1125	1.49	0.13	1063	43.4
	F4	2724	452	0.17	0.15	406	10192	107	0.78	1540	664
	Sum	3873	461	3.90	0.83	694	19400	156	1.87	15601	2248
	Pseudo-total	3649	483	3.98	0.89	622	20229	119	8.62	14409	2368
	% Recovery	106	95	98.0	93.7	112	96	131	21.7	108	94.9
-15	F1	1008	1.04	4.41	0.80	243	4272	62.5	1.10	12139	2233
	F2	10.5	1.76	-	-	14.0	5259	0.23	-	1291	9.85
	F3	73.3	0.61	-	-	24.0	1417	0.79	0.24	1627	36.2
	F4	1660	1090	-	-	136	38487	37.0	0.28	2562	55.5
	Sum	2752	1093	4.41	0.80	417	49435	101	1.62	17619	2335
	Pseudo-total	2302	854	4.98	0.93	433	51320	87.9	2.66	19013	2657
	% Recovery	120	128	88.6	85.3	96.4	96.3	114	60.8	92.7	87.9
-20	F1	507	1.99	2.29	0.36	94.0	2642	31.0	0.55	7607	1285
	F2	-	12.1	-	-	2.50	193	0.14	-	617	5.66
	F3	44.7	381	2.12	3.08	577	23908	10.3	3.22	25125	768
	F4	592	735	14.3	7.00	604	74550	20.4	3.68	80830	5984
	Sum	1144	1130	18.75	10.4	1277	101293	61.8	7.45	114179	8044
	Pseudo-total	990	951	19.5	9.99	1078	99352	59.7	8.38	113981	8533
	% Recovery	116	119	96.3	105	118	102	104	88.9	100	94.3
-30	F1	2.48	825	5.46	0.61	520	3772	66.2	1.02	11500	3002
	F2	9.80	2.77	-	-	34.1	1665	0.21	-	799	27.3
	F3	372	3.46	5.26	0.96	1860	17084	10.7	3.57	19288	2065
	F4	1771	1283	16.7	1.03	1571	50507	34.6	3.89	53339	7267
	Sum	2156	2114	27.5	2.59	3985	73027	112	8.47	84925	12361
	Pseudo-total	1674	2393	32.5	2.94	4112	82948	95.8	10.6	98805	14522
	% Recovery	126	90.1	84.5	88.1	96.9	88.0	117	80.0	86.0	85.1

Table A1. (continues)

Samples Depth (cm)	Step	Al	As	Cd	Co	Cu	Fe	Mn	Ni	S	Zn
		Elements (mg/kg)									
Wet season											
0	F1	108	1.08	0.13	0.10	20.3	1042	3.60	0.10	1657	48.5
	F2	15.3	3.09	-	-	6.00	1607	0.08	0.09	632	3.61
	F3	43.0	21.0	0.16	-	73.0	64.6	0.53	0.23	328.9	70.4
	F4	1599	202	0.09	-	78.0	10990	22.8	0.44	3451	145
	Sum	1765	227	0.38	0.10	177	13704	27.0	0.85	6069	268
	Pseudo-total	1256	253	-	-	260	13129	21.5	-	5891	339
	% Recovery	140	89.6	-	-	68.2	104	126	-	103	79.1
-5	F1	148	1.31	0.21	0.14	25.1	1367	3.48	0.18	2186	80.0
	F2	20.7	2.49	-	-	10.9	1097	0.08	-	375	9.10
	F3	58.6	44.9	0.19	-	133	76.9	0.82	0.21	307	70.7
	F4	1867	369	0.17	0.11	294	17276	28.8	0.56	5247	334
	Sum	2095	418	0.57	0.25	463	19817	33.1	0.95	8116	494
	Pseudo-total	1854	478	-	-	515	21268	33.1	1.15	9816	615
	% Recovery	113	87.3	-	-	89.9	93.2	100	82.8	82.7	80.3
-10	F1	263	4.46	0.35	0.24	31.0	2393	4.99	0.19	3284	134
	F2	15.7	2.35	-	-	3.60	1189	0.08	-	403	4.20
	F3	88.3	11.4	-	-	2.94	88.65	1.52	0.70	215	15.1
	F4	3519	276	0.08	0.09	162	14940	61.0	0.59	4084	267
	Sum	3886	294	0.43	0.33	200	18611	67.6	1.47	7986	420
	Pseudo-total	2832	272	-	-	217	15313	55.1	0.79	4933	410
	% Recovery	137	108	-	-	92.2	122	123	187	162	103
-15	F1	356	10.3	0.46	0.38	41.3	3698	6.77	0.30	8252	177
	F2	13.3	3.66	-	-	1.78	1897	0.09	0.09	593	2.54
	F3	84.6	12.0	-	-	2.20	165	1.21	0.25	350	4.74
	F4	4144	478	-	-	73.1	17028	64.9	0.61	4990	142
	Sum	4598	504	0.46	0.38	118	22787	73.0	1.24	14185	326
	Pseudo-total	4007	561	-	-	129	22189	69.9	1.21	14298	323
	% Recovery	115	89.8	-	-	91.8	103	104	103	99.2	101
-20	F1	567	38.8	0.83	0.89	101	6537	10.1	0.68	10211	295
	F2	14.0	59.3	-	-	0.22	154	-	-	668	1.36
	F3	27.1	346	0.37	9.22	305	51334	5.44	2.45	56184	91.1
	F4	238	682	1.67	22.0	305	154081	13.7	4.30	178756	552
	Sum	846	1126	2.87	32.1	711	212106	29.3	7.43	245819	939
	Pseudo-total	873	1235	3.30	40.3	926	239844	32.7	9.08	273327	1150
	% Recovery	97.0	91.2	86.8	79.6	76.7	88.4	89.6	81.8	89.9	81.7
-30	F1	798	51.6	1.25	1.09	67.7	7864	15.6	0.90	13957	448
	F2	13.7	32.5	-	-	0.30	275	-	-	882	2.36
	F3	18.3	122	0.78	1.06	327	14378	3.79	1.40	16107	255
	F4	461	411	7.57	1.15	525	26491	7.90	1.57	30384	2807
	Sum	1291	617	9.60	3.31	920	49009	27.3	3.87	61329	3512
	Pseudo-total	1180	603	10.8	4.18	969	59602	27.1	4.09	73190	4541
	% Recovery	109	102	89.1	79.1	94.9	82.2	101	94.4	83.8	77.3

Oxidized tailings		Mine tailings

136

Table A1. (continues)

Results for the grayish impoundment:

Samples Depth (cm)	Step	Elements (mg/kg)									
		Al	As	Cd	Co	Cu	Fe	Mn	Ni	S	Zn
Dry season											
0	F1	328	93.8	0.30	3.07	79.5	18928	2.57	0.68	16573	119
	F2	-	10.5	-	0.08	-	49.6	-	-	1082	-
	F3	63.6	361	-	12.7	101	73466	8.3	2.20	73585	50.8
	F4	280	683	1.81	29.8	273	172148	15.7	3.74	194192	670
	Sum	673	1148	2.11	45.6	453	264591	26.6	6.62	285431	841
	Pseudo-total	688	1165	2.31	46.3	469	284419	26.3	8.12	302094	823
	% Recovery	98	98.5	91.1	98.6	96.7	93.0	101	81.6	94.5	102
-5	F1	361	65.2	0.25	2.33	50.5	14473	2.11	0.61	16694	96.4
	F2	-	6.52	-	-	-	52.0	-	-	419	-
	F3	73.6	245	-	6.08	53.5	52642	6.03	1.77	53816	27.2
	F4	123	97.9	0.51	3.58	36.4	29233	2.59	0.83	39885	211
	Sum	557	415	0.76	12.0	140	96400	10.7	3.21	110814	334
	Pseudo-total	565	418	0.90	11.9	139	101195	10.5	4.50	118844	320
	% Recovery	99	99.2	85.1	101	101	95.3	102	71.3	93.2	105
-10	F1	201	55.7	0.28	2.58	63.5	14330	1.80	0.50	11823	121
	F2	-	12.9	-	-	-	45.2	-	-	724	-
	F3	87.6	378	-	14.7	105	78549	9.18	1.94	78549	53.4
	F4	414	899	2.77	44.2	368	239225	20.0	3.99	266746	1030
	Sum	702	1346	3.06	61.5	537	332149	31.0	6.43	357841	1204
	Pseudo-total	689	1385	3.1	62.9	549	361231	31.1	8.13	378000	1091
	% Recovery	102	97.2	97.7	97.7	97.7	91.9	99.6	79.2	94.7	110
-15	F1	237	61.4	0.40	2.75	81.7	14855	2.03	0.57	12949	156
	F2	-	7.49	-	-	-	49.8	-	-	474	-
	F3	95.8	424	-	16.5	112	83674	10.3	3.02	87172	52.9
	F4	340	663	2.82	28.3	270	154690	15.7	3.87	170398	1060
	Sum	673	1156	3.22	47.5	463	253268	28.1	7.47	270993	1269
	Pseudo-total	547	1121	3.30	45.8	453	258842	26.8	9.28	272581	1211
	% Recovery	123	103	97.6	104	102	97.8	105	80.5	99.4	105
-20	F1	181	47.5	0.32	1.52	70.9	8812	1.34	0.43	8157	111
	F2	-	7.57	-	-	0.11	33.1	-	-	874	-
	F3	86.0	421	0.61	15.2	111	78620	11.4	3.80	79499	185
	F4	426	1048	7.52	43.7	449	241023	25.7	6.77	267226	4066
	Sum	693	1524	8.45	60.4	631	328487	38.5	11.0	355755	4362
	Pseudo-total	612	1537	8.7	59.9	636	348822	38.3	12.3	370399	3244
	% Recovery	113	99.2	96.8	101	99.3	94.2	100	89.4	96.0	134
-30	F1	167	52.8	0.36	1.63	135	8821	1.22	0.35	7648	128
	F2	12.4	10.3	-	-	0.12	35.0	-	-	770	-
	F3	100	490	-	21.6	131	100020	12.2	4.57	103201	96.3
	F4	387	1072	3.26	42.1	398	223424	25.2	7.09	249274	1222
	Sum	667	1626	3.62	65.3	664	332300	38.6	12.0	360894	1446
	Pseudo-total	802	1678	4.58	66.7	687	368000	39.1	13.6	386229	1585
	% Recovery	83	96.9	79.1	97.9	96.8	90.3	98.8	88.2	93.4	91.2

137

Table A1. (continues)

Samples Depth (cm)	Step	Al	As	Cd	Co	Cu	Fe	Mn	Ni	S	Zn
		Elements (mg/kg)									

Samples Depth (cm)	Step	Al	As	Cd	Co	Cu	Fe	Mn	Ni	S	Zn
Wet season											
0	F1	56.2	14.3	-	0.46	16.1	2198	2.13	-	3125	13.9
	F2	1.75	5.91	-	-	-	30.6	-	-	1137	-
	F3	11.3	242	0.12	8.34	70.6	54107	5.03	1.80	59559	27.2
	F4	43.5	451	1.32	23.1	183	147608	9.39	2.82	177033	425
	Sum	113	713	1.44	31.9	269	203943	16.6	4.62	240855	466
	Pseudo-total	82.6	776	1.71	38.4	332	240826	18.4	5.63	277448	542
	% Recovery	137	91.9	84.2	83.0	81.1	84.7	90.2	82.1	86.8	85.9
-5	F1	142	24.3	-	0.57	14.5	2906	2.42	0.08	4271	19.3
	F2	3.67	9.62	-	-	-	50.4	-	-	1576	-
	F3	12.7	169	0.23	7.72	63.5	43182	3.91	1.04	48020	60.0
	F4	75.7	519	2.33	31.2	215	185616	10.0	2.50	246743	727
	Sum	234	722	2.56	39.5	293	231755	16.3	3.61	300610	806
	Pseudo-total	208	785	3.48	48.1	386	271849	18.4	5.05	336226	1167
	% Recovery	112	92.0	73.8	82.2	76.0	85.3	88.5	71.6	89.4	69.1
-10	F1	64.7	17.4	-	0.51	11.0	2520	1.34	0.09	3673	10.7
	F2	12.7	5.15	-	-	0.09	34.5	-	-	655	-
	F3	12.1	264	0.10	9.79	73.2	53474	5.51	2.30	58415	15.0
	F4	42.2	736	0.79	30.4	241	192533	15.2	4.97	228708	242
	Sum	132	1023	0.90	40.7	326	248562	22.0	7.36	291451	268
	Pseudo-total	119	941	1.05	44.4	388	248716	21.8	8.68	290195	320
	% Recovery	111	109	84.9	91.8	84.0	99.9	101	84.8	100	83.7
-15	F1	76.1	22.8	-	0.75	12.8	4082	1.28	0.12	4475	22.6
	F2	2.95	3.99	-	-	-	25.2	-	-	788	-
	F3	5.69	298	0.11	9.67	78.8	59014	6.04	2.40	64192	23.1
	F4	20.2	789	1.83	31.9	289	214866	16.1	4.98	253417	579
	Sum	105	1114	1.94	42.3	381	277987	23.4	7.50	322872	624
	Pseudo-total	160	1086	2.14	47.2	451	287160	23.7	8.28	323735	683
	% Recovery	65.4	103	90.7	89.6	84.5	96.8	99.0	90.6	99.7	91.4
-20	F1	103	32.2	0.11	1.17	22.2	5862	1.51	0.21	5609	35.4
	F2	5.02	5.10	-	-	-	39.5	-	-	691	-
	F3	11.9	295	0.22	12.3	82.1	58964	6.10	2.73	64574	48.1
	F4	30.8	842	1.36	35.2	243	196672	17.1	5.98	235017	429
	Sum	151	1174	1.69	48.7	347	261537	24.7	8.92	305892	513
	Pseudo-total	183	1251	1.92	57.5	443	307704	27.9	10.3	338824	597
	% Recovery	82.6	93.8	88.2	84.7	78.3	85.0	88.5	86.8	90.3	86.0
-30	F1	112	41.0	0.20	1.51	29.8	7910	1.76	0.32	7303	62.5
	F2	6.83	6.56	-	-	-	38.9	-	-	889	0.10
	F3	5.96	265	0.26	11.2	68	54498	5.00	2.82	59194	64.6
	F4	28.6	982	4.41	40.0	292	220175	17.7	7.20	262828	1399
	Sum	154	1295	4.87	52.8	390	282622	24.5	10.3	330214	1526
	Pseudo-total	98.2	1290	5.84	57.1	490	316599	25.6	10.8	356251	2010
	% Recovery	157	100	83.5	92.4	79.6	89.3	95.5	95.5	92.7	75.9

Oxidized tailings		Mine tailings
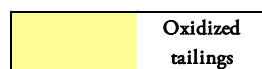
Table A2. Saturation indexes with respect to the main mineral phases in the pore-water of the two mine tailings impoundments. Solubility products and solid phases from other sources than the WATEQ4F database (Ball and Nordstrom, 1991) are indicated with letters.

Results for the yellowish impoundment:

| Depth (cm) | | Wet season (February 2006) | | | | | | | | | | | |
Phase	Min. formula	-5	-15	-25	-35	-45	-60	-100	-150	-200	-250	-300	-350
		Saturation index											
Alum	$KAl(SO_4)_2 \cdot 12H_2O$	-6.40	-6.76	-4.94	-4.52	-4.87	-	-	-6.74	-5.56	-6.35	-9.95	-6.25
Alunite	$KAl_3(SO_4)_2(OH)_6$	1.58	-2.20	-6.36	-5.39	-2.16	-	-	3.26	3.39	1.07	-9.55	-0.09
Alunogen [a]	$Al_2(SO_4)_3 \cdot 17H_2O$	-7.39	-7.09	-5.22	-4.26	-4.44	-4.34	-5.51	-6.93	-5.51	-8.03	-15.8	-8.07
Anglesite	$PbSO_4$	-1.01	-0.54	-0.97	0.11	0.21	-	0.16	0.51	0.46	0.39	0.30	0.26
Bianchite	$ZnSO_4 \cdot 6H_2O$	-3.22	-4.10	-3.03	-3.04	-2.92	-2.76	-2.55	-2.18	-2.23	-2.16	-2.09	-2.18
Bilinite [d]	$Fe^{2+}Fe^{3+}_2(SO_4)_4 \cdot 22H_2O$	-4.87	-2.92	-0.54	0.50	-	-	-	-	-	-	-	-
Chalcantite	$CuSO_4 \cdot 5H_2O$	-3.37	-	-2.81	-2.01	-2.77	-3.75	-3.24	-4.01	-2.76	-3.23	-3.54	-2.52
Copiapite [d]	$Fe^{2+}Fe^{3+}_4(SO_4)_6(OH)_2 \cdot 20H_2O$	-4.23	-1.78	-0.59	-0.02	-	-	-	-	-	-	-	-
Coquimbite [d]	$Fe_2(SO_4)_3 \cdot 9H_2O$	-41.0	-39.2	-37.8	-38.2	-	-	-	-	-	-	-	-
Epsomite [a]	$MgSO_4 \cdot 7H_2O$	-3.43	-3.19	-2.16	-1.75	-1.96	-1.96	-2.14	-1.84	-1.70	-1.85	-1.69	-1.81
Fe(OH)3	$Fe(OH)_3$	0.39	-0.60	-3.82	-4.21	-	-	-	-	-	-	-	-
Goethite	$FeOOH$	4.93	3.94	0.72	0.33	-	-	-	-	-	-	-	-
Goslarite	$ZnSO_4 \cdot 7H_2O$	-3.03	-3.91	-2.84	-2.85	-2.73	-2.57	-2.36	-1.99	-2.04	-1.98	-1.90	-1.99
Gypsum	$CaSO_4 \cdot 2H_2O$	-0.53	-0.03	-0.09	0.01	-0.01	0.02	-0.07	-0.02	0.09	-0.07	-0.03	-0.13
Halotrichite [a]	$FeAl_2(SO_4)_4 \cdot 22H_2O$	-11.0	-10.5	-7.69	-5.34	-5.65	-5.47	-6.84	-7.93	-6.46	-9.04	-16.7	-9.37
Hexahydrite [b]	$MgSO_4 \cdot 6H_2O$	-3.58	-3.34	-2.31	-1.90	-2.11	-2.10	-2.28	-1.98	-1.84	-1.99	-1.83	-1.96
H3O-Jarosite	$(H_3O)Fe_3(SO_4)_2(OH)_6$	5.00	4.51	0.10	-0.77	-	-	-	-	-	-	-	-
K-Jarosite	$KFe_3(SO_4)_2(OH)_6$	9.47	7.86	3.03	2.02	-	-	-	-	-	-	-	-
Na-Jarosite	$NaFe_3(SO_4)_2(OH)_6$	4.71	3.60	-1.63	-2.68	-	-	-	-	-	-	-	-
Jurbanite	$AlOHSO_4$	0.65	0.18	-0.19	0.23	0.76	2.22	1.47	1.15	1.45	0.35	-3.40	0.12
Melanterite	$FeSO_4 \cdot 7H_2O$	-3.91	-3.71	-2.75	-1.36	-1.49	-1.40	-1.61	-1.28	-1.22	-1.28	-1.20	-1.57
Pickeringite [a]	$MgAl_2(SO_4)_4 \cdot 22H_2O$	-10.8	-10.3	-7.41	-6.03	-6.41	-6.31	-7.66	-8.78	-7.22	-9.89	-17.5	-9.90
Rozenite [d]	$FeSO_4 \cdot 4H_2O$	-4.09	-3.89	-2.93	-1.54	-1.67	-1.58	-1.79	-1.46	-1.40	-1.46	-1.37	-1.75
Schwertmannite [c]	$Fe_8O_8(OH)_6SO_4$	23.3	16.7	-6.46	-9.43	-	-	-	-	-	-	-	-
Siderotil [d]	$FeSO_4 \cdot 5H_2O$	-4.09	-3.89	-2.93	-1.54	-1.67	-1.58	-1.79	-1.46	-1.40	-1.46	-1.38	-1.76
Szomolnokite [d]	$FeSO_4 \cdot H_2O$	-4.52	-4.32	-3.35	-1.96	-2.09	-2.01	-2.21	-1.88	-1.82	-1.88	-1.79	-2.18
Zincosite	$ZnSO_4$	-7.97	-8.86	-7.77	-7.77	-7.66	-7.50	-7.30	-6.92	-6.97	-6.91	-6.83	-6.92
Gunningite	$ZnSO_4 \cdot H_2O$	-4.40	-5.29	-4.20	-4.20	-4.09	-3.93	-3.73	-3.35	-3.40	-3.34	-3.26	-3.35

Table A2. (continues)

Depth (cm)		Dry season (May 2005)					Dry season (June 2005)				Dry season (May 2010)				
Phase	Min. formula	-5	-17	-25	-40	-60	-15	-25	-45	-70	-20	-40	-100	-150	-200
		Saturation index					Saturation index				Saturation index				
Alum	KAl(SO$_4$).12H$_2$O	-5.47	-6.55	-6.54	-6.20	-6.18	-6.54	-6.51	-6.54	-6.47	-8.49	-8.55	-8.53	-8.63	-9.38
Alunite	KAl$_3$(SO$_4$)$_2$(OH)$_6$	-9.8	-11.1	-11.2	-6.91	2.90	-8.29	-8.08	-5.64	2.28	-12.0	-10.6	-8.27	0.26	1.88
Alunogen [a]	Al$_2$(SO$_4$)$_3$.17H$_2$O	-1.51	-3.76	-3.85	-3.10	-3.06	-3.69	-3.74	-3.76	-3.68	-7.18	-7.30	-7.25	-7.40	-8.76
Anglesite	PbSO$_4$	-0.09	-0.35	0.38	0.36	0.72	-0.10	0.12	0.03	-0.31	-1.45	-0.18	-0.06	-0.20	-0.10
Bianchite	ZnSO$_4$.6H$_2$O	-2.88	-3.08	-2.98	-2.54	-2.35	-2.83	-2.79	-2.58	-2.44	-2.92	-2.89	-2.87	-2.93	-2.89
Bilinite [d]	Fe^{2+}Fe$^{3+}_2$(SO$_4$)$_4$.22H$_2$O	4.37	2.29	1.44	1.24	-	1.36	1.01	0.73	-	-2.24	-	-	-	-
Chalcantite	CuSO$_4$.5H$_2$O	-1.34	-2.36	-2.19	-1.77	-	-2.02	-2.13	-1.76	-	-2.77	-2.63	-3.35	-5.94	-6.06
Copiapite [d]	Fe^{2+}Fe$^{3+}_4$(SO$_4$)$_6$(OH)$_2$.20H$_2$O	5.01	1.73	-0.14	0.63	-	1.38	0.30	0.99	-	-4.47	-	-	-	-
Coquimbite [d]	Fe$_2$(SO$_4$)$_3$.9H$_2$O	-35.0	-36.8	-37.8	-37.9	-	-37.1	-37.9	-37.8	-	-39.9	-	-	-	-
Epsomite [a]	MgSO$_4$.7H$_2$O	-0.57	-1.36	-1.37	-1.24	-1.22	-1.34	-1.40	-1.43	-1.49	-2.18	-2.24	-2.32	-2.42	-2.59
Fe(OH)$_3$	Fe(OH)$_3$	-6.27	-5.74	-6.26	-4.68	-	-4.47	-4.75	-3.42	-	-4.96	-	-	-	-
Goethite	FeOOH	-1.68	-1.19	-1.71	-0.14	-	0.08	-0.21	1.13	-	-0.42	-	-	-	-
Goslarite	ZnSO$_4$.7H$_2$O	-2.75	-2.90	-2.80	-2.36	-2.17	-2.65	-2.61	-2.40	-2.25	-2.73	-2.70	-2.68	-2.74	-2.70
Gypsum	CaSO$_4$.2H$_2$O	0.78	0.17	0.19	0.16	0.13	0.11	0.05	0.04	0.05	-0.45	-0.49	-0.51	-0.53	-0.69
Halotrichite [a]	FeAl$_2$(SO$_4$)$_4$.22H$_2$O	-1.42	-4.30	-4.25	-3.59	-3.33	-4.90	-4.50	-4.95	-4.30	-9.22	-8.78	-8.74	-9.06	-10.5
Hexahydrite [b]	MgSO$_4$.6H$_2$O	-0.66	-1.49	-1.50	-1.37	-1.35	-1.48	-1.54	-1.57	-1.64	-2.33	-2.39	-2.46	-2.57	-2.73
H$_3$O-Jarosite	(H$_3$O)Fe$_3$(SO$_4$)$_2$(OH)$_6$	-1.84	-2.38	-3.91	-1.36	-	-0.50	-1.51	0.80	-	-3.22	-	-	-	-
K-Jarosite	KFe$_3$(SO$_4$)$_2$(OH)$_6$	-2.43	-2.56	-4.05	-1.00	-	-0.26	-1.17	1.54	-	-2.90	-	-	-	-
Na-Jarosite	NaFe$_3$(SO$_4$)$_2$(OH)$_6$	-4.51	-4.72	-6.41	-3.66	-	-2.10	-3.42	-0.52	-	-5.77	-	-	-	-
Jurbanite	AlOHSO$_4$	0.77	-0.18	-0.24	0.67	2.32	0.29	0.30	0.70	2.03	-1.20	-0.99	-0.59	0.80	0.74
Melanterite	FeSO$_4$.7H$_2$O	-0.29	-0.83	-0.69	-0.79	-0.57	-1.49	-1.04	-1.47	-0.90	-2.32	-1.75	-1.77	-1.93	-2.01
Pickeringite [a]	MgAl$_2$(SO$_4$)$_4$.22H$_2$O	-1.99	-5.21	-5.21	-4.33	-4.27	-5.03	-5.15	-5.20	-5.19	-9.38	-9.56	-9.58	-9.83	-11.4
Rozenite [d]	FeSO$_4$.4H$_2$O	-0.31	-0.98	-0.84	-0.94	-0.72	-1.66	-1.21	-1.64	-1.06	-2.50	-1.93	-1.95	-2.12	-2.19
Schwertmannite [c]	Fe$_8$O$_8$(OH)$_6$SO$_4$	-22.9	-20.1	-24.2	-12.7	-	-11.0	-13.3	-3.47	-	-15.5	-	-	-	-
Sideroti [d]	FeSO$_4$.5H$_2$O	-0.36	-0.99	-0.85	-0.95	-0.73	-1.66	-1.21	-1.64	-1.07	-2.50	-1.93	-1.95	-2.12	-2.20
Szomolnokite [d]	FeSO$_4$.H$_2$O	-0.56	-1.36	-1.23	-1.33	-1.11	-2.06	-1.62	-2.05	-1.48	-2.93	-2.36	-2.38	-2.55	-2.62
Zincosite	ZnSO$_4$	-7.29	-7.75	-7.66	-7.23	-7.03	-7.54	-7.51	-7.31	-7.16	-7.67	-7.64	-7.62	-7.68	-7.64
Gunningite	ZnSO$_4$.H$_2$O	-3.78	-4.19	-4.10	-3.67	-3.47	-3.98	-3.94	-3.74	-3.59	-4.10	-4.07	-4.05	-4.11	-4.07

140

Table A2. (continues)

Results for the grayish impoundment:

Depth (cm)		Wet season (February 2006)								
Phase	Min. formula	-10	-25	-50	-100	-150	-200	-250	-350	-400
		Saturation index								
Alum	$KAl(SO_4)_2 \cdot 12H_2O$	-2.51	-1.13	-1.98	-8.09	-1.76	-1.90	-1.81	-6.13	-6.31
Alunite	$KAl_3(SO_4)_2(OH)_6$	-11.5	-9.9	-10.5	2.09	-8.26	-7.23	-5.84	3.15	4.08
Alunogen [a]	$Al_2(SO_4)_3 \cdot 17H_2O$	-3.47	-1.77	-2.99	-6.92	-2.67	-2.93	-2.73	-2.95	-3.31
Anglesite	$PbSO_4$	-	-	-	-	-	-	-	-	-
Bianchite	$ZnSO_4 \cdot 6H_2O$	-3.81	-3.69	-3.15	-2.22	-2.65	-2.76	-2.70	-2.60	-2.49
Bilinite [d]	$Fe^{2+}Fe^{3+}_2(SO_4)_4 \cdot 22H_2O$	3.54	4.69	3.12	-	-	-	-	-	-
Chalcantite	$CuSO_4 \cdot 5H_2O$	-2.16	-1.74	-0.75	-4.04	-0.84	-1.67	-1.81	-4.44	-3.55
Copiapite [d]	$Fe^{2+}Fe^{3+}_4(SO_4)_6(OH)_2 \cdot 20H_2O$	2.10	3.96	1.32	-	-	-	-	-	-
Coquimbite [d]	$Fe_2(SO_4)_3 \cdot 9H_2O$	-36.2	-35.0	-36.5	-	-	-	-	-	-
Epsomite [a]	$MgSO_4 \cdot 7H_2O$	-2.76	-2.29	-2.61	-1.84	-1.89	-1.59	-1.43	-1.49	-1.49
Fe(OH)3	$Fe(OH)_3$	-8.21	-8.73	-8.35	-	-	-	-	-	-
Goethite	$FeOOH$	-3.62	-4.10	-3.76	-	-	-	-	-	-
Goslarite	$ZnSO_4 \cdot 7H_2O$	-3.67	-3.59	-3.01	-2.03	-2.50	-2.60	-2.53	-2.42	-2.31
Gypsum	$CaSO_4 \cdot 2H_2O$	0.82	1.15	0.82	-0.03	0.60	0.41	0.38	0.24	0.18
Halotrichite [a]	$FeAl_2(SO_4)_4 \cdot 22H_2O$	-3.08	-1.07	-2.67	-7.88	-2.26	-2.70	-2.52	-3.00	-3.37
Hexahydrite [b]	$MgSO_4 \cdot 6H_2O$	-2.85	-2.34	-2.70	-1.99	-1.99	-1.71	-1.55	-1.62	-1.63
H3O-Jarosite	$(H_3O)Fe_3(SO_4)_2(OH)_6$	-5.85	-5.77	-6.34	-	-	-	-	-	-
K-Jarosite	$KFe_3(SO_4)_2(OH)_6$	-2.95	-2.60	-3.14	-	-	-	-	-	-
Na-Jarosite	$NaFe_3(SO_4)_2(OH)_6$	-8.06	-7.99	-8.37	-	-	-	-	-	-
Jurbanite	$AlOHSO_4$	-0.68	0.07	-0.44	1.18	-0.03	0.03	0.30	2.40	2.46
Melanterite	$FeSO_4 \cdot 7H_2O$	0.01	0.24	-0.05	-1.24	0.05	-0.10	-0.12	-0.36	-0.36
Pickeringite [a]	$MgAl_2(SO_4)_4 \cdot 22H_2O$	-6.14	-3.90	-5.51	-8.78	-4.49	-4.48	-4.12	-4.42	-4.80
Rozenite [d]	$FeSO_4 \cdot 4H_2O$	-0.01	0.34	-0.08	-1.42	-0.01	-0.20	-0.22	-0.50	-0.50
Schwertmannite [c]	$Fe_8O_8(OH)_6SO_4$	-37.6	-40.6	-38.7	-	-	-	-	-	-
Siderotil [d]	$FeSO_4 \cdot 5H_2O$	-0.07	0.24	-0.14	-1.42	-0.05	-0.23	-0.25	-0.52	-0.52
Szomolnokite [d]	$FeSO_4 \cdot H_2O$	-0.27	0.18	-0.35	-1.84	-0.31	-0.54	-0.56	-0.88	-0.89
Zincosite	$ZnSO_4$	-8.23	-7.89	-7.59	-6.96	-7.14	-7.33	-7.28	-7.26	-7.16
Gunningite	$ZnSO_4 \cdot H_2O$	-4.71	-4.41	-4.07	-3.39	-3.61	-3.79	-3.74	-3.71	-3.60

Table A2. (continues)

Phase	Min. formula	Dry season (May 2010)					
Depth (cm)		-20	-40	-100	-150	-200	-250
		Saturation index					
Alum	$KAl(SO_4)_2 \cdot 12H_2O$	-5.25	-4.18	-2.87	-1.28	-2.15	-2.04
Alunite	$KAl_3(SO_4)_2(OH)_6$	-16.1	-15.2	-10.2	-6.51	-7.13	1.33
Alunogen [a]	$Al_2(SO_4)_3 \cdot 17H_2O$	-7.51	-6.33	-4.13	-1.98	-3.41	-2.82
Anglesite	$PbSO_4$	-0.06	0.15	0.35	0.88	0.38	-
Bianchite	$ZnSO_4 \cdot 6H_2O$	-3.78	-3.68	-3.12	-2.81	-2.79	-2.73
Bilinite [d]	$Fe^{2+}Fe^{3+}_2(SO_4)_4 \cdot 22H_2O$	1.39	0.42	-	-	-	-
Chalcantite	$CuSO_4 \cdot 5H_2O$	-3.40	-2.30	-1.22	-1.91	-2.21	-
Copiapite [d]	$Fe^{2+}Fe^{3+}_4(SO_4)_6(OH)_2 \cdot 20H_2O$	0.28	0.19	-	-	-	-
Coquimbite [d]	$Fe_2(SO_4)_3 \cdot 9H_2O$	-39.7	-39.2	-	-	-	-
Epsomite [a]	$MgSO_4 \cdot 7H_2O$	-4.20	-3.36	-2.80	-2.06	-1.65	-1.39
$Fe(OH)_3$	$Fe(OH)_3$	-8.42	-8.94	-	-	-	-
Goethite	$FeOOH$	-3.88	-4.38	-	-	-	-
Goslarite	$ZnSO_4 \cdot 7H_2O$	-3.60	-3.51	-2.94	-2.67	-2.62	-2.55
Gypsum	$CaSO_4 \cdot 2H_2O$	-0.01	0.34	0.37	0.93	0.27	0.22
Halotrichite [a]	$FeAl_2(SO_4)_4 \cdot 22H_2O$	-8.81	-7.00	-4.23	-1.46	-3.51	-2.89
Hexahydrite [b]	$MgSO_4 \cdot 6H_2O$	-4.34	-3.49	-2.92	-2.16	-1.78	-1.53
H_3O-Jarosite	$(H_3O)Fe_3(SO_4)_2(OH)_6$	-8.80	-9.28	-	-	-	-
K-Jarosite	$KFe_3(SO_4)_2(OH)_6$	-6.23	-6.46	-	-	-	-
Na-Jarosite	$NaFe_3(SO_4)_2(OH)_6$	-11.1	-11.5	-	-	-	-
Jurbanite	$AlOHSO_4$	-2.50	-2.09	-0.73	0.42	-0.12	1.46
Melanterite	$FeSO_4 \cdot 7H_2O$	-1.59	-0.97	-0.42	0.15	-0.40	-0.37
Pickeringite [a]	$MgAl_2(SO_4)_4 \cdot 22H_2O$	-11.7	-9.67	-6.90	-3.96	-5.05	-4.20
Rozenite [d]	$FeSO_4 \cdot 4H_2O$	-1.74	-1.10	-0.54	0.11	-0.54	-0.51
Schwermannite [c]	$Fe_8O_8(OH)_6SO_4$	-40.8	-44.3	-	-	-	-
Siderotil [d]	$FeSO_4 \cdot 5H_2O$	-1.75	-1.12	-0.56	0.06	-0.55	-0.53
Szomolnokite [d]	$FeSO_4 \cdot H_2O$	-2.15	-1.48	-0.91	-0.18	-0.91	-0.89
Zincosite	$ZnSO_4$	-8.48	-8.32	-7.75	-7.29	-7.44	-7.39
Gunningite	$ZnSO_4 \cdot H_2O$	-4.92	-4.77	-4.20	-3.76	-3.89	-3.83

[a] Reardon (1988).
[b] Delany and Lundeen (1990)
[c] Yu et al. (1999).
[d] Tosca et al. (2005).

Table A3. Theoretical mineral sequences following evaporation with the PHREEQC-2 code of the pore-water solutions of the oxidation zone of both impoundments.

Evaporated water (%)	Precipitated amounts (mol/kg$_{SOLUTION}$)					
	Rozenite	Hexahydrite	Halotrichite	Szomolnokite	Pickeringite	Melanterite
0	0.00	0.00	0.00	0.00	0.00	0.00
1	0.00	0.00	0.00	0.00	0.00	0.00
2	0.00	0.00	0.00	0.00	0.00	0.00
3	0.00	0.00	0.00	0.00	0.00	0.00
4	0.00	0.00	0.00	0.00	0.00	0.00
5	0.00	0.00	0.00	0.00	0.00	0.00
6	0.00	0.00	0.00	0.00	0.00	0.00
7	0.00	0.00	0.00	0.00	0.00	0.00
8	0.00	0.00	0.00	0.00	0.00	0.00
9	0.00	0.00	0.00	0.00	0.00	0.00
10	0.00	0.00	0.00	0.00	0.00	0.00
11	0.00	0.00	0.00	0.00	0.00	0.00
12	0.00	0.00	0.00	0.00	0.00	0.00
13	0.00	0.00	0.00	0.00	0.00	0.00
14	0.00	0.00	0.00	0.00	0.00	0.00
15	0.00	0.00	0.00	0.00	0.00	0.00
16	0.00	0.00	0.00	0.00	0.00	0.00
17	0.00	0.00	0.00	0.00	0.00	0.00
18	0.00	0.00	0.00	0.00	0.00	0.00
19	0.01	0.00	0.00	0.00	0.00	0.00
20	0.03	0.00	0.00	0.00	0.00	0.00
21	0.06	0.00	0.00	0.00	0.00	0.00
22	0.08	0.00	0.00	0.00	0.00	0.00
23	0.10	0.00	0.00	0.00	0.00	0.00
24	0.13	0.00	0.00	0.00	0.00	0.00
25	0.15	0.00	0.00	0.00	0.00	0.00
26	0.17	0.00	0.00	0.00	0.00	0.00
27	0.20	0.00	0.00	0.00	0.00	0.00
28	0.22	0.00	0.00	0.00	0.00	0.00
29	0.24	0.00	0.00	0.00	0.00	0.00
30	0.26	0.00	0.00	0.00	0.00	0.00
31	0.27	0.00	0.01	0.00	0.00	0.00
32	0.28	0.00	0.02	0.00	0.00	0.00
33	0.29	0.00	0.02	0.00	0.00	0.00
34	0.30	0.00	0.03	0.00	0.00	0.00
35	0.31	0.00	0.04	0.00	0.00	0.00
36	0.33	0.00	0.05	0.00	0.00	0.00
37	0.33	0.03	0.06	0.00	0.00	0.00
38	0.34	0.06	0.06	0.00	0.00	0.00
39	0.35	0.09	0.07	0.00	0.00	0.00
40	0.29	0.11	0.07	0.07	0.00	0.00
41	0.10	0.11	0.07	0.26	0.00	0.00
42	0.00	0.12	0.07	0.37	0.00	0.00
43	0.00	0.14	0.08	0.38	0.00	0.00
44	0.00	0.17	0.08	0.40	0.00	0.00
45	0.00	0.12	0.03	0.46	0.06	0.00
46	0.00	0.11	0.00	0.50	0.09	0.00
47	0.00	0.13	0.00	0.52	0.10	0.00
48	0.00	0.14	0.00	0.54	0.10	0.00

143

Table A3. (continues)

Evaporated water (%)	Precipitated amounts (mol/kg$_{SOLUTION}$)					
	Rozenite	Hexahydrite	Halotrichite	Szomolnokite	Pickeringite	Melanterite
49	0.00	0.16	0.00	0.56	0.11	0.00
50	0.00	0.18	0.00	0.57	0.12	0.00
51	0.00	0.19	0.00	0.59	0.12	0.00
52	0.00	0.21	0.00	0.61	0.13	0.00
53	0.00	0.22	0.00	0.62	0.13	0.00
54	0.00	0.24	0.00	0.64	0.14	0.00
55	0.00	0.25	0.00	0.66	0.14	0.00
56	0.00	0.26	0.00	0.67	0.15	0.00
57	0.00	0.27	0.00	0.69	0.15	0.00
58	0.00	0.29	0.00	0.70	0.15	0.00
59	0.00	0.30	0.00	0.71	0.16	0.00
60	0.00	0.31	0.00	0.73	0.16	0.00
61	0.00	0.32	0.00	0.74	0.16	0.00
62	0.00	0.32	0.00	0.74	0.17	0.00
63	0.00	0.33	0.00	0.75	0.17	0.00
64	0.00	0.34	0.00	0.76	0.17	0.00
65	0.00	0.35	0.00	0.76	0.16	0.00
66	0.00	0.36	0.00	0.77	0.16	0.00
67	0.00	0.38	0.00	0.77	0.15	0.00
68	0.00	0.40	0.00	0.77	0.12	0.00
69	0.00	0.46	0.00	0.77	0.07	0.00
70	0.00	0.53	0.00	0.77	0.00	0.00
71	0.00	0.53	0.00	0.77	0.00	0.00
72	0.00	0.54	0.00	0.77	0.00	0.00
73	0.00	0.54	0.00	0.77	0.00	0.00
74	0.00	0.54	0.00	0.77	0.00	0.00
75	0.00	0.54	0.00	0.77	0.00	0.00
76	0.00	0.54	0.00	0.78	0.00	0.00
77	0.00	0.53	0.00	0.78	0.00	0.00
78	0.00	0.53	0.00	0.78		
79	0.00	0.52	0.00	0.78		
80	0.00	0.52	0.00	0.78		
81	0.00	0.53	0.00	0.78		
82	0.00	0.53	0.00	0.78		
83	0.00	0.53	0.00	0.78		
84	0.00	0.53	0.00	0.78		
85	0.00	0.53	0.00	0.78		
86	0.00	0.53	0.00	0.78		
87	0.00	0.53	0.00	0.78		
88	0.00	0.53	0.00	0.78		
89	0.00	0.53	0.00	0.78		
90	0.00	0.53	0.00	0.00		

144

Table A4. Results obtained for BCR sequential extraction for the experimental plot for the yellowish impoundment.

Samples Depth (cm)	Step	Elements (mg/kg)										
		Al	As	Ca	Cd	Co	Cu	Fe	Mn	Ni	S	Zn
Wet season												
10	F1	1568	0.54	20973	0.10	1.36	1.73	15.3	21.9	3.69	1153	7.73
	F2	2015	3.42	771	-	0.82	5.20	569	54.2	1.45	79.8	5.46
	F3	2760	2.09	2303	-	0.78	2.82	89.9	15.7	1.85	25.5	3.59
	F4	13518	2.52	5143	-	5.33	9.15	11010	54.5	11.1	-	15.4
	Sum	19861	8.57	29190	0.10	8.28	18.9	11684	146	18.1	1258	32.2
	Pseudo-total	18893	8.71	26635	-	7.95	18.0	10464	140	16.1	1665	32.4
	% Recovery	105	98.3	110	-	104	105	112	104	113	75.5	99.5
Hardpan	F1	992	0.21	12365	0.19	0.18	38.9	339	3.16	0.59	10665	66.3
	F2	655	0.97	77.9	-	0.11	23.4	23212	3.18	0.34	2782	27.4
	F3	1091	1.05	197	-	0.19	39.0	837	1.93	0.72	625	25.6
	F4	6742	150	1844	-	2.86	24.4	31541	27.6	6.21	679	22.1
	Sum	9479	152	14485	0.19	3.34	126	55929	35.9	7.86	14751	141
	Pseudo-total	9499	166	13175	-	3.89	111	55399	36.2	8.83	14392	129
	% Recovery	100	91.6	110	-	85.8	113	101	99.1	89.0	102	109
-5	F1	26.9	1.49	6529	-	-	3.71	75.4	0.44	0.15	5427	10.8
	F2	8.98	2.18	100	-	-	3.52	4016	-	0.09	1363	4.54
	F3	59.2	5.87	58.3	-	-	39.1	436	0.58	0.33	658	11.5
	F4	2683	527	35.5	0.10	0.12	179	32611	40.1	0.51	8785	272
	Sum	2778	537	6723	0.10	0.12	226	37139	41.1	1.08	16232	299
	Pseudo-total	2077	542	6922	-	-	260	35111	35.2	0.83	16982	340
	% Recovery	134	99.0	97.1	-	-	87.0	106	117	131	95.6	88.1
-10	F1	31.1	1.29	5311	-	0.10	4.41	89.2	0.44	0.21	4552	11.9
	F2	11.3	2.18	52.3	-	-	3.88	3982	-	-	1350	4.10
	F3	29.9	4.45	52.1	-	-	49.7	289	0.34	0.24	689	10.4
	F4	2703	138	21.6	0.09	0.11	216	16580	50.4	0.51	4810	310
	Sum	2775	145	5437	0.09	0.20	274	20939	51.1	0.96	11401	336
	Pseudo-total	2441	778	4868	-	-	403	37027	41.6	1.05	15157	443
	% Recovery	114	18.7	112	-	-	68.0	56.6	123	92.0	75.2	76.0
-15	F1	94.6	1.27	6724	0.17	-	27.1	2096	1.47	0.19	7709	69.2
	F2	8.05	2.98	48.2	-	-	4.17	2194	-	0.09	852	3.00
	F3	26.9	63.9	60.3	0.40	-	765	384	0.21	0.27	1561	108
	F4	2741	1171	31.5	0.59	-	238	21106	33.6	0.43	6911	328
	Sum	2871	1239	6864	1.16	-	1034	25781	35.3	0.98	17033	508
	Pseudo-total	2576	1557	5850	1.27	-	1204	26082	35.4	0.77	16942	582
	% Recovery	111	79.6	117	90.9	-	85.9	98.8	100	128	101	87.3
-20	F1	128	2.60	7609	0.33	0.10	44.9	3062	2.40	0.24	9006	136
	F2	9.62	23.3	48.7	-	-	4.81	1242	-	-	486	8.06
	F3	45.1	259	56.8	0.87	1.68	337	18492	4.92	1.34	21433	352
	F4	857	884	21.5	3.13	1.47	568	34499	8.28	1.23	30946	1339
	Sum	1040	1169	7736	4.33	3.25	955	57295	15.6	2.81	61871	1835
	Pseudo-total	1442	2366	7365	8.31	5.61	2001	92124	22.8	4.72	95907	4027
	% Recovery	72.1	49.4	105	52.1	58.0	47.7	62.2	68.4	59.6	64.5	45.6
-30	F1	129	1.70	7651	0.61	0.25	56.3	3079	5.44	0.44	9057	212
	F2	9.67	7.05	49.0	-	-	6.68	1249	-	-	489	7.51
	F3	45.4	64.8	57.2	0.61	1.04	206	18595	3.20	1.14	21553	234
	F4	862	821	21.6	1.17	0.37	455	34692	34.8	0.59	31119	486
	Sum	1046	895	7779	2.39	1.66	724	57615	43.4	2.16	62217	939
	Pseudo-total	1949	1177	5537	3.39	2.39	954	51125	36.9	2.70	51187	1462
	% Recovery	53.7	76.0	140	70.3	69.3	75.9	113	118	80.2	122	64.2

145

Table A4. (continues)

Samples Depth (cm)	Step	Elements (mg/kg)										
		Al	As	Ca	Cd	Co	Cu	Fe	Mn	Ni	S	Zn
Dry season												
10	F1	288	1.17	22318	0.10	1.05	0.92	-	19.9	3.25	522	7.71
	F2	2262	2.14	1372	-	1.03	3.21	534	61.9	1.92	-	4.06
	F3	2337	0.16	2637	-	0.72	2.64	98.8	19.5	1.84	-	4.59
	F4	21549	-	10328	-	8.35	14.8	15237	81.0	19.6	-	31.9
	Sum	26435	3.47	36654	0.10	11.2	21.6	15870	182	26.6	522	48.3
	Pseudo-total	22048	7.08	37891	0.20	10.9	17.4	9592	196	23.4	362	44.2
	% Recovery	120	49.0	96.7	50.1	102	124	165	93.1	114	144	109
5	F1	699	-	21199	4.51	3.38	130	-	52.0	6.40	1756	1195
	F2	2506	0.36	1071	1.14	1.60	137	735	70.3	2.98	306	358
	F3	4951	2.17	2111	0.30	1.38	65.2	75.3	20.3	3.30	-	116
	F4	16942	-	9491	0.14	9.51	28.5	4269	82.9	20.7	-	53.6
	Sum	25097	2.53	33873	6.10	15.9	361	5079	225	33.3	2062	1723
	Pseudo-total	31640	9.00	33952	5.58	15.4	355	18959	236	30.8	1829	1740
	% Recovery	79.3	28.1	100	109	103	102	26.8	95.7	108	113	99.0
Hardpan	F1	1202	-	18109	0.58	0.57	71.8	552	9.08	4.36	14376	156
	F2	1388	-	186	0.11	0.19	34.3	20660	6.77	0.46	3608	47.0
	F3	1610	-	123	-	0.17	56.8	587	2.72	0.79	884	26.7
	F4	9230	121	2088	0.09	4.27	44.9	46562	33.7	11.3	1470	28.3
	Sum	13430	121	20506	0.78	5.20	208	68361	52.3	16.9	20338	258
	Pseudo-total	12992	158	19439	0.81	4.67	172	73185	52.2	9.82	19969	256
	% Recovery	103	76.6	105	97.0	111	121	93.4	100	172	102	101
-5	F1	99.0	-	320	0.09	-	12.3	277	1.26	0.17	604	41.1
	F2	37.5	-	37.40	-	-	0.26	638	0.18	0.16	179	-
	F3	48.6	0.82	-	-	-	2.88	851	0.25	0.27	493	8.16
	F4	1117	72.1	36.6	-	0.09	165	14521	12.1	0.51	4277	247
	Sum	1302	72.9	394	0.09	0.09	181	16287	13.8	1.10	5553	296
	Pseudo-total	1250	180	469	0.17	0.16	216	25039	13.3	0.70	7928	325
	% Recovery	104	40.6	84.0	52.7	52.2	83.5	65.0	104	158	70.0	91
-15	F1	232	-	4761	0.33	0.19	25.2	2194	3.83	0.27	5802	141
	F2	-	-	34.9	-	-	0.11	1566	0.10	0.19	468	-
	F3	34.5	1.67	-	-	-	2.84	516	0.32	0.32	562	4.11
	F4	4687	334	29.2	-	0.09	135	39642	67.6	0.55	11818	274
	Sum	4953	336	4825	0.33	0.28	163	43918	71.9	1.32	18650	420
	Pseudo-total	4042	411	5239	0.40	0.25	179	46709	66.4	0.73	19038	434
	% Recovery	123	81.7	92.1	82.8	114	91.2	94.0	108	182	98.0	96.6
-20	F1	185	0.87	5085	0.33	0.17	17.2	1862	3.34	0.28	5768	137
	F2	-	-	43.1	-	-	0.07	2057	0.09	0.16	539	-
	F3	31.9	0.77	40.6	-	-	33.9	710	0.35	0.35	716	9.49
	F4	2153	134	35.0	-	-	101	5108	49.5	0.34	1695	161
	Sum	2370	136	5203	0.33	0.17	152	9738	53.2	1.13	8719	307
	Pseudo-total	2699	132	5490	0.39	0.18	145	12504	47.8	0.46	9392	287
	% Recovery	87.8	103	94.8	85.0	94.2	105	77.9	111	244	92.8	107
-30	F1	1219	215	4907	3.48	1.41	105	13803	22.2	1.19	17110	1229
	F2	-	42.4	31.7	-	-	-	690	0.16	0.15	333	3.10
	F3	24.8	222	20.4	0.34	6.46	172	41284	6.02	2.46	43904	103
	F4	744	866	28.5	3.92	5.61	454	63102	7.21	1.84	63638	1686
	Sum	1988	1345	4988	7.74	13.5	731	118879	35.6	5.63	124986	3022
	Pseudo-total	2166	1311	4742	6.71	11.7	623	125393	35.7	4.36	128284	2777
	% Recovery	91.8	103	105	115	115	117	94.8	99.5	129	97.4	109

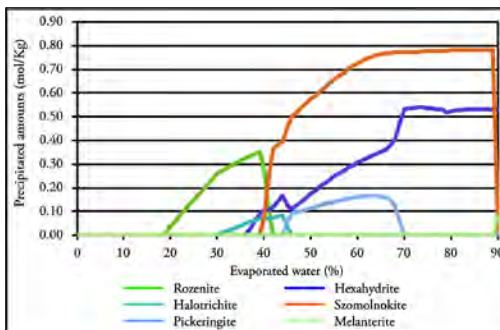|	Fly ash		Hardpan		Oxidized tailings		Mine tailings

146

Table A5. Results obtained for BCR sequential extraction for the experimental plot for the grayish impoundment.

Samples Depth (cm)	Step	Elements (mg/kg)										
		Al	As	Ca	Cd	Co	Cu	Fe	Mn	Ni	S	Zn
Wet season												
10	F1	1062	0.63	18716	0.09	1.04	1.26	8.79	19.8	3.02	1770	5.94
	F2	2025	4.12	705	-	0.77	4.57	556	52.0	1.39	105	5.20
	F3	3124	2.10	2548	-	0.77	2.87	103	16.4	1.87	29.2	3.18
	F4	12885	2.19	4731	-	5.10	8.87	9817	54.0	10.9	1.76	15.9
	Sum	19096	9.04	26699	0.09	7.68	17.6	10485	142	17.1	1906	30.2
	Pseudo-total	18646	7.73	27224	-	7.60	17.4	7650	134	16.1	1028	28.3
	% Recovery	102	117	98.1	-	101	101	137	106	106	185	107
Hardpan	F1	2131	0.48	3835	-	1.08	15.4	1651	7.13	1.28	7461	30.7
	F2	777	1.22	86.4	-	0.49	10.7	20670	3.01	3.20	3190	23.7
	F3	2566	2.30	465	-	1.32	13.1	1962	4.95	1.67	4960	10.7
	F4	6517	151	1446	-	2.91	9.47	31331	26.3	6.31	1278	24.8
	Sum	11991	155	5832	-	5.79	48.6	55614	41.4	12.5	16889	89.9
	Pseudo-total	11562	187	5591	-	5.86	51.2	57759	41.0	9.66	18614	115
	% Recovery	104	82.9	104	-	98.8	94.9	96.3	101	129	90.7	78.3
-5	F1	246	11.1	198	-	0.58	7.20	3193	1.11	0.26	3253	15.1
	F2	6.44	5.53	10.2	-	0.08	-	51.6	-	-	532	-
	F3	10.0	181	56.8	-	5.71	40.3	47072	3.85	1.56	52004	14.6
	F4	59.9	149	8.9	0.57	7.40	59.8	57027	3.30	1.40	83683	200
	Sum	323	346	274	0.57	13.8	107	107343	8.26	3.22	139472	230
	Pseudo-total	306	356	389	0.82	15.6	120	121934	8.78	3.73	163412	259
	% Recovery	105	97.4	70.5	69.7	88.3	89.1	88.0	94.1	86.4	85.3	88.6
-10	F1	56.4	7.67	108	-	0.15	5.33	798	0.17	-	995	13.9
	F2	5.48	8.18	15.5	-	-	-	42.7	-	-	1941	0.31
	F3	10.0	199	40.2	0.15	8.14	64.2	46559	4.48	1.30	51971	35.3
	F4	54.3	682	46.6	2.24	39.8	279	237514	13.1	3.24	298362	723
	Sum	126	897	210	2.39	48.1	348	284914	17.7	4.54	353268	772
	Pseudo-total	166	896	775	3.51	52.4	403	303233	18.3	4.91	368421	1177
	% Recovery	75.9	100	27.1	68.3	91.8	86.5	94.0	96.8	92.6	95.9	65.6
-15	F1	37.4	4.54	130	-	0.14	9.44	718	0.14	-	994	22.9
	F2	1.51	2.62	23.4	-	-	-	20.0	-	-	1087	0.21
	F3	10.0	232	39.3	0.13	7.83	67.3	44157	5.17	1.84	48718	30.5
	F4	49.9	789	33.4	5.80	35.4	313	217806	16.7	4.55	260493	1884
	Sum	98.9	1028	226	5.94	43.4	389	262701	22.0	6.38	311292	1938
	Pseudo-total	182	1087	349	8.15	50.7	490	308046	24.0	7.29	343678	2854
	% Recovery	54.2	94.6	65.0	72.8	85.5	79.4	85.3	91.5	87.6	90.6	67.9
-20	F1	32.0	6.11	160	-	0.17	13.0	857	0.16	0.20	1206	21.9
	F2	0.88	5.03	15.6	-	-	-	29.5	-	-	1777	0.55
	F3	2.20	249	53.7	0.14	9.05	71.3	51737	5.61	2.23	56906	27.1
	F4	50.6	824	38.9	6.91	36.3	306	225788	16.4	4.84	270259	2240
	Sum	85.7	1084	269	7.05	45.5	390	278411	22.2	7.27	330149	2289
	Pseudo-total	92.4	1187	238	9.94	55.5	535	338317	25.9	7.99	382074	3557
	% Recovery	92.8	91.3	113	70.9	82.1	73.0	82.3	85.5	90.9	86.4	64.4
-30	F1	62.5	9.56	198	-	0.50	32.5	1893	0.31	0.19	2118	14.5
	F2	5.28	3.60	14.2	-	-	0.28	45.5	-	0.10	823	1.40
	F3	9.20	312	60.5	0.10	12.9	80.5	66613	6.52	3.05	72911	13.9
	F4	54.6	823	30.3	0.70	32.7	229	190804	17.3	6.37	230708	218
	Sum	132	1148	303	0.80	46.1	342	259355	24.1	9.71	306560	247
	Pseudo-total	181	1121	742	0.89	49.9	383	282307	25.1	10.3	317263	254
	% Recovery	73	102	40.8	90.0	92.3	89.3	91.9	95.9	93.8	96.6	97.5

Table A5. (continues)

Samples Depth (cm)	Step	Elements (mg/kg) Al	As	Ca	Cd	Co	Cu	Fe	Mn	Ni	S	Zn
Dry season												
10	F1	1333	-	18826	0.65	6.57	5.32	-	68.4	7.70	2608	132
	F2	2603	-	736	0.19	3.36	19.1	785	80.8	4.11	711	92.4
	F3	3236	0.87	1665	0.10	1.81	18.5	106	20.2	4.57	588	41.6
	F4	25735	-	7294	0.10	8.20	28.6	16881	79.9	18.2	-	42.5
	Sum	32907	0.87	28520	1.03	19.9	71.6	17772	249	34.6	3907	308
	Pseudo-total	33025	10.6	30230	0.99	20.0	64.3	15039	262	34.6	3607	305
	% Recovery	100	8.24	94.3	105	99.6	111	118	95.1	100	108	101
5	F1	723	4.04	15823	-	0.62	3.49	1778	5.62	0.99	13903	16.6
	F2	32.2	4.06	57.8	-	-	-	652	0.30	0.15	381	-
	F3	206	3.88	39.8	-	0.75	6.72	2456	1.12	0.61	3854	8.35
	F4	3644	26.0	783	-	4.08	6.49	20467	32.5	8.90	1616	24.2
	Sum	4605	38.0	16704	-	5.45	16.7	25354	39.5	10.6	19755	49.2
	Pseudo-total	3791	10.8	10662	0.12	4.65	13.1	7450	36.9	8.73	13524	42.1
	% Recovery	121	351	157	-	117	127	340	107	122	146	117
Hardpan	F1	625	-	9670	-	0.31	3.71	1016	2.93	0.65	8916	9.75
	F2	1201	-	151	-	0.27	4.57	25968	1.54	0.92	4984	5.88
	F3	1623	-	279	-	0.42	5.62	1851	2.66	1.28	1398	8.29
	F4	11314	34.4	3423	-	5.73	10.8	20905	48.7	12.8	623	34.0
	Sum	14763	34.4	13523	-	6.73	24.7	49740	55.9	15.7	15921	57.9
	Pseudo-total	14420	40.5	13939	0.11	6.47	24.0	38607	56.6	14.1	10860	60.8
	% Recovery	102	84.9	97.0	-	104	103	129	98.8	112	147	95.3
-5	F1	259	4.07	104	-	0.48	10.7	2409	2.51	0.37	2877	13.9
	F2	-	6.63	24.3	-	-	-	93.9	-	0.14	1011	-
	F3	-	232	29.4	-	10.2	69.3	62747	5.10	2.21	65988	19.5
	F4	22.1	629	43.7	0.95	27.0	223	216502	12.9	3.80	235809	321
	Sum	281	872	201	0.95	37.6	303	281752	20.5	6.52	305685	354
	Pseudo-total	290	381	120	1.02	34.4	270	274445	20.5	5.46	289298	335
	% Recovery	97.0	229	168	93.5	109	112	103	100	119	106	106
-15	F1	269	8.68	81.81	0.14	0.84	7.46	4526	1.62	0.46	3846	56.7
	F2	-	0.29	-	-	-	-	45.3	-	0.14	355	-
	F3	140	105	-	0.10	4.64	34.4	36527	2.92	1.89	39696	24.5
	F4	157	16.7	-	0.39	1.53	15.5	13288	0.71	0.39	19804	165
	Sum	565	131	81.8	0.64	7.01	57.3	54385	5.25	2.87	63701	246
	Pseudo-total	418	233	83.2	0.69	9.33	79.9	81613	6.27	2.14	91642	250
	% Recovery	135	56.3	98.3	92.8	75.1	71.7	66.6	83.8	134	69.5	98.5
-20	F1	43.5	8.37	80.8	0.29	0.55	13.1	2793	0.37	0.18	2924	115
	F2	-	2.36	36.1	-	-	-	-	-	0.17	1251	-
	F3	-	112	25.1	-	4.94	34.7	31291	2.82	0.97	33501	14.4
	F4	36.7	193	37.6	1.02	14.5	99.1	91483	3.85	1.21	104506	375
	Sum	80.2	316	180	1.31	20.0	147	125567	7.04	2.53	142182	505
	Pseudo-total	252	536	96.2	1.92	30.2	247	238539	15.2	3.47	259305	666
	% Recovery	31.8	58.9	187	67.9	66.2	59.6	52.6	46.2	73.1	54.8	75.8
-30	F1	51.5	11.2	47.3	0.18	0.48	12.0	2656	0.45	0.15	2365	73.0
	F2	-	2.70	17.1	-	-	-	48.6	-	0.14	977	-
	F3	103	148	33.6	0.44	8.10	60.0	48290	4.09	1.60	50326	111
	F4	104	361	19.6	3.42	19.3	140	143075	7.56	2.61	161480	1202
	Sum	259	523	118	4.04	27.9	212	194069	12.09	4.51	215150	1386
	Pseudo-total	191	505	93.9	4.72	25.3	192	191245	11.0	3.32	203629	1656
	% Recovery	135	104	125	85.6	110	110	101	110	136	106	83.7

	Fly ash		Hardpan	Oxidized tailings	Mine tailings

ANEXO II. PUBLICACIONES

PUBLICACIONES

Artículos publicados en revistas internacionales JCR-SCI derivados de esta tesis:

Dino Quispe, Rafael Pérez-López, Luis F.O. Silva, José Miguel Nieto. Changes in mobility of hazardous elements during coal combustion in Santa Catarina power plant (Brazil). Fuel 94 (2012) 495-503.

Dino Quispe, Rafael Pérez-López, Patricia Acero, Carlos Ayora, José Miguel Nieto. The role of mineralogy on element mobility in two sulfide mine tailings from the Iberian Pyrite Belt (SW Spain). Chemical Geology 345 (2013) 119-129.

Dino Quispe, Rafael Pérez-López, Patricia Acero, Carlos Ayora, José Miguel Nieto, Rémi Tucoulou. Formation of a hardpan in the co-disposal of fly ash and sulfide mine tailings and its influence on the generation of acid mine drainage. Chemical Geology 355 (2013) 45-55.

Otras publicaciones internacionales JCR-SCI:

Rafael Pérez-López, Julio Castillo, **Dino Quispe**, José Miguel Nieto. Neutralization of acid mine drainage using the final product from CO_2 emissions capture with alkaline paper mill waste. Journal of Hazardous Materials 177 (2010) 762-772.

Rafael Pérez-López, **Dino Quispe**, Julio Castillo, José Miguel Nieto. Acid neutralization by dissolution of alkaline paper mill wastes and implications for treatment of sulfide-mine drainage. American Mineralogist 96 (2011) 781-791.

Manuel Caraballo, Francisco Macías, José Miguel Nieto, Julio Castillo, **Dino Quispe**, Carlos Ayora. Hydrochemical performance and mineralogical evolution of a dispersed alkaline substrate (DAS) remediating the highly polluted acid mine drainage in the full-scale passive treatment of Mina Esperanza (SW Spain). American Mineralogist 96 (2011) 1270-1277.